FINAL REPORT

Fluid Dynamic Aspects of Jet Noise Generation

New York University

Aerospace and Energetics Laboratory

Westbury, L.I., N.Y.

October 1, 1973 - September 30, 1974

Grant Number NGR-33-016-177

TABLE OF CONTENTS

LIST OF FIGURES

LIST OF FIGURES (Cont'd)

NOMENCLATURE

A, A'	Sinusoidal signal amplitudes
D	Nozzle exit diameter
F, $\bar{F}$	Functions of time
f	Fundamental frequency of the periodic signals
IA	Input attentuation of the analyzer
i	Integer between 0 and 99
K	Total number of (100 point) samples or summations
k, ℓ	Integers between 1 and K
M	Mean flow Mach number
M_j	Jet Mach number
m	Exponent between $1/2$ and 1
N, n	Stationary random functions of time
P	Mean static pressure
p	Fluctuating static pressure
R_{FF}	Average auto-correlation of the function F(t)
$R_{FS'}$	Average cross-correlation between F(t) and S'(t)
S	Periodic signal
S'	Sinusoidal reference signal
SPFL	Static pressure fluctuation level as defined in Equation III-2
T	Period of the harmonic signals
T_o	Mean stagnation temperature of the flow
T_R	Total running time of the flow

NOMENCLATURE (Cont'd)

t	Time
t'	Averaging time
t_d, τ	Delay times
Δt	Sampling increment
$\vec{x} = (x, y, z)$	
x	Streamwise coordinate
y	Vertical transverse coordinate
z	Horizontal transverse coordinate (= 0 in all cases)
φ	Relative phase

Subscripts

e	Nozzle exit
rms	Root-mean-square amplitude

I. INTRODUCTION

Recent experimental investigations of the problem of jet noise fall within two main categories. In the first, a direct attempt is made to obtain a reduction of the radiated sound by a modification of the jet flow. This includes the use of secondary flows (Reference 1) or the alteration of the shape, size or configuration of the standard circular nozzle (Reference 2,3). A review of the various approaches to the problem along these lines can be found in Reference 4. The success of these attempts in significantly suppressing radiated noise has consistently been coupled with a large reduction of jet thrust. These losses might be avoidable if more rational suppressor design principles were established.

With this in mind, the other course of investigation involves a more fundamental attempt to determine the location of the noise sources within jet flows, their relative importance to the overall radiated field, and the mechanisms by which noise generation occurs. Information of this type has been obtained from detailed measurements of the level and spectral composition of the radiated sound in the far-field (as, for example, in References 5,6), by the use of directional microphones to isolate the contribution to the radiated sound of small regions of the flow (Reference 7), and by cross-correlation between the radiated acoustic field and either the velocity fluctuations (Reference 8) or the pressure fluctuations

(References 9-11) in the source field.

In addition, detailed studies of the level and spectral distribution of the pressure fluctuations within small model jet flows have been made by Nagamatsu and several associates (References 12-14). Part of the present investigation is directed toward a similar survey of the static pressure fluctuations within the cold supersonic jet flow exhausting from a relatively large 7 inch exit diameter convergent-divergent nozzle. The nozzle is designed to yield shock-free (balanced) flow with a jet Mach number $M_j=2$. Both the flow in this perfectly expanded case, and an overexpanded flow with $M_j=1.8$ are surveyed.

An important aspect of the problem of jet noise which could lead to a better understanding of noise generating mechanisms is the propagation of pressure disturbances in the presence of flow. Research in this area has included a study by Chih-ming and Kovasznay (Reference 15) of periodic wave propagation across a two-dimensional layer of turbulence, and analytical investigations by Slutsky and Tamagno (Reference 16) and Gottlieb (Reference 17) of the field due to an harmonic source radiating from a two-dimensional region of flow, across a velocity discontinuity, into a medium at rest. Although the last reference also includes results for the reverse case of a source radiating into a region of flow from one at rest, the use of an improper boundary condition at the interface is believed to invalidate the results for both cases. The problem

of a source within a cylindrical flow region was treated by Slutsky (Reference 18), and was extended by Liu and Maestrello (Reference 19) to the case of a real axisymmetric flow with diverging boundaries. An experimental investigation of refraction (Reference 20) has included measurements in the acoustic far-field of a pure-tone point source located inside a low speed jet flow.

Mixing induced disturbances at the periphery of an axisymmetric jet flow not only propagate into the sorrounding medium but also toward the centerline of the flow. A recent analysis by Ferri, Ting and Werner (Reference 21) has shown that the non-linear propagation of a circumferential disturbance at the edge of a cylindrical supersonic flow toward the axis of the flow will exhibit effects such as focussing and distortion of wave profile. (Also included in this investigation is a study, in the same vein as those described in the previous paragraph, of the propagation of an acoustic disturbance from the core of a supersonic jet through the shear layer). An experimental verification of these phenomena requires the ability to first induce a known disturbance at the edge of a supersonic flow and then to observe the disturbance as it propagates into the flow. A major effort of the present study is the development of the experimental procedures and data processing necessary to accomplish this. Although a method of detecting a weak acoustic signal in turbulent airflows has been investigated (Reference 22), its scope, as will be

discussed in Section IV, is rather limited.

The development of a signal tracing capability, as well as its implementation to a mapping of the pressure fields induced within the two supersonic jet flows described above by a single acoustic disturbance at the periphery of the flows, represents a continuation of the experimental program outlined in References 23 and 24.

II. EXPERIMENTAL FACILITIES AND PROCEDURES

A. Jet Facility

The axisymmetric cold jet flows under investigation were established through a convergent-divergent nozzle with a throat diameter of 5.25 inches and an exit diameter of 7 inches (Fig. 1). The settling chamber for the nozzle is a steel cylinder (7 ft long and 1.5 ft I.D.), closed at one end with a blind flange, and designed for a nominal pressure of 1600 psi. Air was supplied to the chamber from a 1700ft^3 bank at a maximum pressure of 2000psi through three regulating valves (Fig. 2). The air temperature ranged between T_o = 450-490°R depending on ambient conditions. The nozzle exhausted into an open space at a height of approximately 5 ft above the ground. Also shown in Fig. 2 is the laboratory coordinate system referred to hereafter.

Two jet flows were studied. In the first, the chamber pressure was maintained at 80 psia, yielding a mass flow of 40 lbm/sec and a nozzle exit static pressure of 10 psia. The shadowgraph in Fig. 3 exhibits the initial shock structure associated with this overexpanded jet. The second configuration, which required a chamber pressure of approximately 110 psia and a mass flow of 60 lbm/sec, had an exit static pressure equal to the ambient atmospheric pressure. Assuming the same initial bank pressure of 2000 psi, maximum valve openings allowed for only 45 seconds of total running time in this balanced configuration and 100 seconds in the former overexpanded one before bank pressure had to be re-established by a compressor. For both flow conditions the exit Mach number M_e = 2, being determined by the nozzle geometry. Defining the jet Mach number, M_j, as the Mach number that would result from an isentropic expansion of a given chamber (total) pressure to atmospheric pressure, it is clear that M_j = 2 for the balanced jet, while M_j = 1.8 for the overexpanded jet.

B. Probes and Supporting Structure

Probes were supported in the flow by the structure shown in Fig. 4. A massive base can be moved down a 10 ft long track fixed to the ground and oriented along the x-axis, as well as normal to this streamwise direction. A motorized mechanism attached to the base allowed for a 13 inch vertical traverse of the flow at a speed of approximately 2 in/sec. Two pressure probes can be mounted, either singly or together (separated by 1.5 inches in the vertical y-direction), at the end of a knife-edged wing (Fig. 5) which was then fixed to the top of the traversing mechanism and extended into the flow. The wing also served to enclose the transducer cables.

Static pressure fluctuation measurements were made using two probes, both consisting of Kulite piezoresistive pressure transducers (Type CQS125-100) housed in the ends of 6 inch long stainless steel tubes fitted with Bruel and Kjaer #UA0385 ogive nose cones, Fig. 5. One tube has a constant $\frac{1}{4}$ inch O.D. and the other a $\frac{3}{8}$ inch O.D. tapering to $\frac{1}{4}$ inch. The transducer senses the pressure in a cavity (formed by the B & K nose cone) which is in contact with the outside pressure field through a wire mesh ring. A "blind," solid steel nose cone was constructed for use in determining how large a part of the transducer output signal was due to spurious, non-pressure noise such as that resulting from vibration of instrumentation cables. Specifications for the two transducers, identified as #1 and #7, as well as a typical circuit diagram are presented in Fig. 6. The resonance frequency of 130 kHz indicates a flat ($\pm$ 1 db) transducer frequency response of DC-40 kHz as shown in Fig. 7. The Helmholtz resonance of the probe cavity mentioned above should not significantly affect measurements within this range

of frequencies. It is believed that this resonance frequency is much higher than the 20 kHz found in Reference 25 for the cavity of a similar 1 inch diameter B & K nose cone. In fact, simple scaling considerations would indicate a frequency on the order of 80 kHz. The sensitivities of the transducers were verified using a 1 kHz pressure field of known level (154 dB).

C. Instrumentation

A diagram of the instrumentation set-up for recording the transducer outputs and generating the acoustic signal to be traced through the flow is shown in Fig. 8. The output voltage of transducer #1 was amplified and filtered by a Princeton Applied Research amplifier (Model 113) which has a maximum gain of 10^4. The RMS level of the amplifier output was monitored on a voltmeter. A Bruel & Kjaer Type 2606 measuring amplifier with a maximum gain of 96 db served the same purpose for the output of transducer #7, its meter indicating the RMS level of this output. Typical amplifier bandpasses used were 30-300,000 Hz on the PAR and 22.5-200,000 Hz on the B & K. The low frequency roll-offs were needed to eliminate the effect of 2 Hz mass flow fluctuations (created by valve oscillation) on the measurements. Both amplifier outputs were displayed on a 2 channel oscilloscope and recorded on a 7-channel Honeywell 5600 tape recorder.

The system for generating the acoustic signal consisted of a 100 watt Altec 290-E loudspeaker, with a 3 inch exit diameter catenoidal horn, driven by a H-P 3310A function generator (operating in the sine mode) through a Bogen 100 watt power amplifier. The sync output of the function generator acted as an external trigger for a General Radio pulse generator (Type 1340). The resulting pulse train, adjusted for proper amplitude, was

recorded along with the transducer outputs and served to synchronize them with the loudspeaker generated signal. Tape recordings were made primarily at 60 ips although a speed of 15 ips was also used. The tranducer outputs were all simultaneously recorded both in FM double extended mode and Direct mode. The pulse train was recorded only in Direct mode. At 60 ips, the recorder bandwidth is DC-40 kHz for FM and 300-300,000 Hz for Direct. At 15 ips these become DC-10 kHz and 100-75,000 Hz, respectively. When the traversing mechanism was used, a marker signal locating the position of the probe along the y-axis in the flow was recorded in FM mode.

Basically, three experimental procedures were followed to acquire data. With one of the probes located at various fixed positions inside the jet, 15 to 20 second recordings were made of the transducer output at each position. The RMS level of the static pressure fluctuations represented by this output was determined from an on-line reading of the appropriate meter, while the recordings were later analyzed to obtain the spectral distribution of the fluctuations. Again with only one probe, the traversing mechanism was used to vertically scan the static pressure fluctuations across the jet. In this case the transducer output was recorded during the scan along with a signal marking the approximate position of the moving probe. In the last procedure, the set-up for which is shown in Fig. 9, both probes (separated by 1.5 inches in the vertical direction) were placed in the field of the acoustic signal generator (located 4 inches below the centerline of the nozzle and 2 inches downstream of the exit). The two transducer outputs were recorded both with and without jet flow. In the former case, 40 seconds of data was recorded to allow the subsequent processing to separate the acoustic signal from the jet pressure fluctuations.

The systems used to analyze the recordings are shown in Fig. 10. The jet traverse recordings were played through the RMS circuit of the B & K measuring amplifier and then displayed on the oscilloscope together with the marker signal, thus giving a trace of RMS level of static pressure fluctuations vs position traversed along the y-axis. In all other cases, RMS playback levels were monitored on a voltmeter. Spectral distributions of the recorded static pressure fluctuations at various points in the flow were obtained using a General Radio narrow band wave analyzer (Model 1900A) linked to a General Radio (Model 1521-B) graphic level recorder. The signal recovery processing was accomplished by feeding the recorded transducer pick-ups in the field of the acoustic signal generator into one of the channels of a Saicor SAI-42 correlation and probability analyzer operating in the enhance (ensemble averaging) mode. In this mode, 100 values of the incoming signal are sampled (at a predefined increment), digitized and added to 100 memory bins each time a trigger pulse, of prescribed amplitude and duration, is sensed at the EXT SYNC terminal of the analyzer. These external triggers were provided by the pulse generator being itself triggered by the recorded synchronization pulse train. This procedure was followed because the pulse amplitude required by the analyzer is greater than that which can be recorded, and also due to the fact that some distortion occurs to the pulses in the recording/playback process. Thus, the pulse generator served, in a way, to transform the recorded pulse train into one having the required properties. At the end of the processing, the levels in the 100 bins of the analyzer were displayed across the oscilloscope screen and photographed.

An electronic simulation of this signal recovery processing was carried out using the system shown in Fig. 11. A General Radio (Type 1390B) random noise generator served to simulate the jet static pressure fluctuations while the sinusoidal output of the function generator represented the acoustic trace signal. The two were summed and filtered by the PAR 113 operated in its differential amplifier mode. The resulting sum was handled as if it were the amplified output of a transducer in the flow with the exception that recording was bypassed in some of the simulation studies. The meter could be used to monitor the RMS levels of the noise and signal, separately or combined.

III. STATIC PRESSURE FLUCTUATION MEASUREMENTS

A. General Remarks

Prior to dealing with the primary objective of this investigation, which was to develop and implement a procedure for externally injecting and then tracing an acoustic signal through the jet flow, a survey was made of fluctuating static pressure levels in the flow. This survey was useful in two respects. It first of all provided a good idea of the sort of background noise levels which would have to be contended with in recovering the injected signal, and secondly, it furnished some significant data aimed toward a localization of possible noise producing sources in supersonic jets. Although such measurements are common in the literature, as for example in References 10-14,26, it is also common to find these studies employing flows exhausting from nozzles with exit diameters on the order of 1 or 2 inches. Considering the probes ordinarily used, this leads to a ratio of jet diameter to probe diameter in the range 4-10. For the present investigation this ratio is 28, thus substantially decreasing the errors in measurement due to changes in the pressure field induced by the introduction of the probe in the flow. The effects of the probe wing support shown in Fig. 5 should be small due to the limited upstream influence in the supersonic flow regimes of the jet; and was minimized still further by making most of the measurements of this survey using only the upper, more slender probe (housing transducer #1), thus eliminating the bulky structure required to support the lower probe.

The validity of using the B & K ogive nose cones, described in Section II and shown in Fig. 5, to accurately represent the static pressure fluctuations in subsonic and transonic flow has recently been verified (Reference 11) with the use of an intersecting laser technique which does not require any obstructions

to be placed in the flow. It was also found that in supersonic flow there is a complex structure of weak shocks attached to the nose cone which would tend to give extraneously high pressure fluctuation measurements. But of three nose cones tested, the B & K was found to yield the most consistent results. It should be added that any vibration of the probes would tend to aggravate these problems of induced pressure disturbances, although such effects would be primarily confined to relatively low frequencies.

In general, the measured pressure fluctuations at a point $\vec{x}$ in the flow can be separated into several terms:

$$p_{meas}(\vec{x},t) = p(\vec{x},t) + p_{probe}(\vec{x},t) + p_{vib}(\vec{x},t) + p_{elec}(t) \qquad \text{(III-1)}$$

where $p(\vec{x},t)$ is the true jet static pressure fluctuation (i.e., the excursion from the mean static pressure, $P(\vec{x})$); $p_{probe}(\vec{x},t)$ is the pressure disturbance induced by the presence of the probe and support as discussed above; and $p_{vib}(\vec{x},t)$, $p_{elec}(t)$ are pressure equivalents of electrical noise induced by vibration of the transducer and cables, and by the measuring electronics, respectively. By a procedure to be described, the overall RMS level of the third term above was found to be typically about 22 dB below that of the sum of all the terms. The noise floor of transducer #1 and its amplifier was 125 dB (in equivalent pressure level re. 0.0002 μBar), while for transducer #7 it was 122 dB. This put the fourth term at least 35 db below any of the measured levels. Thus, the disturbance created by the presence of the probe, particularly in the supersonic regions of the jet, is likely to be the most significant source of error in the measurements. (An estimate, either experimental or

analytical, of the magnitude of this error is beyond the scope of the present study although some attempts have been made by previous investigators (e.g., References 9 & 11)). All of the above components of the measured pressure fluctuations are assumed to be stationary random functions of time.

It should be noted that error considerations of this kind are not of critical importance for the signal tracing aspects of this investigation. In that case, the measured pressure fluctuations will consist of the injected acoustic signal, as sensed by the transducer, plus a random component attributable to the various sources described in the previous paragraph. The individual contributions to this random noise background are significant only in the sense that they increase the total RMS level thus lowering the effectiveness of the signal recovery processing.

In what follows, the static pressure fluctuation level (SPFL) at a point $\vec{x}$ in the flow is calculated according to the formula,

$$SPFL(\vec{x}) = 20 \log_{10} \frac{p_{rms}(\vec{x})}{p_o} \text{ dB} \qquad \text{(III-2)}$$

where

$$p_{rms}(\vec{x}) = \sqrt{\frac{1}{t'} \int_o^{t'} p^2_{meas}(\vec{x},t)\, dt}$$

and $p_o = 0.0002$ μbar $= 2.9 \times 10^{-9}$ psi.

A distinction is made from ordinary sound pressure level (SPL) since besides acoustic disturbances the static pressure fluctuations in a flow also include aerodynamic disturbances convected along streamlines.

All the static pressure fluctuation (and acoustic signal tracing) measurements for this study were made in the plane $z = 0$ (Fig. 2).

B. Static Presssure Fluctuation Levels in the Overexpanded Jet

A somewhat simplified illustration of the jet flow exhausting from the nozzle with an overexpanded exit static pressure of 10 psia is presented in Fig. 12a. The lengths of the supersonic core and supersonic mixing zone were determined from equations empirically derived by Nagamatsu and Horvay (Reference 27) which express these lengths in terms of the jet Mach number (in this case, $M_j = 1.8$). The position of the sonic line along the jet centerline was approximately verified by a series of pitot and static pressure probe measurements. It was also assumed that the jet spreads initially at a total angle of 12°.

The variation of overall SPFL along the centerline of this jet is shown in Fig. 13. Due to the supersonic exit Mach number, a point on the centerline does not "see" the nozzle lip or any part of the subsequent mixing layer until it is at least about one nozzle diameter (D) downstream of the exit. Consequently, the levels measured at $x/D \leq .5$ give a good indication of the pressure fluctuations existing in the flow, before it exhausts into the atmosphere, due to upstream turbulence created in the valves and settling chamber and to radiation from the nozzle boundary layer. The high levels ($\sim$ 165 dB) obtained in this region are not surprising since

there was no attempt made to quiet the flow entering the nozzle by the use of screens or flow straightners. Such a procedure becomes necessary when the details of the far-field radiated sound due to the jet alone are sought (as is the case, for example, in Reference 6 where upstream disturbances were lowered to negligible levels). Since the jet is overexpanded the supersonic core will contain a cell structure of shocks and expansions which is partially shown in Fig. 12a. Where the conical shocks of this structure converge on the centerline, a small Mach disc is formed, the first of which can be seen in the shadowgraph of Fig. 3. Very marked increases in pressure fluctuation level were found near both of the first two of these discontinuties, that is, at $x/D \cong .5$ and $x/D \cong 2$. The level was also found to vary erratically ($\pm$ 3 dB) during the course of a measurement at each of these positions. Such phenomena could have been the result of some interaction between the weak shocks attached to the probe and the Mach discs, especially when the probe is vibrating, or due to the convection of the high level upstream disturbances through the jet shock structure. If the latter is the more important effect, as is believed to be the case at least for the overall increase in level, these regions could be significant sources of radiated noise. The remaining measurements made along the centerline indicate an increase in level up to a maximum at about 9 diameters downstream of the exit (i.e., the end of the supersonic core), and a fall-off afterwards. Similar results were obtained by Nagamatsu and Sheer (Reference 14) for an $M_j = 1.4$ flow from a 1 inch exit diameter convergent nozzle. Using a specially designed $1/8$ inch probe, they found a peak static pressure fluctuation level on the jet axis also

at the end of the supersonic core (i.e., at approximately 7 diameters). An absolute comparison of levels cannot be made since the results are presented there in terms of RMS voltage outputs of the transducer.

Spectral densities of the static pressure fluctuations at selected points along the jet centerline are presented in Figs. 14-20. The initial distribution ($X/D = 1$, Fig. 14) shows that there is a significant amount of low frequency (50-300 Hz) energy at the outset of the flow. This could be due to both long wavelength disturbances originating in the settling chamber and to low frequency mass flow fluctuations. The pressure fluctuations at this position were analyzed for high frequency content and show that, beyond 30 kHz, complex resonance phenomena begin to occur. The strong peak at 70 kHz, for example, recurs in every spectrum analyzed at this frequency and is thought to be the Helmholtz resonance of the nose cone cavity. A comparison of this first spectral distribution with the one at $X/D = 2$ (Fig. 15) shows an unusual increase in energy at almost all frequencies of between 5 and 10 dB. Recalling that this is the approximate position of the second Mach disc in the flow, it is possible that such a discontinuity serves to locally amplify upstream disturbances. The steeper fall-off in energy above 4 kHz (10 dB/octave as compared to the previous 7 dB/octave) would seem to indicate that this amplification loses its effectiveness at the higher frequencies or perhaps is extremely localized spatially. The two peaks at 1200 and 1700 Hz are unique to this position ($X/D = 2$) among those at which measurements were made.

Except for the spectrum at $^{x}/_{D}$ = 2.6 (Fig. 16) which is basically similar to that at $^{x}/_{D}$ = 2 (other than actually contains less total energy), those remaining along the centerline show a regular increase in energy within the range 50-2000 Hz up to the end of the supersonic core ($^{x}/_{D}$ = 8.6, Fig. 18), and then downward shifts in this same range for the two beyond this point (Figs. 19 & 20). At least two sources are believed to contribute to the growth of energy within this range of frequencies. First there are the disturbances (largely below 300 Hz) originating upstream of the nozzle which seem to be transmitted and reinforced by the shock cell structure of the supersonic core, and second there are the pressure fluctuations on the centerline induced by the jet mixing whose contribution to frequencies below 2000Hz should increase with distance downstream since the length scale of mixing increases. (It is difficult to determine from the spectra whether the shock structure also serves to amplify these mixing induced fluctuations.) The importance of the supersonic core to the first effect can be seen in the one spectral distribution at a considerable distance downstream of the core ($^{x}/_{D}$ = 15.7, Fig. 20). Compared to the distribution near the core tip (Fig. 18) there is a sharp drop, as high as 12 dB at 70 Hz, in the energy of frequencies between 50 and300 Hz, while for frequencies above 500 Hz the drop is less pronounced (3 or 4 dB). This would indicate that the very low frequency disturbances propagating through the core region of the jet cannot be sustained, or are dissipated, once mixing begins to occur. The general subsidence of fluctuations over all frequencies is accounted for by the decreasing mean flow velocity in this now fully turbulent region of the jet.

Above 2000 Hz all the latter spectra show a fall-off of energy at an almost constant rate of 8 or 9 dB/octave with minor shifts in level as the measuring position is varied.

To determine the degree to which spurious electrical noise induced by the vibration sensitivity of the transducer and cables affected these results, a series of measurements were made at $^{X}/D = 2.6$, the spectral analyses of which are shown in Fig. 21. The uppermost curve is the spectral distribution of the static pressure fluctuations measured at this point by the probe fitted with the usual B & K nose cone. Its similarity to one obtained previously at this position (Fig. 16) is an indication of the reproducibility of the results. The two lower distributions are of transducer output signals obtained with the B & K nose cone replaced by one which seals-off the transducer from the jet pressure fluctuations (see Fig. 5). As indicated, some pressure disturbances (particularly at frequencies below 500 Hz) were reaching the transducer until the threads by which this "blind" nose cone was attached to the probe were sealed with a silicone compound. With this accomplished, it could be seen from the lowermost curve that, over a wide range of frequencies, the spectral distribution of the electrical noise induced by vibration was at least 20 dB below that of the static pressure fluctuations at this position. It is possible that, even with the precautions taken, some pressure disturbances were still being transmitted through the "blind" nose cone to the transducer, in which case the estimate above is conservative.

The overall measured levels in the two cases were 144 dB and 166 dB. The conclusions reached here are valid for other measurments in the flow since the general vibration level was not noticed to change appreciably with position.

The spectra of the static pressure flucturations measured within the supersonic core of the overexpanded jet (Figs. 14-17) all contain a strong peak at a freqency which varies between 800 and 900 Hz. It is thought that this is a manifestation of the phenomenon known as supersonic screech, that is, the coupling of some discrete upstream disturbance with the shock structure of the jet through a feedback loop. The spectral density of the radiated sound field at a distance of 10 feet from the nozzle exit and an angle of 45° from the centerline is included as Fig. 22 to lend support to this conclusion. Measured with a separate acoustic microphone and amplifier, the radiated sound clearly shows a screech frequency (or shock tone) at about 800 Hz. The reasons for the variation in the frequency at which the peak occurs were not established.

The variation of overall SPFL with vertical distance from the centerline ($^{Y}/_{D}$), at selected downstream stations, is presented in Figs. 23a-b. The initial profiles show peak fluctuations occuring in the jet mixing region. There are rapid decreases in level outside the flow, while the interior is characterized by regions of constant level around the centerline. The sharp rise in fluctuations near the centerline at $^{X}/_{D} = 2$ has been discussed previously in relation to the flow discontinuity which exists at this position. Here it can be seen that the effect is very local in terms of the transverse direction to the flow. The tendency for the mixing region peaks to first move in toward the centerline and then

to diverge outward is an indication of the initial contraction of the flow streamlines resulting from the overexpanded nozzle exit pressure of 10 psia. Although there is a general trend in these initial profiles for the level to rise for all Y/D as the downstream distance increases, this occurs at an accelerated rate in the core of the jet until at X/D = 8.6 the most intense static pressure fluctuations along the cross-section are found near the centerline. Beyond this point, near the end of the supersonic core, the flow becomes fully turbulent and the jet centerline is also the center of mixing. The last two profiles show more even distributions of level across the flow and a decreasing trend with distance downstream. Considering the increased diameter of the jet (i.e., 3D or more) and the high levels of fluctuating pressure existing over much of the area, this section of the jet, downstream of the core tip, would probably make the largest contribution to the radiated sound field.

A recent investigation (Reference 28) of a small $M_e \cong 2$ jet has included profiles of RMS hot-wire voltage fluctuations in the flow. The similarity in the shape and development of these profiles to those measured here would perhaps call for an examination of the relationship between the two measured properties of the jets.

C. Static Pressure Fluctuation Levels in the Balanced Jet

The changes that occur in the jet flow field when the nozzle exit static pressure is raised from 10 psia to the level of the ambient atmospheric pressure are depicted in Fig. 12b. Besides the disappearance of any finite flow discontinuities in the supersonic regions of the jet, the entire flow structure is elongated in the streamwise

x-direction. Again, the extent of the various regions of flow were determined according to the results of Reference 27. The measurements made in the overexpanded jet were basically repeated for this now shock-free, balanced jet and are presented in Figs. 24 - 33.

The first, that of the variation of overall SPFL along the centerline of the jet (Fig. 24), shows that the initial level of static pressure fluctuations (mainly originating upstream of the nozzle exit) is approximately the same as before (~ 165 dB). Missing, though, are the strong peaks in level near the exit which were previously associated with the shock structure of the overexpanded jet. After a similar increase with distance downstream, a maximum level of about 171 dB is reached between $^{x}/D$ = 9 and 12. Although this again corresponds to the approximate position of the supersonic core tip (i.e., $^{x}/D$ = 10), the maximum level is now 6 dB lower than that obtained, at $^{x}/D$ = 8.6, along the centerline of the overexpanded jet (Fig. 13). Thus even with the 33% lower mass flow, the static pressure fluctuations along the centerline of the overexpanded jet are generally higher than those for the balanced jet. This is directly relatable to the shock structure present in one flow and not in the other. It is interesting to note that at $^{x}/D \cong 15$, where the effects of the shock structure are not as important, the levels in the two jets are about the same (~ 170 dB).

There are some striking differences in the spectra obtained for the two flows. The original low freqency (50-300 Hz) content in the static pressure fluctuations is still present as can be seen in Fig. 25. But now, in the shock-free flow, the energy within this band of frequencies does not grow

appreciably with distance downstream. For example, at 50 Hz there is a 4 dB variation among all the measured positions while, previously, a growth in level of 20 dB occurred, at this frequency, from $^{x}/D = 1$ to $^{x}/D = 8.6$. With this very low frequency effect absent, the contribution of the jet mixing to the static pressure fluctuations on the centerline can be more clearly identified. Before the rapid fall-off in energy at high frequencies, a "shoulder" can be seen to exist in all the spectral distributions. Besides growing in level consistently with each position further downstream, this "shoulder" is centered about a monotonically decreasing frequency for each such position. At $^{x}/D = 1$ (Fig. 25) it is located around 1500 Hz with a level of approximately 120 dB, while at $^{x}/D = 15$ (Fig. 31) its center frequency is more like 350 Hz and its level has almost reached 140 dB. It has already been mentioned that, as the mixing region of the jet increases in size, the pressure disturbances created would reasonably be expected to contain energy at correspondingly decreasing frequencies. The shifting frequency above is a clear demonstration of this effect. The strong peaks between 800 and 900 Hz that appeared in the spectra for the over-expanded jet are also now missing. This is more support for the previous conclusion that the peaks are associated with a shock-related phenomenon (screech). For high frequencies, the spectral distributions behave similarly for the two flows. Except for the first (Fig. 25) which falls-off above 4 kHz at 7 dB/octave, all the distributions in the balanced jet (Figs. 25 - 31) show a decrease in energy above 3 kHz at a constant rate of 8 or 9 dB/octave.

The profiles of overall SPFL at various cross sections of the balanced jet (Figs. 32 & 33) also show significant changes. The first three profiles are basically the same with the only change being that the peaks in level occurring in the mixing layer of the jet are located in line with the nozzle lip since the flow now exits more or less parallel to the centerline. The sharp rise in level at $^{x}/D = 2$ near the centerline, previously associated with the Mach disc present at that position, no longer exists. Although the profiles again show a pattern of increasing levels with distance downstream, the shift of the peak to the centerline does not occur. What is seen instead is a broadening of the peaks as the mixing region grows in size. Even after the flow is believed to have become fully turbulent (i.e., $^{x}/D > 10$), the highest levels of static pressure fluctuations occur at some distance off-center. The remarkable growth of the very low frequency energy along the centerline of the overexpanded jet, which does not take place here, is thought to be responsible for the special significance the centerline has to the profiles in that flow. As the turbulence becomes fully developed and the mean flow velocity drops, the profiles in both flows (i.e., at $^{x}/D \cong 15$) become rather flat and show a trend toward decreasing levels. The broader peaks in the profiles of the balanced jet, combined with its longer flow dimensions, should cause it to have a more intense radiated field than the overexpanded jet, even with the many local areas of very high static pressure fluctuations present in that flow. There is a certain amount of speculation involved in these conclusions concerning the radiated fields of the two jets since a direct relationship

has not been established between the distribution of static pressure fluctuations within a jet flow and its radiated sound field.

Due to the limited number of measurements in this survey of the static pressure fluctuations in the two flows, the results are intended to show only general trends. A detailed investigation of the phenomena observed here would require a more extensive series of measurements.

IV. ACOUSTIC SIGNAL TRACING IN SUPERSONIC JET FLOWS

A. Basis for Signal Recovery Processing

As discussed in the Introduction, an experimental study of the propagation of pressure waves in the interior of a jet flow, with the intention of discerning effects such as refraction of ray trajectory and nonlinear distortion of wave profile, requires a means of measuring certain properties of a trace signal which has become a relatively small component of the pressure fluctuations at a point in the flow. The parameters of interest for such a deterministic signal are its amplitude, relative phase (or time delay), and spectral composition (i.e., signal shape). The variation of signal phase at various sets of nearby points in the flow could be used to yield wavefront orientations, and thus, to trace the path of ray trajectories. Changes of signal shape during propagation would be an obvious indication of nonlinear distortion, while any detected increase in amplitude for a circumferential distribution of signal sources would serve to verify the focussing phenomena theorized in Reference 21 . These last two manifestations are of course related since pressure amplitude is a governing factor in the nonlinear steepening of compression waves. Strictly speaking a single temporal disturbance of reasonable form and duration could yield the information required to investigate these effects, but as a practical matter, the separation or recovery of this trace signal from the high level random pressure fluctuations present in the jet can only be realized if it is periodic.

Leaving the actual physical situation for the moment, the problem can be stated as follows. Given a function of time,

$$F(t) = S(t) + N(t) \ , \qquad \text{(IV-1)}$$

which is the sum of a periodic, deterministic signal (S) with period T, and stationary random noise (N), how does one extract a useful representation of the signal (i.e., determine any of its unknown parameters) if the RMS amplitude of N(t) is much greater than that of S(t)? The problem is, in a general sense, one of filtering, that is, the removal of as much of the obscuring noise as possible from F(t). This procedure could be characterized as a transformation $\mathcal{T}$, such that

$$\bar{F}(t) = \mathcal{T}\left[F(t)\right] = S(t) + n(t) \qquad \text{(IV-2)}$$

where again n(t) is stationary random noise. The effectiveness of such a procedure would be typified by the improvement in signal-to-noise ratio (SNR) from S_{rms}/N_{rms} to S_{rms}/n_{rms}. More generally, instead of the signal S(t) with some noise, the transformation could be such as to yield directly some required property of S(t) with an error, e.g., the amplitude of one of its frequency components.

With this in mind, some of the possible approaches to the problem are frequency filtering, auto and cross correlation, or ensemble averaging. The first method involves filtering out all frequencies in the spectrum of F(t) except those in a narrow band which includes either the fundamental frequency, $f = 1/T$, of the signal or any of its harmonics. If the spectrum of N(t) is spread over a sufficiently wide range of frequencies, this filtering would considerably increase the signal-to-noise ratio thus allowing a more accurate measurement of the amplitudes of the spectral components of S(t). Although this

method could thus be used to obtain an approximate signal shape and amplitude, it does not yield any phase information. The theory of filtering, as well as certain aspects of correlation techniques, are dealt with thoroughly in Reference 29 for application to problems in radio engineering. Of course, a very large literature exists in the field.

The use of correlation methods is practical when S(t) is a sinusoidal signal $A\cos 2\pi ft$. By calculating the average auto-correlation of the function F(t)

$$R_{FF}(\tau) = \frac{1}{t'} \int_o^{t'} F(t)\ F(t-\tau)\ dt \qquad \text{(IV-3)}$$

for t', $\tau \to \infty$; or the average cross-correlation of F(t) with some reference signal, $S'(t) = A' \cos(2\pi ft + \varphi)$,

$$R_{FS'}(\tau) = \frac{1}{t'} \int_o^{t'} F(t)\ S'(t-\tau)\ dt \qquad \text{(IV-4)}$$

for $t' \to \infty$, it is shown in Reference 22 that

$$R_{FF}(\tau) \to \frac{1}{2} A^2 \cos 2\pi f\tau \qquad \text{(IV-5)}$$

and

$$R_{FS'}(\tau) \to \frac{1}{2} AA' \cos(2\pi f\tau + \varphi) \qquad \text{(IV-6)}$$

where φ is a relative phase. These results are obtained under the condition that the noise, N(t), has a zero mean and is uncorrelated with the signals S(t) and S'(t). In most circumstances, these conditions are readily satisfied. Thus the

auto-correlation procedure leads to an estimate of the sinusoidal signal amplitude A, while cross-correlation yields both A and the phase, φ, of the unknown signal relative to some chosen reference. The shortcomings are that, besides not providing any phase information, the auto-correlation processing requires a long delay time τ, and that both techniques are not readily applicable to periodic signals of arbitrary harmonic composition. For an initial signal-to-noise ratio of -20 db, Smith andLambert (Reference 22) using a 1000 Hz signal and an analog correlator obtained improvements in SNR of 20 db for auto-correlation and 40 db for cross-correlation. Typical improvements using frequency filtering are on the order of 30 db. Ensemble averaging, as it is applied in this investigation, involves the sampling of one-hundred equally spaced values of the function F(t) a certain number of times, K. The resulting sequence of values,

$$F_i^{(k)} = F(t_k + i\Delta t) \quad \begin{matrix} i = 0, 1, \ldots, 99 \\ k = 1,2,\ldots K \end{matrix} \qquad \text{(IV-7)}$$

is summed according to

$$\bar{F}_i = \sum_{k=1}^{K} F_i^{(k)} = \sum_{k=1}^{K} S_i^{(k)} + \sum_{k=1}^{K} N_i^{(k)} \quad i=0,1,\ldots 99 \qquad \text{(IV-8)}$$

In the above, Δt is the sample increment and t_k is the time when sampling of the k-th set of 100 values of F(t) is begun. The success of this method depends on choosing the t_k's such that they are synchronous with the periodicity, T, of the signal S(t), that is,

$$t_k = t_d + (k-1)T \quad k=1,2,\ldots,K \qquad \text{(IV-9)}$$

where t_d is a relative time delay which can be related to a phase, φ, by $\varphi = 2\pi\, t_d/T$. Since the sampling of F(t) is continuous, it is assumed that the time to sample each 100 values, 100 Δt, is less than one period, T, which is the separation between each t_k. (If this is not the case, a factor must be introduced into Eq. IV-9 making the separation between the t_k's a certain multiple of the period depending on the duration 100 Δt). In this way, it can be seen that the sequence of sampled values $S_i^{(k)} = S(t_k + i\Delta t)$ will be independent of k since, for a given i, $S(t_k + i\Delta t) = S(t_d + i\Delta t)$ for all k. It follows that,

$$\bar{F}_i = KS_i + \sum_{k=1}^{K} N_i^{(k)} \qquad i = 0,1,\ldots,99 \qquad \text{(IV-10)}$$

where S_i is now a 100 point representation of a cycle of S(t). This can either be a small portion of the cycle or an almost complete cycle depending on Δt. Assuming that N(t) is stationary random noise, uncorrelated with S(t), and with zero mean, the second term in Eq. (IV-10) will grow in amplitide as a function of K at a rate which will depend on the degree of correlation between $N_i^{(k_1)}$ and $N_i^{(k_2)}$ where $k_1 \neq k_2$. In the case of coherence (as was arranged between the $S_i^{(k's)}$) the sum grows linearly with K, while for incoherence it grows like $\sqrt{K}$. This can be seen by forming,

$$\left[\sum_{k=1}^{K} N_i^{(k)}\right]^2 = \sum_{k=1}^{K} N_i^{(k)} \times \sum_{\ell=1}^{K} N_i^{(\ell)}$$

$$= \sum_{k=1}^{K} \left[N_i^{(k)}\right]^2 + \sum_{\substack{k,\ell=1 \\ k\neq\ell}}^{K} N_i^{(k)}\, N_i^{(\ell)}$$

The sum of the cross-terms tends to zero for large K if $N_i^{(k)}$

and $N_i^{(\ell)}$ are incoherent. Therefore,

$$\sum_{k=1}^{K} N_i^{(k)} \longrightarrow \pm \sqrt{\sum_{k=1}^{K} \left[N_i^{(k)} \right]^2}$$

$$= \pm \sqrt{K} \sqrt{\frac{1}{K} \sum_{k=1}^{K} \left[N_i^{(k)} \right]^2}$$

or

$$\sum_{k=1}^{K} N_i^{(k)} \longrightarrow \pm \sqrt{K}\, N_{rms} \qquad \text{(IV-11)}$$

(N_{rms} does not depend on i since N(t) is stationary).
Thus in the case of a signal buried in incoherent noise this method of recovery yields the signal amplitude $\left(\sqrt{\frac{1}{100} \sum_{i=0}^{99} S_i^2}\right)$, relative phase ($\varphi$), and shape ($S_i$) with an improvement in signal-to-noise ratio of,,

$$\frac{KS_{rms}/\sqrt{K}N_{rms}}{S_{rms}/N_{rms}} = \sqrt{K} \qquad \text{(IV-12)}$$

or of

$$20 \log_{10} \sqrt{K} = 10 \log_{10} K \text{ db} .$$

When S(t) is a sinusoid, it would be possible to increase the effectiveness of this technique by combining it with the frequency filtering discussed earlier. That is , by first filtering the spectrum of F(t) outside a band which includes the frequency of the signal, the <u>total</u> SNR improvement after subsequent ensemble averaging would be significantly higher

than that obtained by the use of this method alone. In the general case, however, of a signal with harmonic components, the relative phase shifts induced between the components by electronic filters would make the results unacceptable for subsequent ensemble averaging. The wider filter bandwidth required to pass all the harmonics would also diminish the advantages of filtering. For these reasons, the use of filtering in conjunction with ensemble averaging was not considered further in this investigation.

B. Electronic Simulation Results

To investigate the parameters involved in the procedure just described and to calibrate the physical system to be used, a simulation was made with the set-up shown in Fig. 11. The random noise, N(t) was simulated first by electronically generated "pink" noise, and then separately by "white" noise filtered outside the range 1000-3000 Hz. The signal, S(t), provided by the function generator was a sinusoid with a period $T = 180\ \mu sec$ ($f \cong 5500$ Hz). The signal and noise were summed by the differential amplifier and then fed into the digital analyzer operating as an ensemble averager. Under these controlled conditions, it was possible to measure and vary the input signal-to-noise ratio. The sample increment, Δt, used in all cases was 2 μsec. Initiation of sampling at the times $t_k = t_d + 2(k-1)T$ $(k = 1,2,\ldots,K)$ was accomplished by a sequence of pulses, synchronized with the sinusoidal output of the function generator, acting as triggers for the analyzer. The factor of 2 in the expression for t_k is to take into account the fact

that the sampling of each 100 points took 200 μsec, thus requiring that the separation between successive t_k's be two periods, 2T. That is, slightly more than one cycle of the signal was sampled for each k and only every other pulse could be used to trigger the analyzer. The delay time $t_d = 0$ since no delay developed in the signal between the output of the function generator and the input to the analyzer.

Given the final 100 point representation of the signal at the output of the analyzer, S_i, i = 0, ... , 99, its RMS amplitude would be calculated in the most general case according to $S_{rms} = \sqrt{\frac{1}{100} \sum_{i=0}^{99} S_i^2}$. Since the signal here is a sinusoid, a more convenient measurement of peak-to-peak amplitude, S_{p-p}, was used to determine S_{rms} : $S_{rms} = S_{p-p}/2\sqrt{2}$. (No attempt was made to measure noise levels at the conclusion of processing). The parameters affecting the final signal amplitude are the total number of summations K, the input attentuation (IA) of the analyzer, and whether the processing is done in the full or clip mode. In the full mode there is a proportional relationship between the analog voltage S(t) + N(t), being sampled and the digitized data stored and then summed, whereas the clip mode operates such that <u>any</u> sampled positive voltage is digitized as a + 1 while any negative voltage becomes a-1. It is only in this clip mode that the maximum $\sqrt{K}$ improvement in signal-to-noise ratio discussed previously can be obtained. The reason for this is that different samples of a physical random process (e.g., the pressure fluctuations at a point in a jet) are usually not incoherent, that is, some degree of correlation will

exist between the process at a time t and t + τ. Using the full mode, any such correlation present in N(t) would cause the summation in Eq. IV-10 to grow at a rate faster than $\sqrt{K}$,

$$\sum_{k=1}^{K} N_i^{(k)} \longrightarrow \pm K^m N_{rms} \qquad \text{(IV-13)}$$

where, $\frac{1}{2} < m < 1$, depending on the degree of correlation. The improvement in signal-to-noise ratio after K summations would suffer accordingly:

$$\frac{KS_{rms}/K^m N_{rms}}{S_{rms}/N_{rms}} = K^{1-m} \qquad \text{(IV-14)}$$

The special processing involved in the clip mode tends to nullify any existing correlation, in which case Eqs. IV-11 &12 remain valid. Implicit in the use of this mode, however, is the condition that the input signal-to-noise ratio be somewhat smaller than 1. In the limiting case of N(t) ≡ 0, it can be seen that this mode will take an input sinusoid and process it into a square wave. Such distortion does not occur if the input has a significant random component. All this leads to the conclusion that, in the case of signal recovery from a background of high level random noise, clip is the reasonable mode of operation, while the full mode is useful for "cleaning" slightly noisy signals or for displaying clean signals in a format comparable to other processed data.

Calibration curves for these two modes of operation are shown in Figs. 34 - 36. The signal amplitude at the conclusion of processing in the full mode (Output S_{rms}) can be seen from Fig. 34 to be directly proportional to the signal amplitude being processed (Input S_{rms}) and the number of summations (K), while inversely proportional to the input attenuation (IA). The situation in the clip mode is quite different (Fig. 35). Although still depending directly on the number of summations, the output signal amplutide now varies in direct proportion to the signal-to-ratio of the data being processed (Input S_{rms}/N_{rms}), that is, it is inversely proportional to the RMS amplitude of the noise from which this output signal is recovered. For large signal-to-noise ratios, this linear relationship breaks down and it can be seen that there is a limit to the output signal amplitude which can be obtained for a given number of summations. As indicated by the arrow, for $\frac{S_{rms}}{N_{rms}} > .8$, the distortion discussed in the previous paragraph begins to occur to the output signal. On the other hand, there is a limit (for a given K) on how low a SNR can be processed to yield a signal free enough of noise to be reasonably identified. This subjective limit is indicated on the two curves of Fig. 35 by vertical lines. The limit is lowered by a factor of two (from $\frac{S_{rms}}{N_{rms}} = .003$ to .0015) when the number of summations is increased from 128 x 1024 to 512 x 1024. This verifies the previous conclusion that, in this mode of operation, the maximum possible improvement in SNR should double if the number of summations is quadrupled.

Fig. 35 also shows that the spectral content of the noise, or whether the processing is performed on recorded data, has no effect on the results. The curve in Fig. 36 indicates that the output signal amplitude in the clip mode is independent of the input attenuation setting of the analyzer if it is chosen within a proper range.

A sequence of output signals obtained from the clip mode simulation processing are shown in Fig. 37. The variation of signal amplitude and definition (i.e., final SNR) with input signal-to-noise ratio is clearly demonstrated. That limit of reasonable definition mentioned above can be seen to be somewhere between the fifth and sixth trace.

In the physical problem under consideration, the random noise, $N(t)$, to be dealt with (at some point $\vec{x}$ in the jet flow) is the $p_{meas}(\vec{x},t)$ discussed and surveyed in Section III. These high level random pressure fluctuations act to critically obscure the presence of a periodic acoustic signal $S(\vec{x},t)$ at that point, whose source is an electro-acoustically generated sinusoidal disturbance at the edge of the flow. To make use of the results obtained in the electronic simulation just described, it must be assumed that the jet pressure fluctuations and the acoustic trace signal at each point $\vec{x}$ combine in an additive manner, that is, such that the transducer senses $S(\vec{x},t) + p_{meas}(\vec{x},t)$. Also required is that $p_{meas}(\vec{x},t)$ be stationary, have zero mean, and be fully uncorrelated with $S(\vec{x},t)$. Under these conditions, the transducer output voltage can be recorded, along with a pulse train synchronized with the signal source disturbance, and processed using the clip mode,

ensemble averaging technique to recover a useful representation of the unknown signal, $S(\vec{x},t)$. The success of this processing has been seen to depend on the initial signal-to-noise ratio, $S_{rms}(\vec{x})/p_{rms}(\vec{x})$, and the number of summations performed, K. The definition of the final signal representation could thus be improved by increasing the amplitude of the signal source, or by decreasing the level of jet pressure fluctuations. The only reasonable way to accomplish the latter is by lowering the level of disturbances originating upstream of the nozzle. The maximum number of summations possible in the processing is equal to the number of cycles of the signal that are recorded, i.e.,

$$K_{max} = fT_R \qquad \text{(IV-15)}$$

where f is the signal frequency and T_R is the total duration of each measurement in the flow. The choice of frequency is restricted by the response limits of the signal generator and, more importantly, by any physical requirements of the propagation study. The running time of the jet flow is determined solely by the available air supply.

In the experimental application chosen for this study, an attempt was made to achieve values of these parameters, within the limits of the facilities available, which would optimize the signal recovery processing. Thus, a relatively high acoustic signal frequency of 5500 Hz ($T \cong 180$ μsec) was used along with a total running time for each measurement in the flow of 40 seconds. This allowed for $K_{max} = 220{,}000$ possible summations, and a corresponding maximum possible improvement in signal-to-noise ratio of approximately 53 db.

The output amplitude of the signal generator was also made as high as possible (~ 150 dB at the center of the horn exit plane). As stated previously, no attempt was made to decrease the level of jet pressure fluctuations by quieting the flow upstream of the nozzle.

Once a measurement in the flow was processed, the signal amplitude at the output of the analyzer was used, in conjunction with the results of Fig. 35, to obtain the signal-to-noise ratio $S_{rms}(\vec{x})/p_{rms}(\vec{x})$. The acoustic signal amplitude at the point $\vec{x}$ in the flow, $S_{rms}(\vec{x})$, was then determined by multiplication of this ratio by $p_{rms}(\vec{x})$ as measured during processing (i.e., since the signal level in all cases was very small it could be assumed that $p_{rms}(\vec{x}) \equiv \left[p_{meas}(\vec{x},t)\right]_{rms} \cong \left[S(\vec{x},t) + p_{meas}(\vec{x},t)\right]_{rms}$). Differences in phase between signals at nearby positions in the flow or the development of non-linear distortion in the signal could be estimated directly from the analyzer output representation. It should be noted that due to unsteadiness in the flow, the final signal properties represent an average over 40 seconds.

As a reference, a recording of the acoustic signal at each point $\vec{x}$ in still air (i.e., without the jet flow) was also processed. Since a strong noise background does not exist in this case, the processing was done in the full mode of operation.

C. Results of Signal Recovery within the Two Jets

With the source area (the 3 inch diameter exit of the catenoidal horn) located 4 inches below the centerline and 2 inches downstream of the nozzle exit as shown in Fig. 9, an attempt was made to trace its sinusoidal acoustic disturbance through the two jet flows described in Section III.

This consisted of an attempt to observe, through signal recovery processing, the acoustic signal present at several positions along the centerline of the jets ($Y/D = 0$) and along a parallel line 1.5 inches below ($Y/D = -.2$), for downstream distances ranging only as far as 19 inches ($X/D = 2.7$). Due to the high levels of background pressure fluctuations and the limited initial signal strength, successful recovery was restricted to this initial section of the jets.

Signal traces resulting from the processing of measurements at these positions in the balanced jet are presented in Fig.38-43. (The spikes which appear on some of the traces just to the left of center are due to an effect in the electronics and should be ignored.) At each position (identified according to the labels assigned in Fig. 44), two traces are shown; the upper is of the acoustic signal as it exists at that point in still air, while the lower shows, when the recovery processing succeeds, the signal arriving at that point in the presence of the supersonic flow. Due to the sample increment used in the processing ($\Delta t = 2$ μsec), each of these 100 point traces is of 200 μsec of the signal, that is, of slightly more than one cycle. Next to each trace is an indication of the sound pressure level of the signal it represents. The variation of signal level in still air and within the flow is summarized in Fig. 44.

The acoustic signal field in still air can be seen to be very complex. There is a significant amount of distortion occurring to the original sinusoidal disturbance as it propagates both directly and after reflection from nearby surfaces to each measuring position. The distortion itself can be related to the high level of the initial disturbance, while the spatial

complexity of the field is due to the high frequency of the signal and the proximity of the signal generator to a number of scattering bodies (Fig. 9). One consequence of the high frequency, and the resulting wavelength in still air of about 2.5 inches, is that signals originating from opposite edges of the source disturbance arrive at some positions with significant phase shifts. The variation of signal level (Fig. 44) shows that, in the vicinity of the generator where measurements were made, the acoustic field is very directional with most of the energy concentrated close to the axis of the horn.

Appreciable changes occur to the field in the presence of the balanced supersonic flow. Although a strong directionality pattern still exists (Fig. 45), it is now centered about a ray making an angle of approximately 60° with the axis of the horn. Since the Mach angle in the flow is 30° ($M = 2$), this is a demonstration that, once the initial disturbance crosses the thin mixing layer present in this early stage of the jet, its region of influence is determined (due to the supersonic convection) by the characteristic lines in the flow (two of which are shown). As a result, little if any of the disturbance would be able to reach points upstream of the characteristic which emanates from the nozzle lip. This is clearly the case since no signal is recovered at the first four positions along the centerline and the first two along $y/D = -.2$ (Figs. 38-39). (When the processing does not yield anything which can be reasonably identified as a signal, an estimate is made of the minimum signal level which could have been recovered from the known noise level at each point. This estimate is indicated in Fig. 44 by horizontal dashes. The signal level at these positions is then somewhere below this mark.) The maximum signal levels attained within the flow are lower than those in still air possibly due to the

fact that not all of the source energy is transmitted across the flow boundary, that is, some is reflected back toward the source. A series of measurements along both sides of the flow boundary would be required to investigate the mechanisms involved in the transmission of the disturbance through the shear layer at the boundary. As would be expected, the peak level along $y/D = -.2$ is slightly higher than that along the centerline in still air, but within the flow the reverse is true. This is perhaps an indication of a focussing phenomenon which could be enhanced and explored further using a circumferential distribution of source disturbances around the periphery of the jet. An attempt was made to determine whether the signal level downstream of $x/D = 2.7$ along the centerline increased due to an interior reflection of the disturbance from the opposite edge of the flow (i.e., at $y/D \cong +.5$). Although there were some signs of such an effect, the signals recovered in this region were generally too weak to allow a definite conclusion to be reached.

The traces obtained in the presence of the flow, particularly where the signal levels are high (Figs. 40 - 41), clearly show that the source disturbance remains sinusoidal as it propagates through the jet. The complex pattern of distortion occurring to the signal profiles in still air does not exist in the flow, at least as far as can be seen from the "cleanly" recovered signals. This could be due to the lowering of the initial disturbance level by the reflection at the flow boundary combined with the absence of any scattered fields within the flow. On the other hand, this effect together with the absence of significant phase differences between signals arriving at various points within the flow (i.e., 6a, 6b, 7a, 7b), might involve phenomena requiring further investigation.

The measurements at two positions in the flow (6a and 5b) were repeated and are presented as 6a′ and 5b′ in Fig. 45. Except for slight differences in the still air signals (due to errors in positioning the probe in the spatially intricate field), the results show the basic reproducibility of the measurements and subsequent processing.

In Figs. 46 - 52 are presented the results of a sequence of measurements tracing the acoustic signal within the over-expanded jet (P_e = 10 psia). Other than the absence of data for positions 8a and 8b, they consist of the same set of measurements made in the balanced jet. The interpretation of the results here, however, is more difficult for two reasons. The region of the jet through which the signal is being traced is no longer one of constant mean flow velocity, but rather consists of the previously described shock-cell structure. Furthermore, at the time these measurements in the over-expanded jet were made, the signal being recovered at each point in the flow was the sum of the usual acoustic signal plus a non-pressure (electrical) signal being induced (electromagnetically) in the recording instrumentation by the signal generating system. The two main sources of this spurious signal were found to be the proximity of the loud-speaker power amplifier to the transducer amplifiers and the existence of a section of unshielded cable leading to the loudspeaker. The signals recovered at the first few positions in the flow (Fig. 46) were primrily due to these sources since the points are outside the zone of influence of the acoustic source. This conclusion was verified by repeating the measure-ments at two of these positions (1a and 1b) using the "blind" nose cone shown in Fig. 5 to seal-off the transducer from any acoustic signal. The signal levels obtained from processing

these measurements were only slightly lower than those obtained with the transducer capable of sensing pressure fluctuations, thus indicating that some acoustic signal can perhaps reach these positions by upstream propagation through the subsonic mixing and boundary layers in the flow. The actual error caused by the electrical signal would depend on the phase it has relative to the acoustic signal at each point. (The sources of the electrical signal were largely eliminated prior to making measurements in the balanced flow.)

The signal traces obtained within the overexpanded jet, as well as the variation of signal level shown in Fig. 52, must therefore be interpreted with some caution. However, several of the basic phenomena observed for the signal in the balanced jet can still be seen to occur here. The signal traces recovered with some clarity (Figs. 47 and 48) again show that the disturbance remains sinusoidal as it now propagates through the various flow regions comprising the initial cell structure of the overexpanded jet. There is also, as before, an absence of large differences in phase between many of the signals within the flow. Although the acoustic signal field is again convected downstream (Fig. 52), the shift is significantly less than it was in the balanced flow. There are two possible reasons for this. The most obvious is that the Mach number at which the field is convected drops from $M = 2$ to $M \cong 1.6$ across the first shock in the flow shown in Fig. 52. Less obvious is the fact that, due to this shock, the initial flow streamlines will be deflected toward the centerline of the jet causing the flow boundary to move away from the signal source disturbance. Since the convection would then begin closer to the lines along which measurements were made, it is reasonable that the convected distances are less. These two effects can be pictured more

clearly in terms of the characteristics in the flow. The first can be seen as an increase in the angle of the characteristic lines with respect to the flow direction, and the second as an upward (vertical) shift of the points from which the characteristics emanate.

The failure to recover a signal at positions 3a and 10a (Figs. 47 & 50) in the overexpanded jet was due to the unusually high level of jet pressure fluctuations resulting from the presence, near these positions, of the first two Mach discs in the flow.

Due to the restriction placed on the possible number of measurements by the large high-pressure air supplies required and the problems encountered in developing the signal tracing systems and procedures, a more complete mapping of the signal field within the jets could not be achieved. Any continuing investigation could in addition include a study of the signal transmitted through the jet into the sorrounding still air. The axisymmetry of the jets suggests that a circumferential distribution of sources (with various relative phases) at the periphery of the flow would be more appropriate for the further study of acoustic signal propagation within the flow. Useful information concerning the propagation of disturbances through the shock structure of overexpanded jets could be obtained by tracing the acoustic signal from a source located on the centerline upstream of the nozzle.

V. CONCLUSIONS

Two cold supersonic jet flows have been investigated, both exhausting from a 7 inch exit diameter convergent-divergent nozzle. One was a perfectly expanded (shock-free) flow with a jet Mach number $M_j = 2$, and the other an overexpanded flow with $M_j = 1.8$. Measurements of the static pressure fluctuations within the two flows have indicated the existence of several interesting phenomena. The maximum level of static pressure fluctuations along the centerline of both jets was found to be near the end of their respective supersonic cores. However, even with the lower mass flow, the levels along the centerline of the overexpanded jet were generally higher than those for the balanced jet. This was particularly the case in the area of the Mach discs in the former flow where appreciable increases in level were detected. The spectral composition of these static pressure fluctuations tended to show that the higher levels along the centerline of the overexpanded jet could be related to the shock-cell structure present in that flow. Starting near the exit of the nozzle with a level and spectral distribution of upstream disturbances that was similar in both flows, the static pressure fluctuations in the balanced jet increased with distance downstream due to the addition of energy which could be traced to disturbances originating in the mixing layer, while in addition to this effect, the fluctuations in the overexpanded jet included an amplification of disturbances propagating through the cell structure. This was particularly evident for the low frequency disturbances originating upstream of the nozzle (e.g., due to mass flow fluctuations and the large size of the settling chamber). Since this was the only probable source of disturbances with frequencies on the order of 100 Hz, the growth in energy of the

static pressure fluctuations at these frequencies along the centerline of the overexpanded jet could best be accounted for in terms of the intensification of these disturbances by the shock structure in the core of this jet. Downstream of this structure (i.e., where the jet becomes fully turbulent), the level and spectrum of the fluctuations were again similar to those in the balanced flow. Another shock-related phenomenon (screech) was believed to be the cause of a strong peak in fluctuations between 800 and 900 Hz within the overexpanded jet.

The similarity between the two jets near the exit of the nozzle and then after the flows become fully turbulent was also evident in the profiles of the variation of static pressure fluctuation level with radial distance from the centerline. In the initial flows, these profiles showed a peak level occurring in the mixing layer, and a lower, more constant level about the centerline. Far downstream, the profiles in both jets indicated a more uniform distribution of level across the fully turbulent flows. In between these regions, one significant difference could be seen in the profiles for the two flows. While the peaks in the mixing layer broadened as the scale of mixing grew in the balanced jet, a shift in the peak level to the centerline occurred in the overexpanded jet. The intensification of disturbances in the core of this jet was believed to be responsible for the shift.

The tracing of an acoustic signal through the jets required the development of two systems; one for externally injecting and then detecting the signal within the flow, and another that would allow for observation of the signal amidst the random pressure fluctuations of the flow. An electro-acoustic signal generator was chosen because of its relatively high output over a wide frequency range, the control it allows

over signal shape, and the ease with which it permits synchronization of the signal for subsequent processing. Size and high frequency response were the basic criteria used in selecting the transducers for sensing the signal (and jet pressure fluctuations), although obvious consideration had to be given to the requirement that the high levels of mean and fluctuating jet pressure were within the operating range of the transducers. If not for this requirement, transducers with higher sensitivities could have been chosen.

A survey of the possible procedures available for recovering or separating a periodic signal from a high level random noise background led to the conclusion that ensemble averaging is capable of yielding the most information about the signal (i.e., amplitude, relative phase, and spectral composition). An electronic simulation study of the processing involved in this procedure was made to determine how various parameters affected the outcome and to calibrate the instrumentation being used. The clarity with which the signal is recovered by the processing was found to depend on the square-root of the number of cycles of the signal available for processing. Obviously, it would also directly depend on the initial signal-to-noise ratio of the data being processed. But since the output level of the signal generator was limited and the level of jet pressure fluctuations (noise) could not be easily lowered, an attempt was made to maximize the effectiveness of the processing by increasing the number of cycles of the signal sensed during a measurement in the flow, that is, by choosing a high signal frequency (5500 Hz) and running the flow for as long as possible (40 seconds). This combination permitted a maximum possible improvement in signal-to-noise ratio of about 53 db.

Even with this high degree of improvement in signal definition, the successful application of these procedures to the recovery of the acoustic signal within the jet flows was restricted to a limited region of each flow. The data that was acquired did suggest the existence of several effects. It clearly demonstrated the supersonic convection of the acoustic field and the resulting limited upstream influence of the signal source. Also indicated was a possible increase of signal strength as it propagated toward the centerline of the flow. Missing in the signal traces recovered within the flows, however, was the development of any distortion in the initial sinusoidal profile. Since this was seen to occur for the acoustic field in still air, it would be of interest to investigate why it doesn't within the flows. This would apply as well to the absence of appreciable phase differences between signals arriving at various points in each of the flows. In general, both an analytical and experimental extension of this investigation is required to fully explore the many observed phenomena.

REFERENCES

1. Dosanjh, D.S., Bassiouni, M.R., Bhutiani, P.K., and Ahuja, K.K., "Potential of Coaxial Multinozzle Configurations for Reduction of Noise from High Velocity Jets," Proceedings of the Interagency Symposium on University Research in Transportation Noise, Raleigh, North Carolina, Vol. 1, pp. 162-177, June 1974.
2. Nagamatsu, H.T., Sheer, R.E., Jr., and Gill, M.S., "Characteristics of Multitube Multishroud Supersonic Jet Noise Suppressor," AIAA Journal, Vol. 10, No. 3, pp. 307-313, 1972.
3. Mangiarotty, R.A., and Cuadra, D.E., "Acoustic and Thrust Characteristics of the Subsonic Jet Efflux from Model Scale Sound Suppressors - Part 1, Unheated Jets," Boeing Report No. 06-15071, 1968.
4. Richards, E.J., and Mead, D.J., Noise and Acoustic Fatigue in Aeronautics, John Wiley & Sons Inc., London, 1968.
5. Eldred, K.M., et al., "Far Field Noise Generation by Coaxial Flow Jet Exhausts, Volume 1 - Detailed Discussion," FAA Report No. RD-71-101,1, November 1971.
6. Mollo-Christensen, E., Kolpin, M.A., and Martucelli, J.R., "Experiments on Jet Flows and Jet Noise Far-Field Spectra and Directivity Patterns," J. Fluid Mech., Vol. 18, No.2, pp. 285-301, 1964.

7. Laufer, J., Chu, W.T., Schlinker, R.H., and Kaplan, R.E., "Supersonic Jet Noise Investigations," Proc. Inter. Symp. Univ. Res. Transp. Noise, Raleigh, N.C., Vol. 1, pp. 59-73, June 1974.

8. Lee, H.K., and Ribner, H.S., "Direct Correlation of Noise and Flow of a Jet," J. Acoust. Soc. Amer., Vol. 52, No.5, pp.1280-1290, 1972.

9. Siddon, T.E., "Some Observations on Source Detection Methods with Application to Jet Noise," Proc. Inter. Symp. Univ. Res. Transp. Noise, Raleigh, N.C., Vol. 1, pp. 74-89, June 1974.

10. Scharton, T.D., and White, P.H., "Simple Pressure Source Model of Jet Noise," J. Acoust. Soc. Amer., Vol. 52, No. 1, pp. 399-412, 1972.

11. Scharton, T.D., White, P.H., Rentz, P.E., et al., "Supersonic Jet Noise Investigations Using Jet Fluctuating Pressure Probes," Air Force Aero Propulsion Laboratory Report No. TR-73-35, June 1973.

12. Nagamatsu, H.T., Sheer, R.E., Jr., and Gill, M.S., "Flow and Acoustic Characteristics of Subsonic and Supersonic Jets from a Convergent Nozzle," General Electric Research and Development Center Report No. 69-C-310, September, 1969.

13. Nagamatsu, H.T., Sheer, R.E., Jr., and Bigelow, E.C., "Mean and Fluctuating Velocity Contours and Acoustic Characteristics of Subsonic and Supersonic Jets," AIAA Paper No. 72-157, January 1972.

14. Nagamatsu, H.T., and Sheer, R.E., Jr., "Subsonic and Supersonic Jets and Supersonic Suppressor Characteristics," AIAA Paper No. 73-999, October 1973.

15. Chih-ming, H., and Kovasznay, L.S.G., "Acoustic Wave Propagation Through a Two-Dimensional Turbulent Jet," Proc. Inter. Symp. Univ. Res. Transp. Noise, Stanford, California, Vol. 1, pp.3-17, March 1973.

16. Slutsky, S., and Tamagno, J., "Sound Field Distribution about a Jet," General Applied Science Laboratories Technical Report No. 259, December 1961.

17. Gottlieb, P., "Sound Source Near a Velocity Discontinuity," J. Acoust. Soc. Amer., Vol. 32, pp. 1117-1122, September 1960.

18. Slutsky, S., "Acoustic Field of a Cylindrical Jet Due to a Distribution of Random Sources or Quadrapoles," General Applied Science Laboratories Technical Report No. 281, February 1962.

19. Liu, C.H., and Maestrello, L., "Propagation of Sound Through a Real Jet Flowfield," AIAA Paper No. 74-5, January 1974.

20. Kelsall, T., "Suppression of Refraction in Jet Noise," Proc. Inter. Symp. Univ. Res. Transp. Noise, Raleigh, N.C., Vol. 1, pp. 2-6, June 1974.

21. Ferri, A., Ting, L., and Werner, J., "Supersonic Jet Engine Noise Analysis," Proc. Inter. Symp. Univ. Res. Transp. Noise, Stanford, Ca., Vol. 1, pp. 39-54, March 1973.

22. Smith, M.W., and Lambert, R.F., "Acoustical Signal Detection in Turbulent Airflows," J. Acoust. Soc. Amer., Vol. 32, No. 7, pp. 858-866, 1960.

23. Ferri, A., Slutsky, S., and Panunzio, S., "Fluid Dynamic Aspects of Jet Noise Generation," Proc. Inter. Symp. Univ. Res. Transp. Noise, Stanford, Ca., Vol. 1, pp.55-63, March 1973.

24. Slutsky, S., Panunzio, S., and Barra, V., "Fluid Dynamic Aspects of Jet Noise Generation," Proc. Inter. Symp. Univ. Res. Transp. Noise, Raleigh, N.C., Vol. 1, pp. 178-183, June 1974.

25. Bruel & Kjaer Instruments Inc., "Product Manual," Copenhagen, Denmark, February 1967.

26. Benzakein, M.J., and Knott, P.R., "Supersonic Jet Exhaust Noise," Air Force Aero Propulsion Laboratory Report No. TR-72-52, August 1972.

27. Nagamatsu, H.T., and Horvay, G., "Supersonic Jet Noise," AIAA Paper No. 70-237, January 1970.

28. McLaughlin, D.K., Morrison, G.L., and Troutt, T.R., "Experiments on the Instability Waves in a Supersonic Jet and Their Acoustic Radiation," Proc. Inter. Symp. Univ. Res. Transp. Noise, Raleigh, N.C., Vol. 1, pp. 113-127, June 1974.

29. Wainstein, L.A., and Zubakov, V.D., Extraction of Signals from Noise, Dover Publications Inc., New York, 1962.

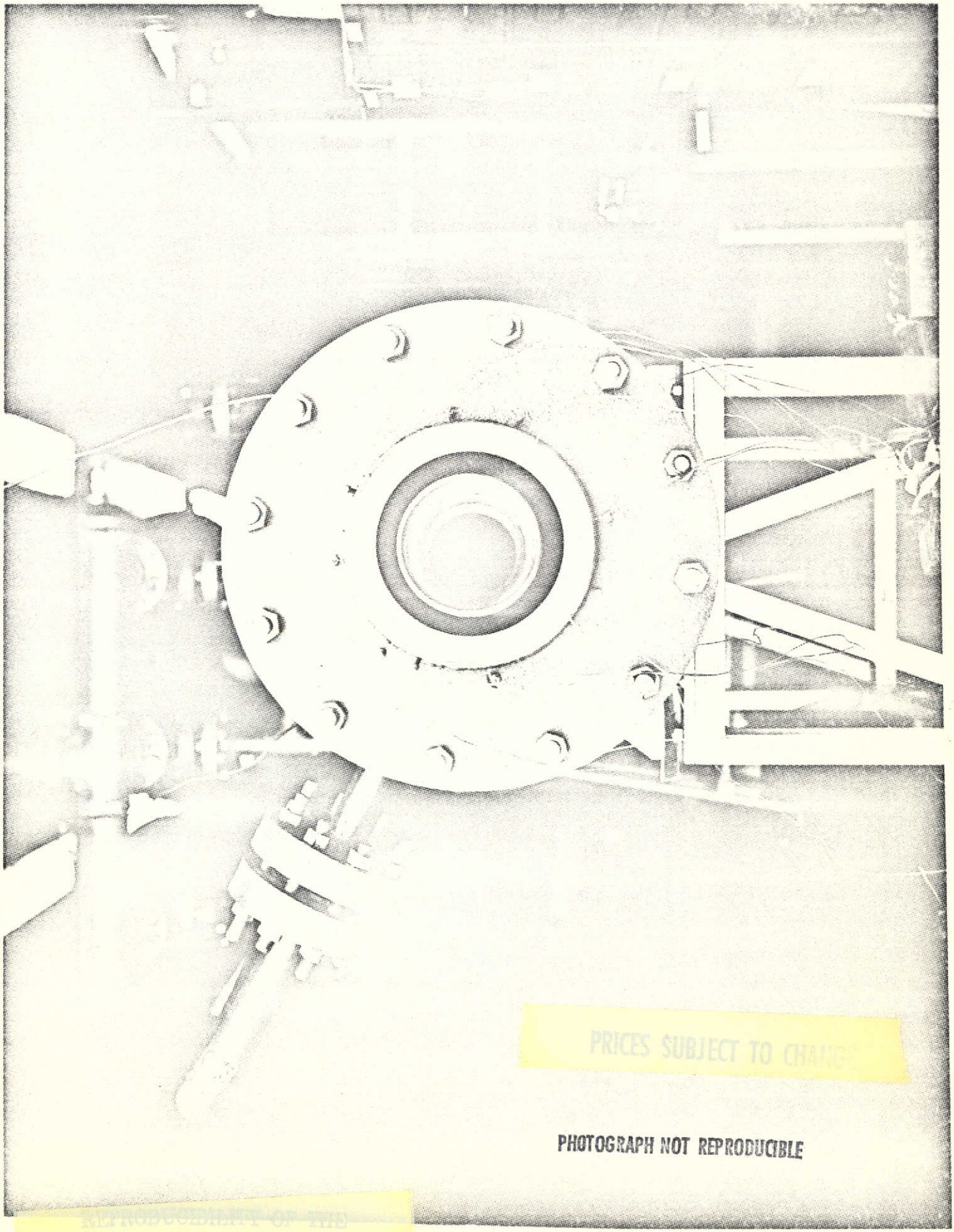

PHOTOGRAPH NOT REPRODUCIBLE

Fig. 1 Jet Nozzle

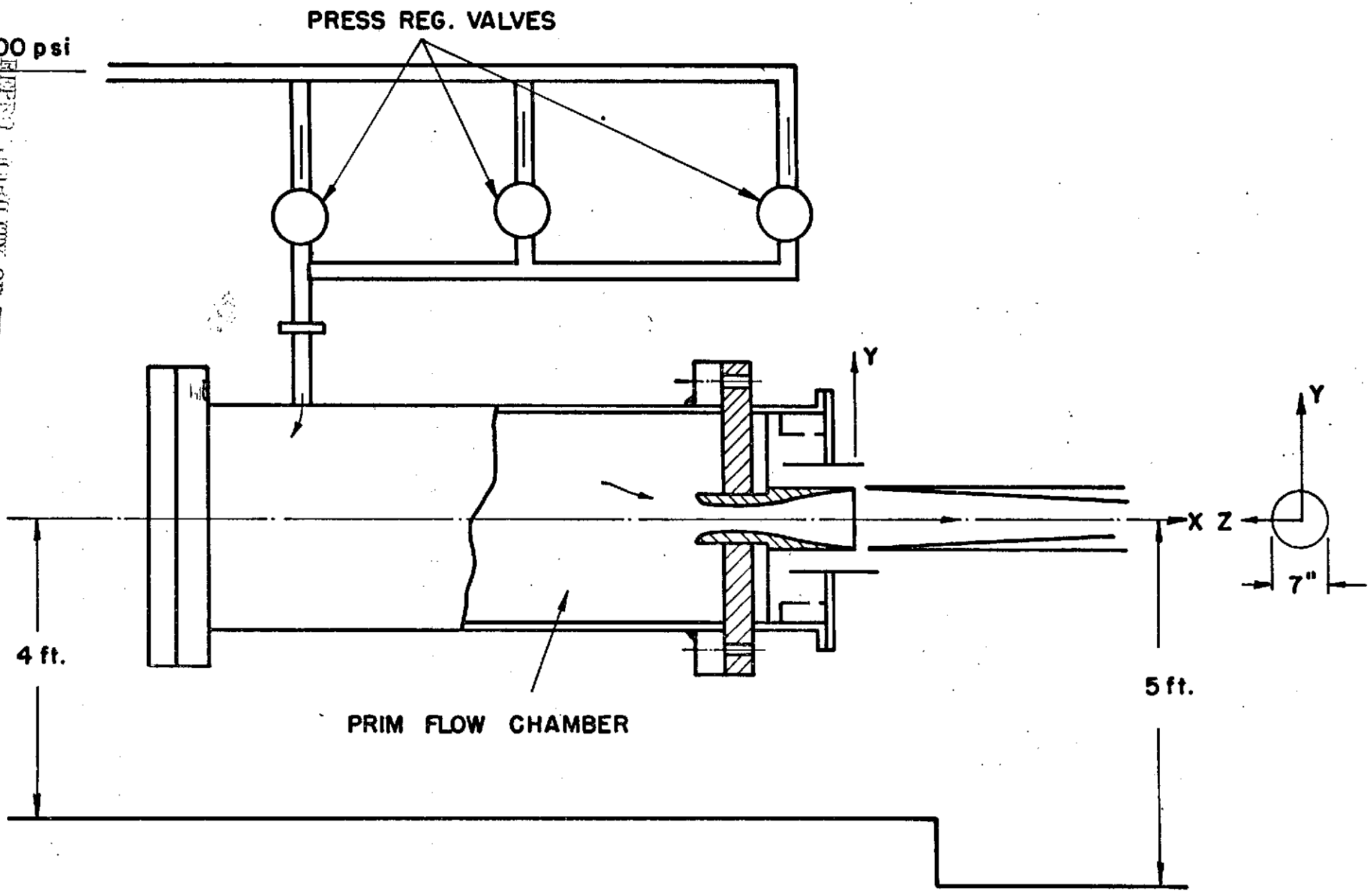

Fig. 2 Facility Configuration

Fig. 3 Shadowgraph of Over-expanded Flow Near Nozzle Exit

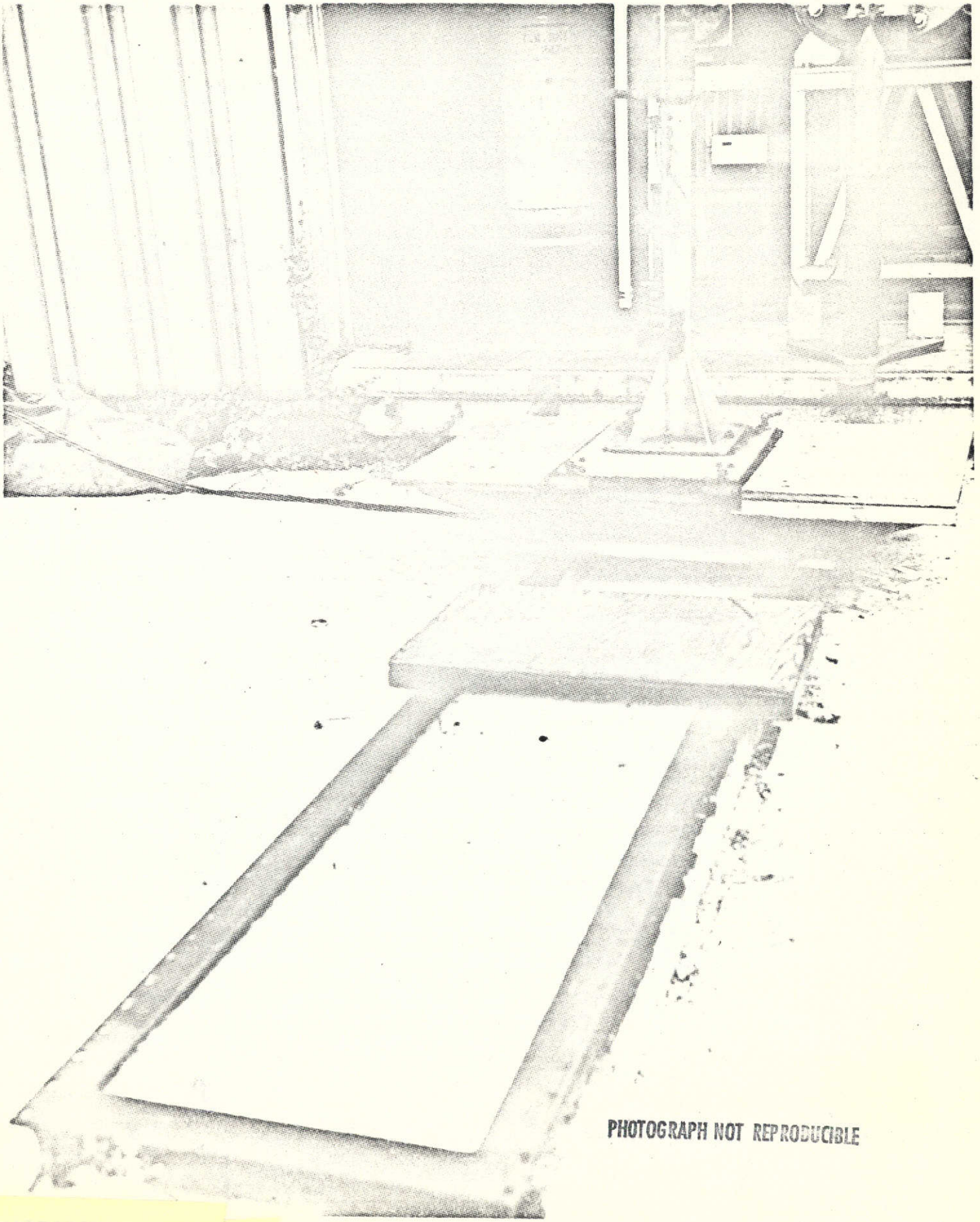

Fig. 4 Probe Support Structure

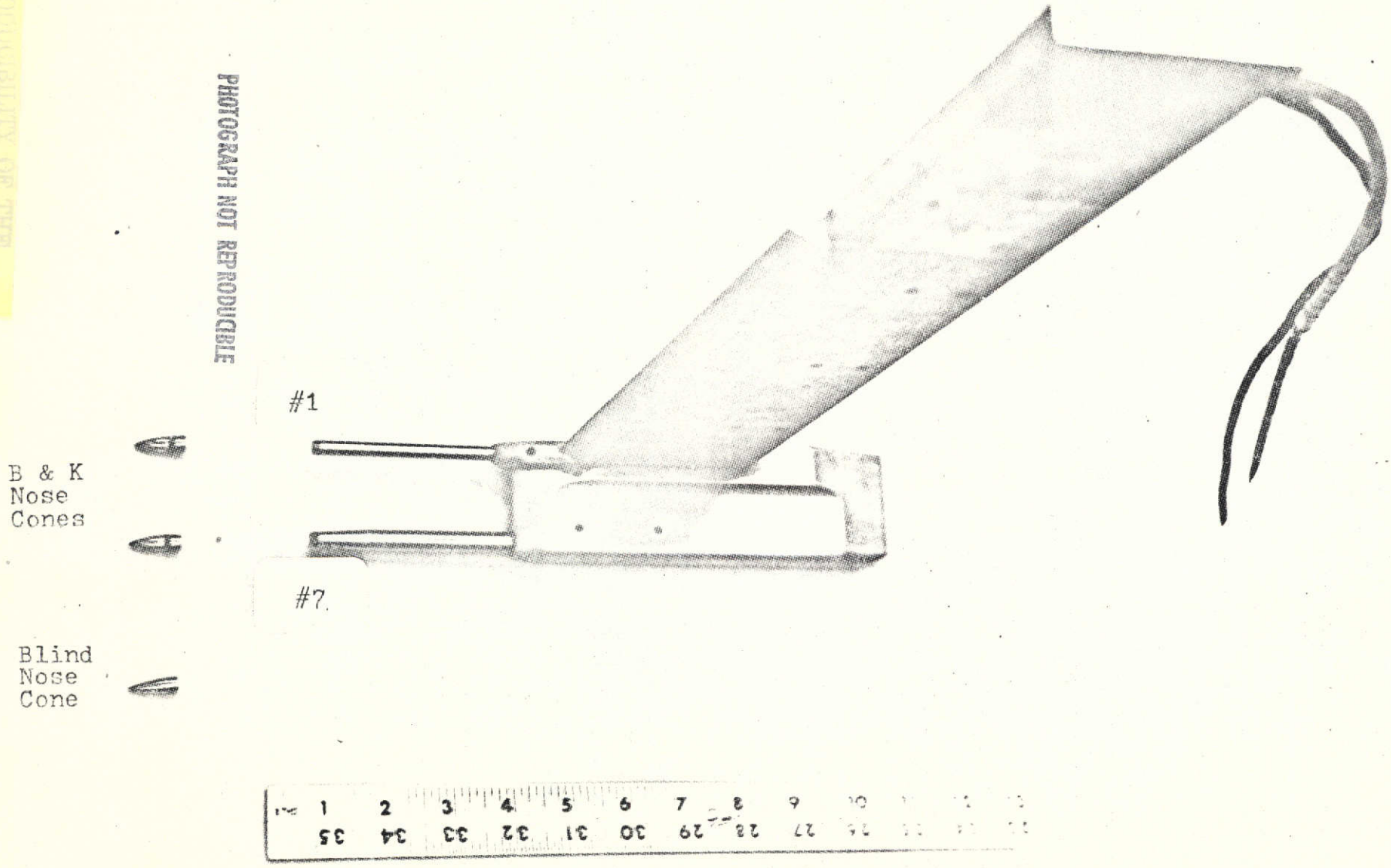

Fig. 5 Wing Support with Probes and Nose Cones

TRANSDUCER	NO. 1	NO. 7
TYPE	KULITE COS-125-100	KULITE COS-125-100
SERIAL NO.	2065-4-1	2065-5-7
RATED PRESSURE	100 psi	100 psi
SENSITIVITY	.293 mv/v/psi	.331 mv/v/psi
MAX. INPUT VOLTAGE	5 VDC	7.5 VDC
OUTPUT IMPEDANCE	304 Ω	326 Ω
OPERATING TEMP.	< 250° F	< 250° F
CHANGE OF SENS. WITH TEMP. (APPROX.)	± 2.5 % /100° F	± 2.5 % /100° F
NATURAL FREQ. (APPROX.)	130 kHz	130 kHz
ACCELERATION SENS. PERPENDICULAR TRANSVERVE	0.0002 % FS/g 0.00004 % FS/g	0.0002 % FS/g 0.00004 % FS/g

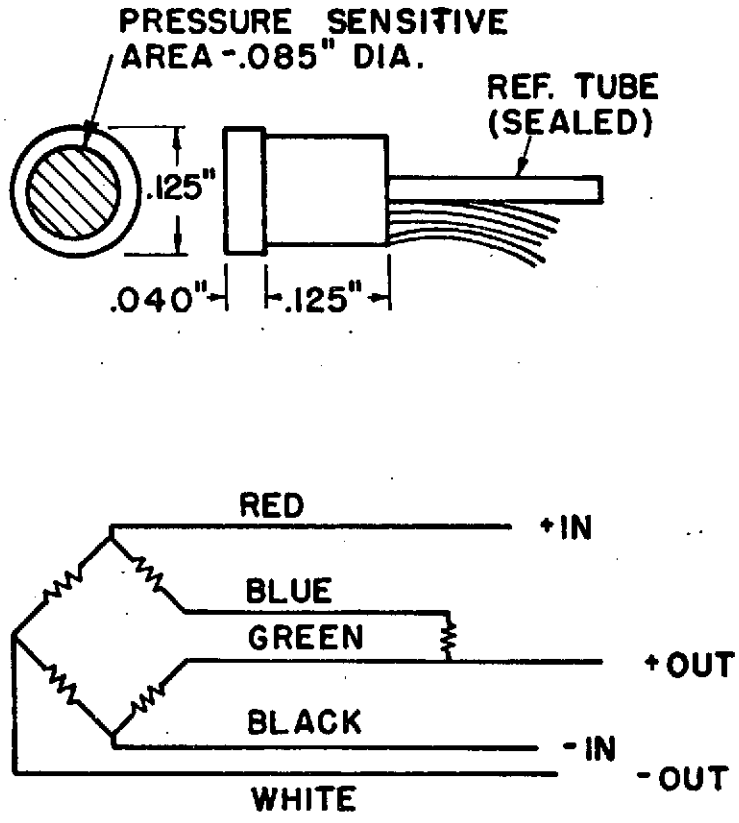

Fig. 6 Transducer Specifications and Circuitry

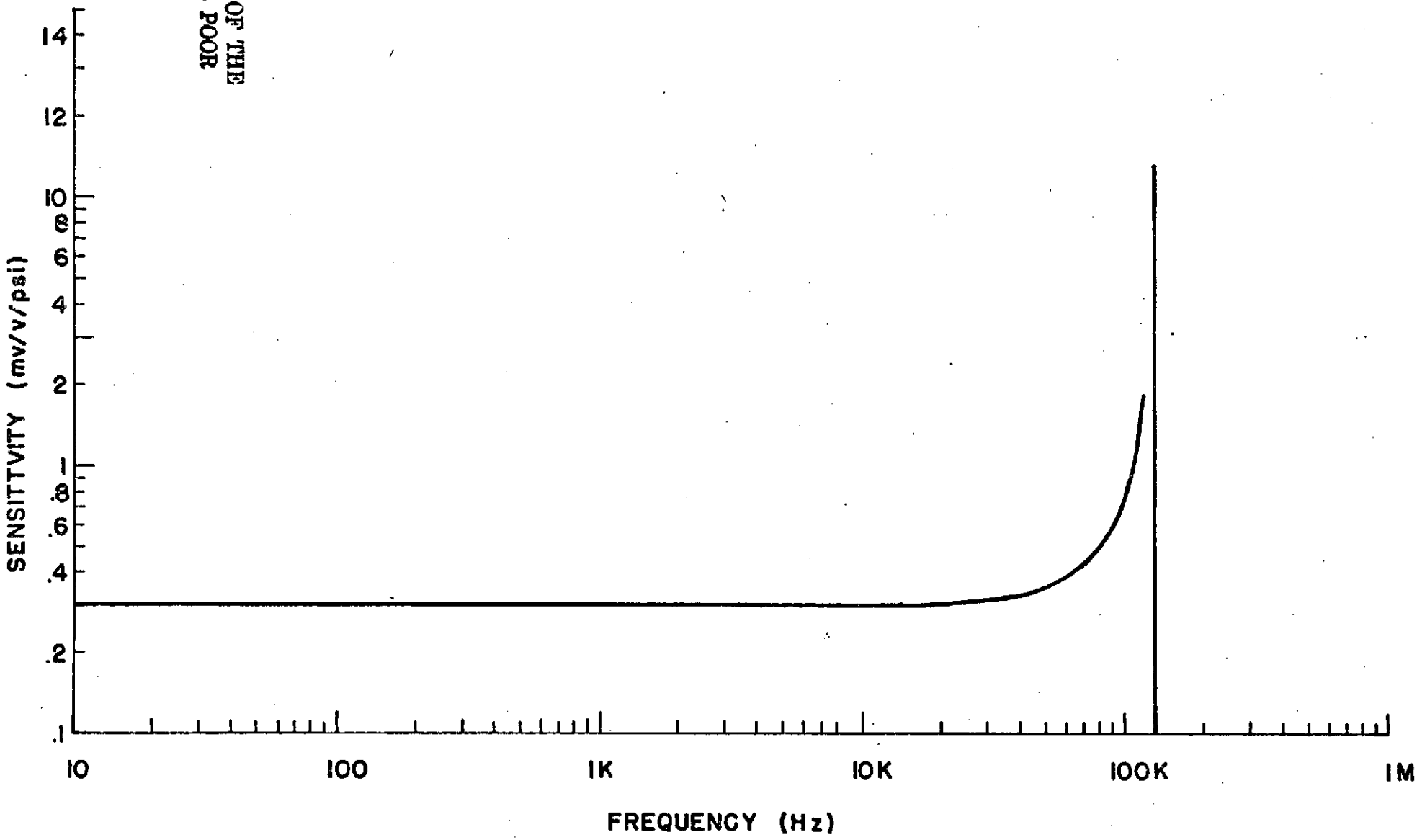

Fig. 7 Typical Frequency Response of Kulite CQS-125 Pressure Transducers

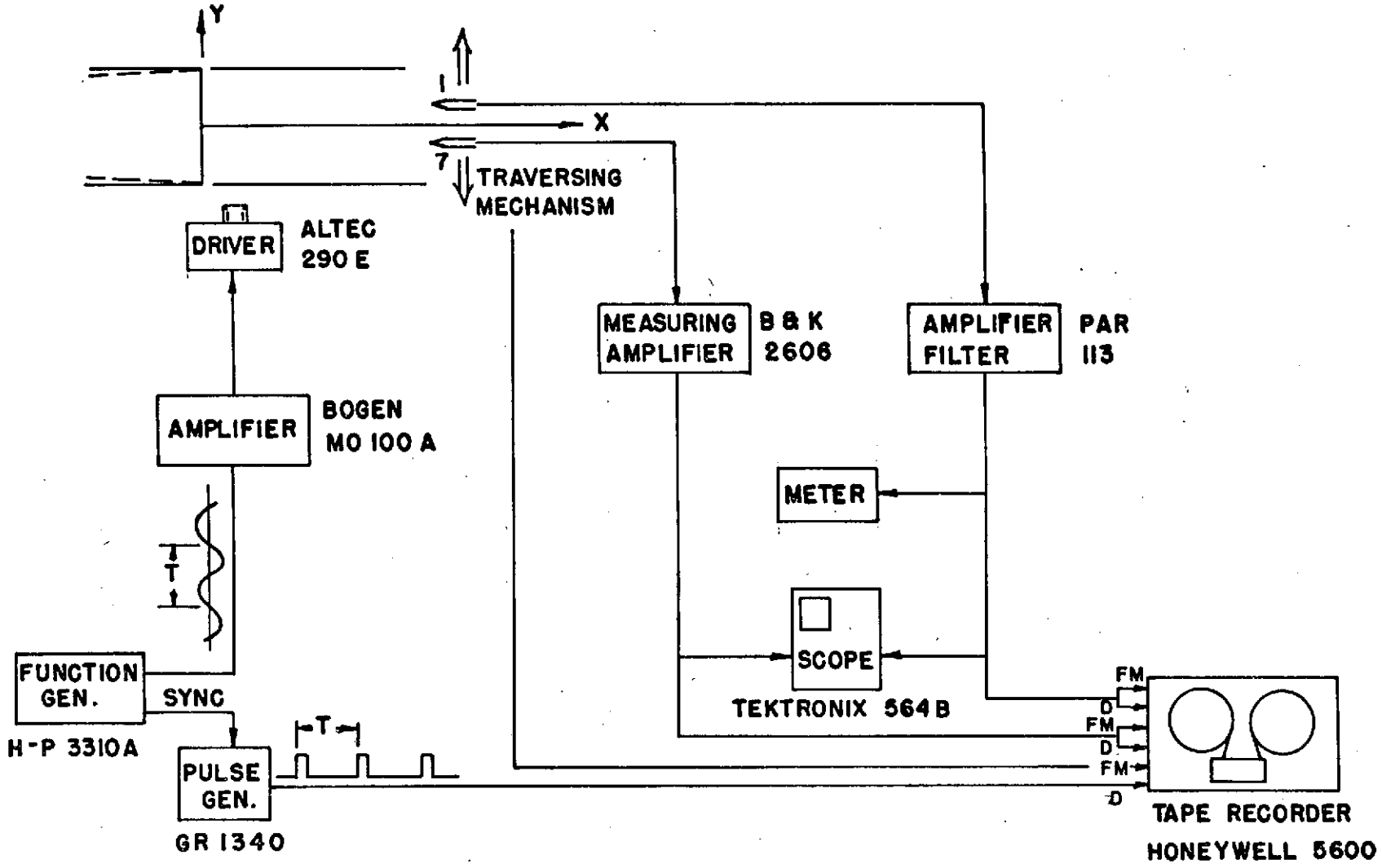

Fig. 8 Recording and Signal Generating Systems

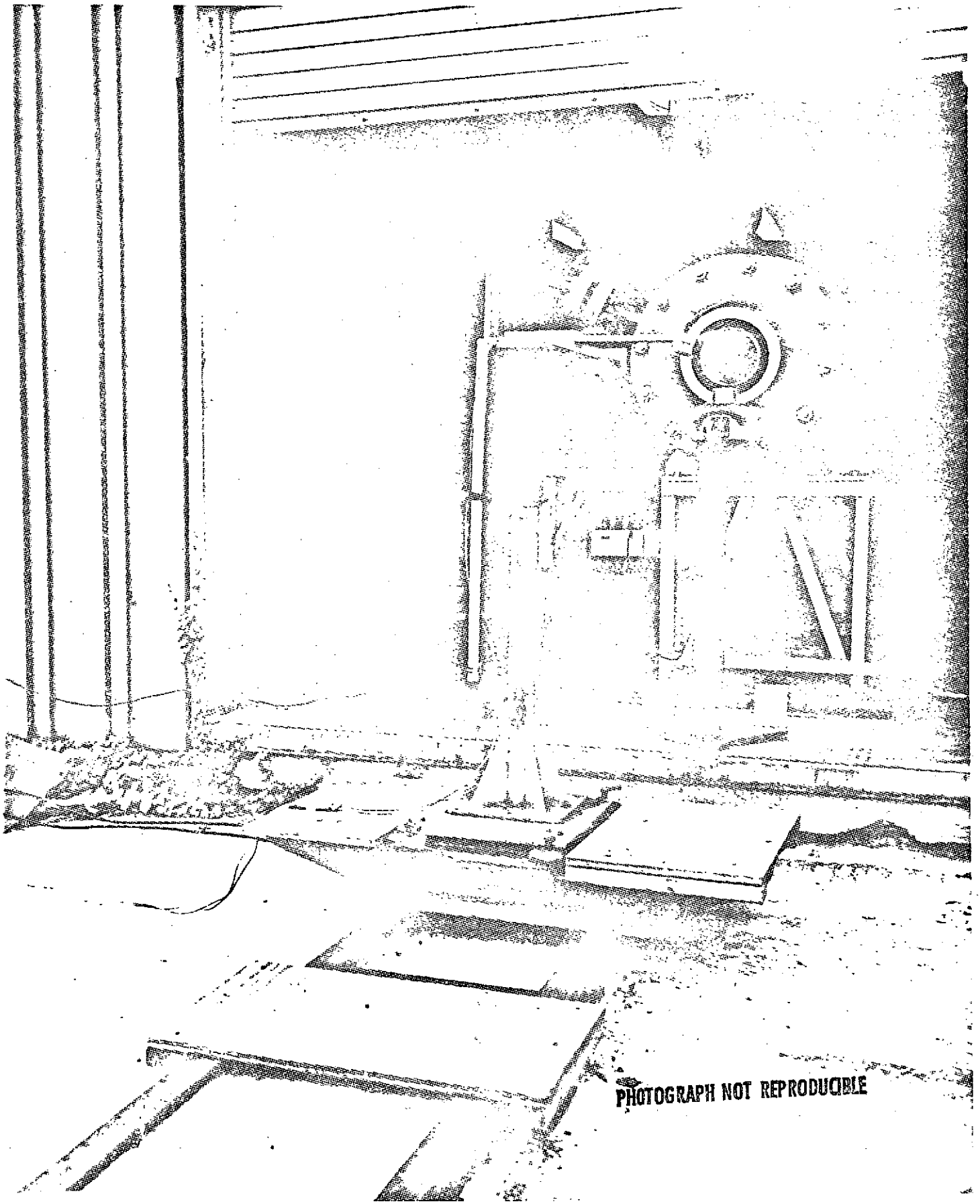

Fig. 9 Experimental Set-Up
for Acoustic Signal Tracing

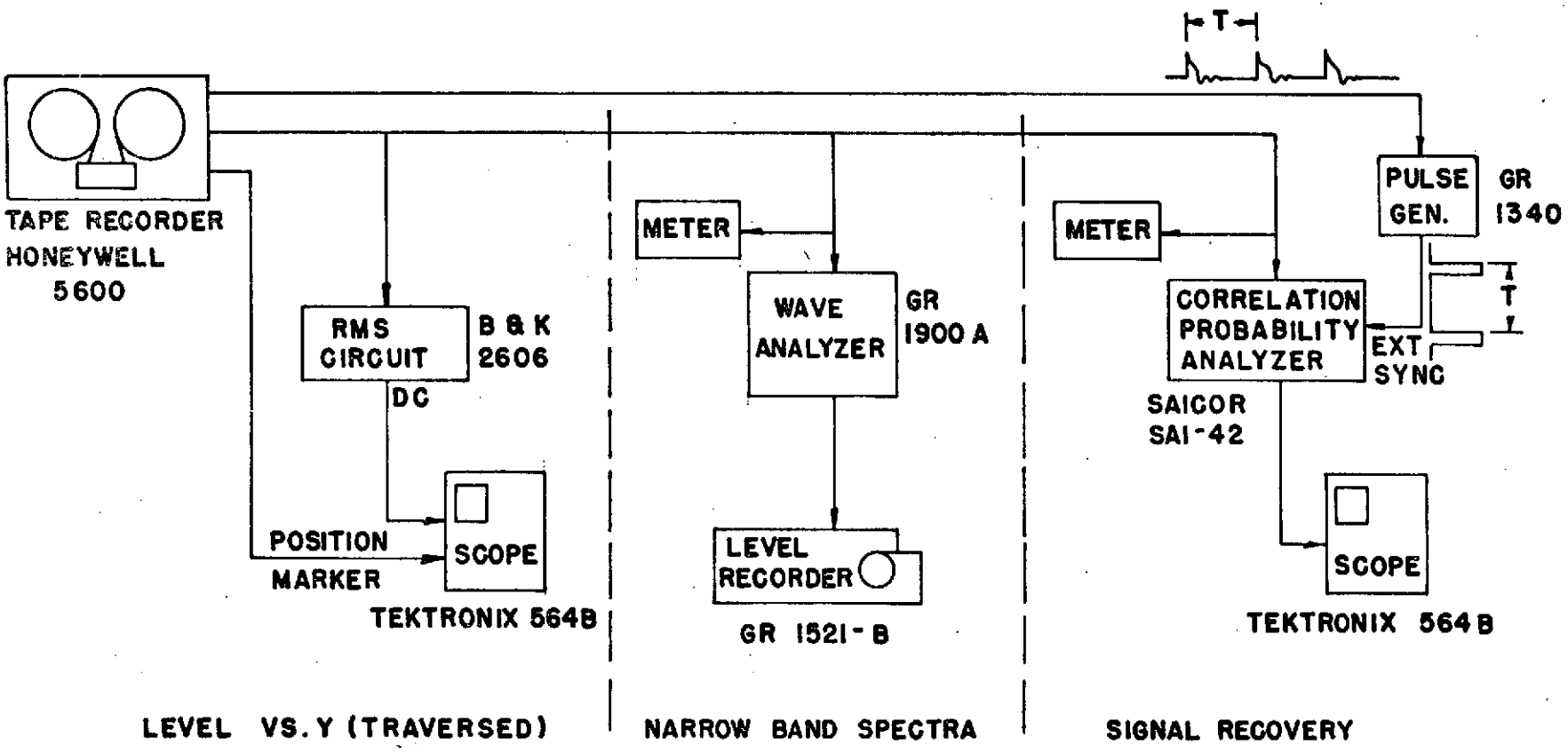

Fig. 10 Data Analysis Systems

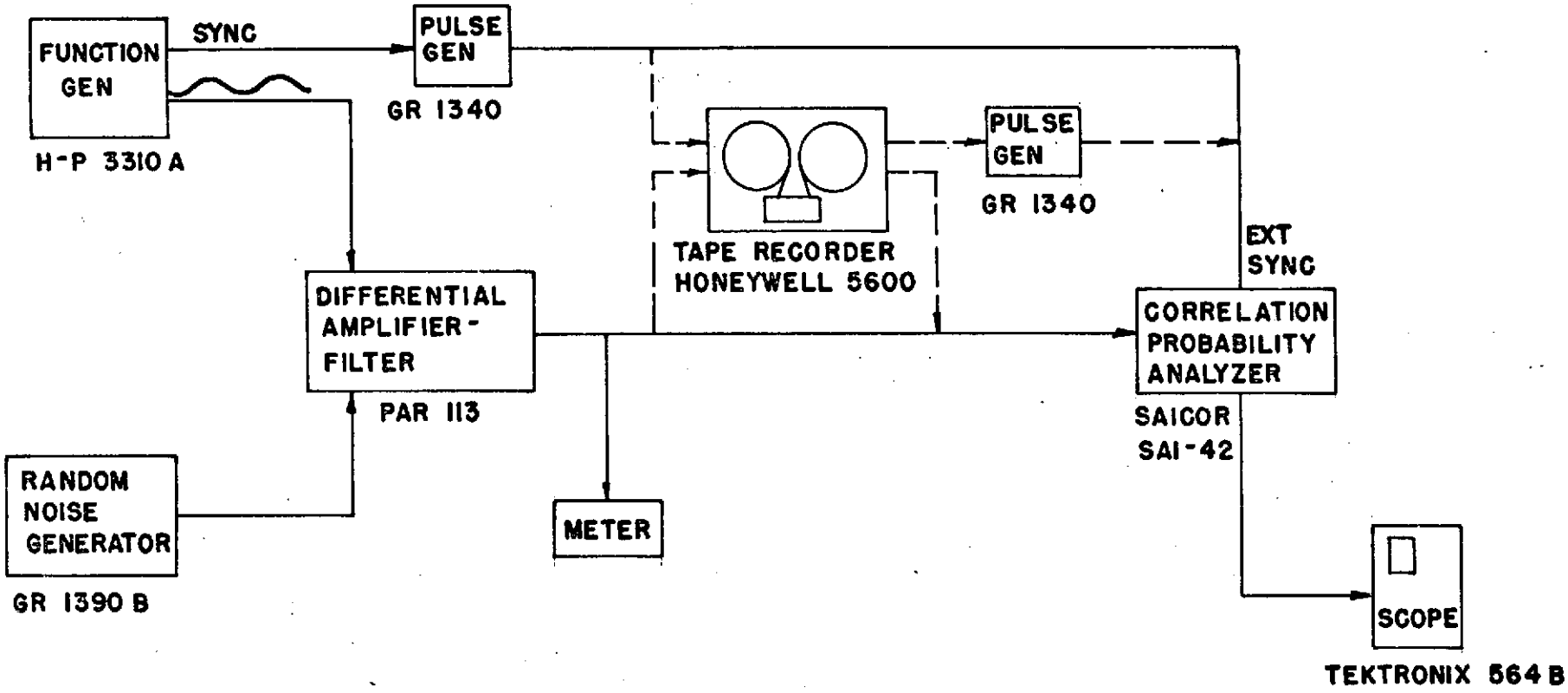

Fig. 11 Signal Recovery Simulation System

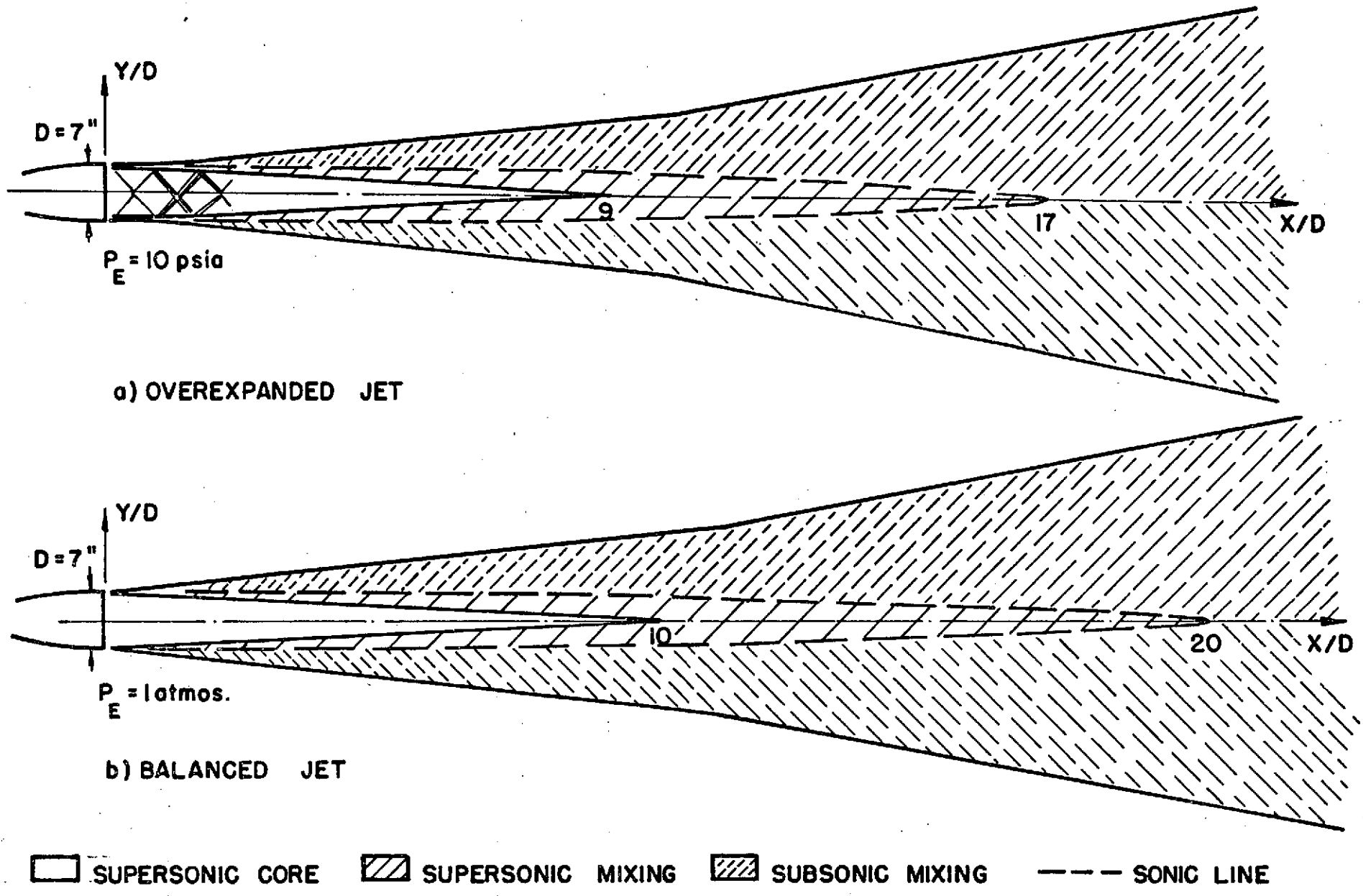

Fig. 12 Schematics of Jet Flow Fields

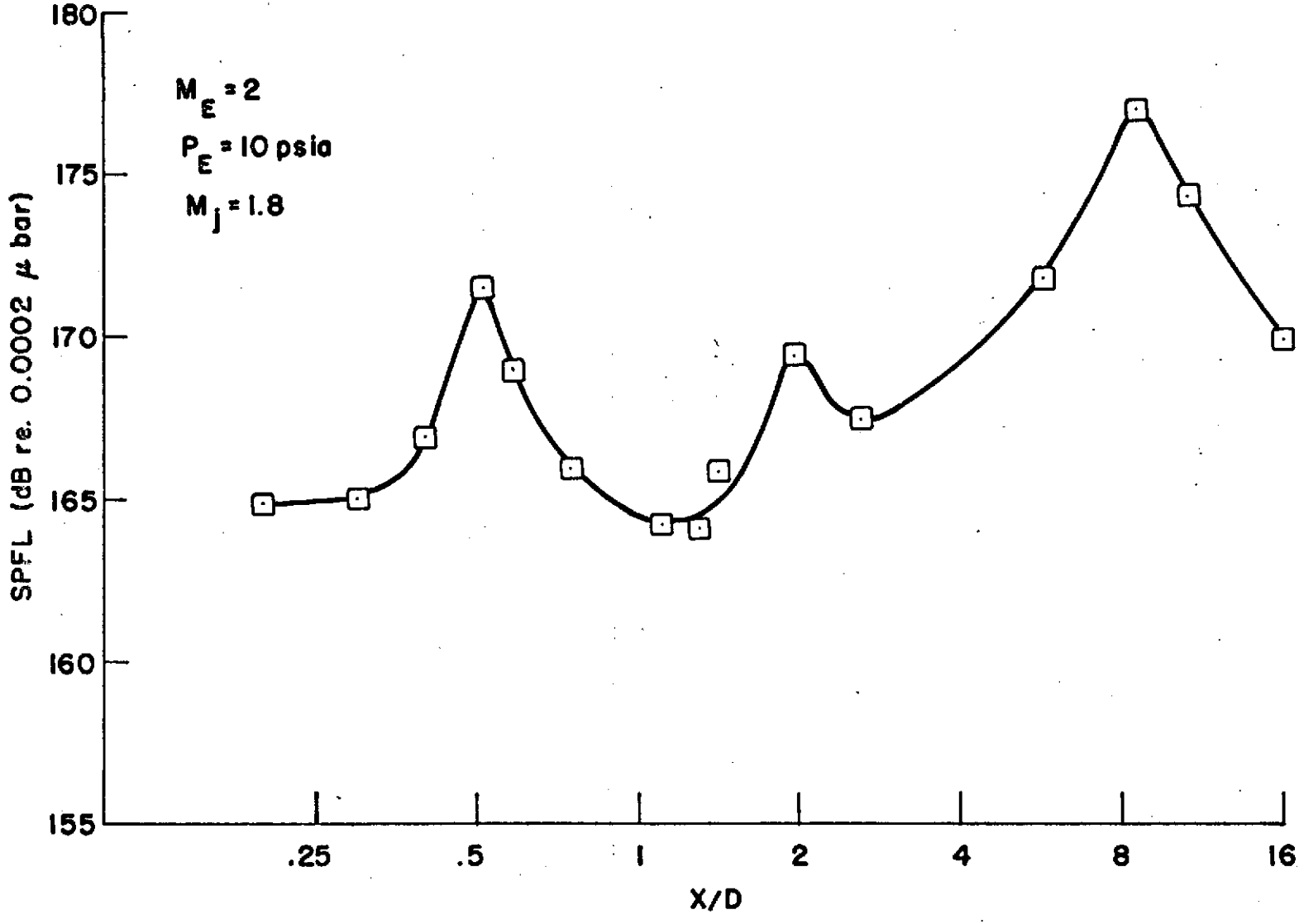

Fig. 13 Variation of Static Pressure Fluctuation Level Along Centerline of Overexpanded Jet

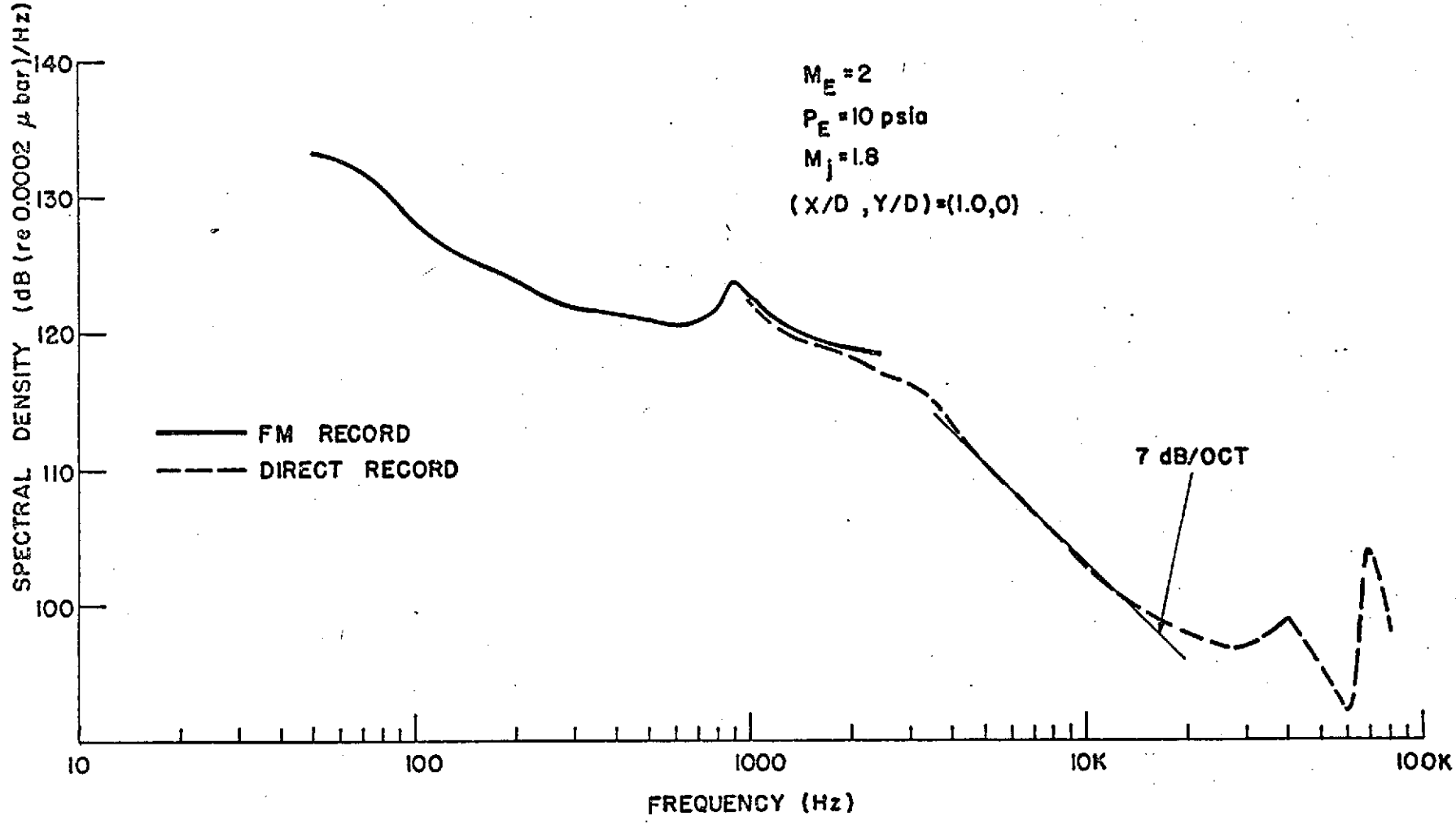

Fig. 14 Spectral Distribution of the Static Pressure Fluctuations at X/D=1 Along Centerline of Overexpanded Jet

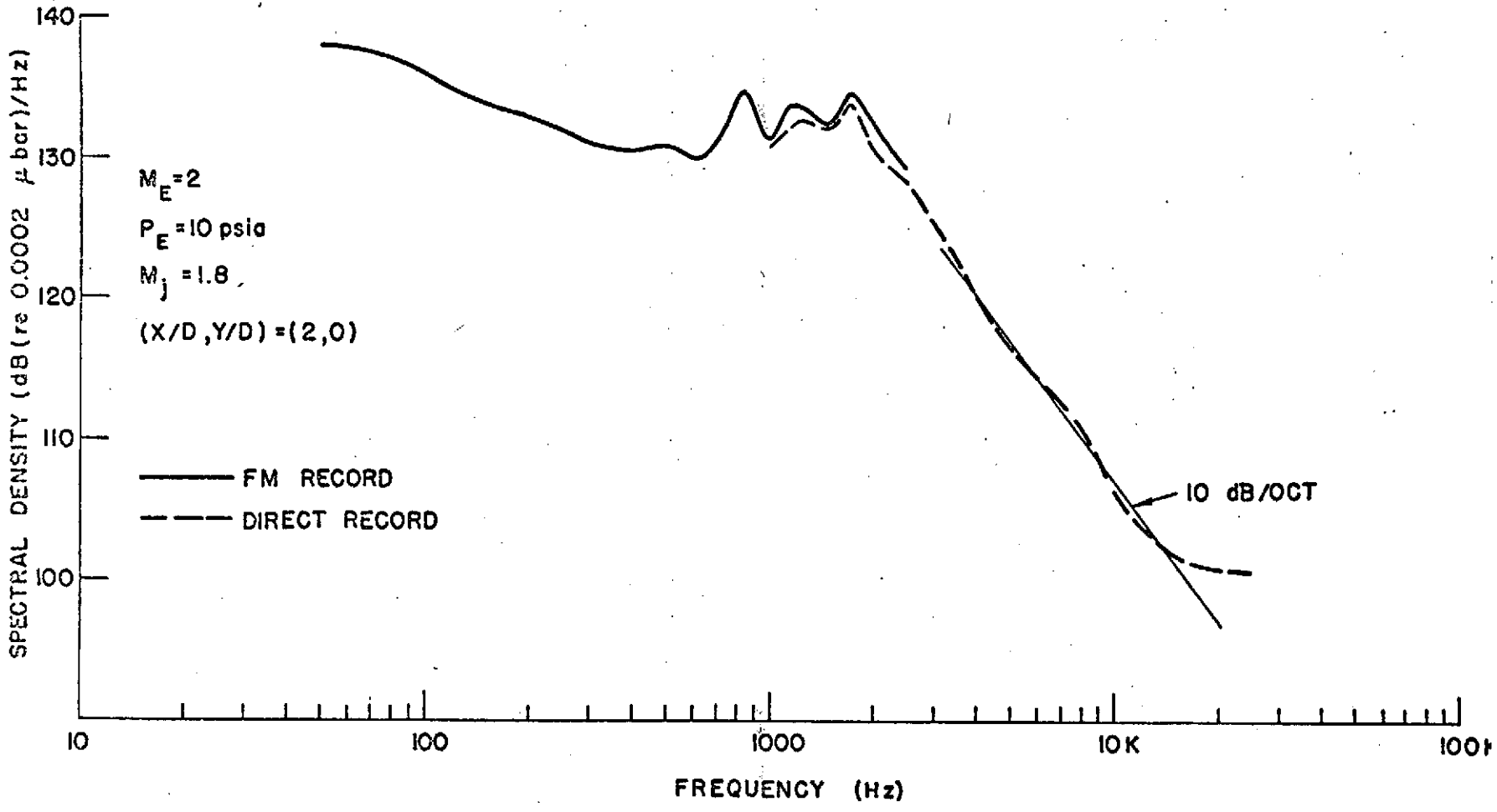

Fig. 15 Spectral Distribution of the Static Pressure Fluctuations at X/D=2 Along Centerline of Overexpanded Jet

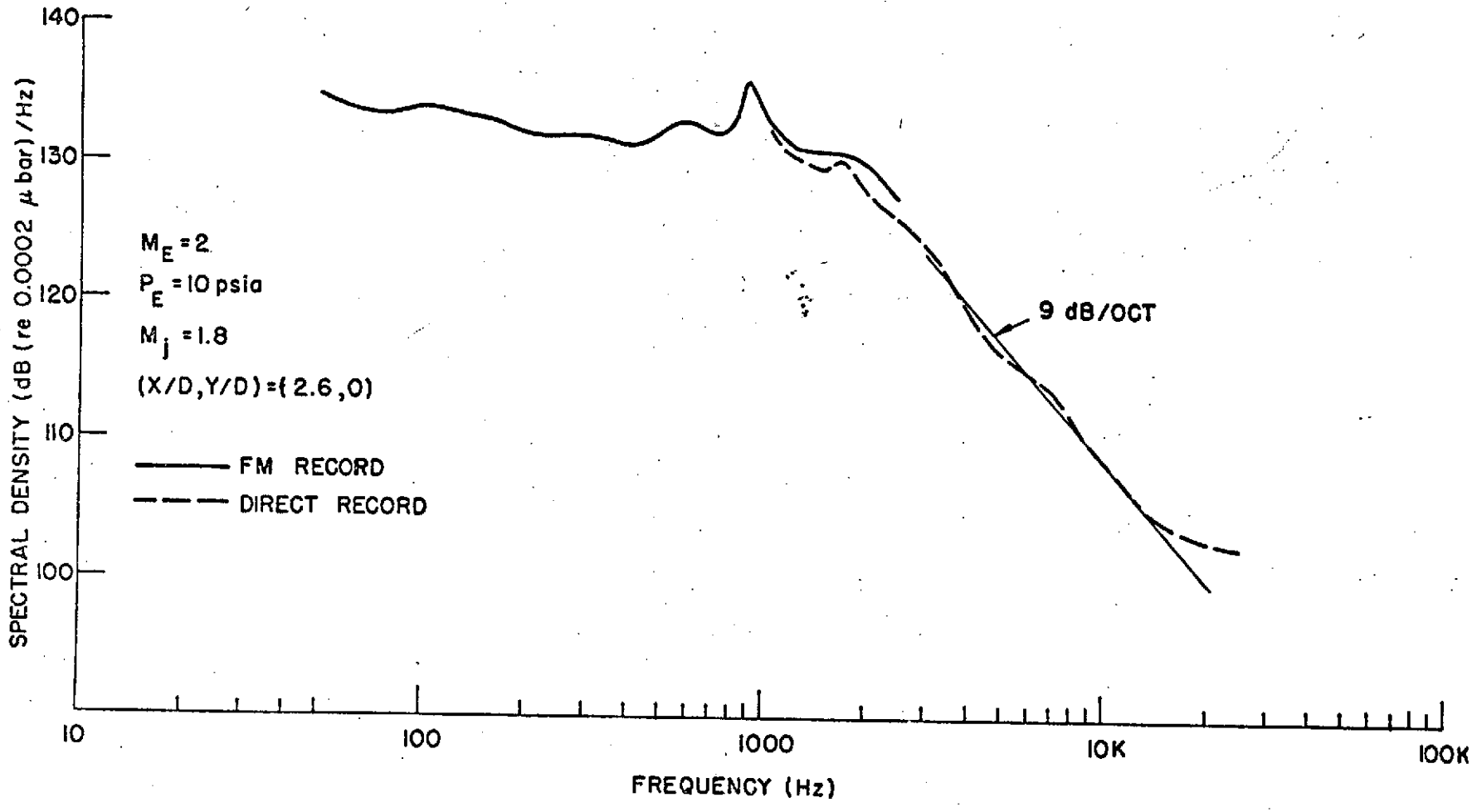

Fig. 16 Spectral Distribution of the Static Pressure Fluctuations at X/D=2.6 Along Centerline of Overexpanded Jet

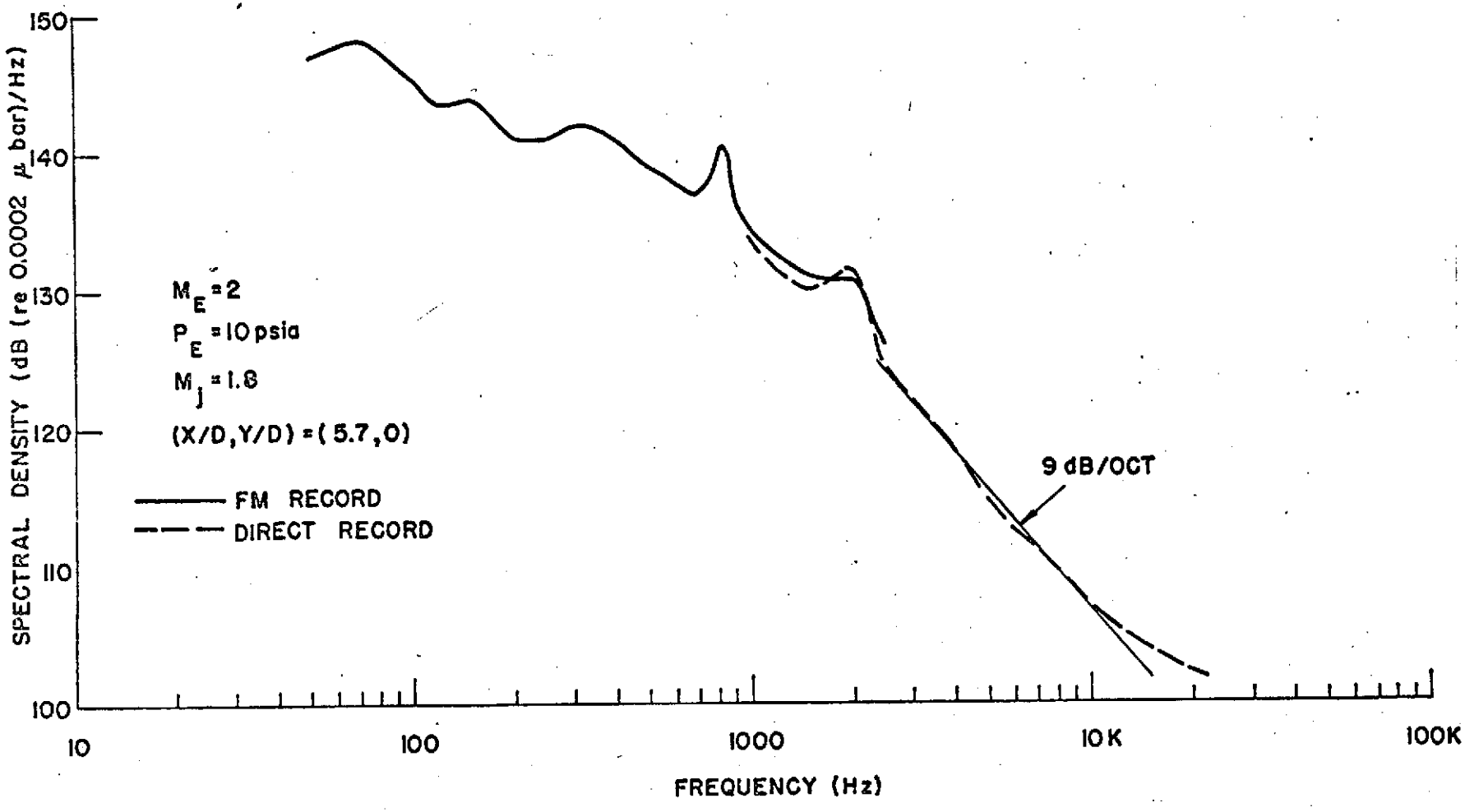

Fig. 17 Spectral Distribution of the Static Pressure Fluctuations at X/D=5.7 Along Centerline of Overexpanded Jet

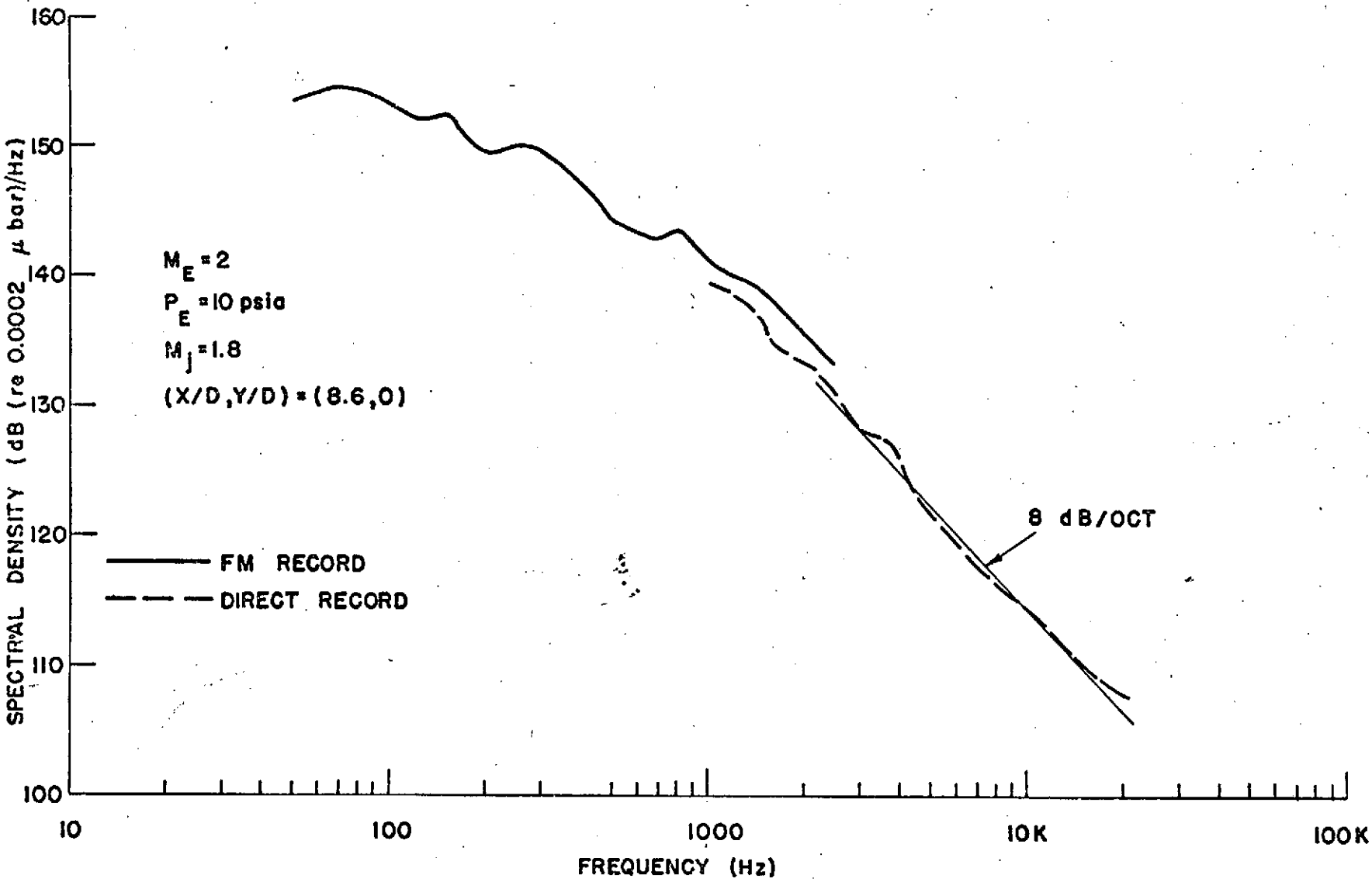

Fig. 18 Spectral Distribution of the Static Pressure Fluctuations at X/D=8.6 Along Centerline of Overexpanded Jet

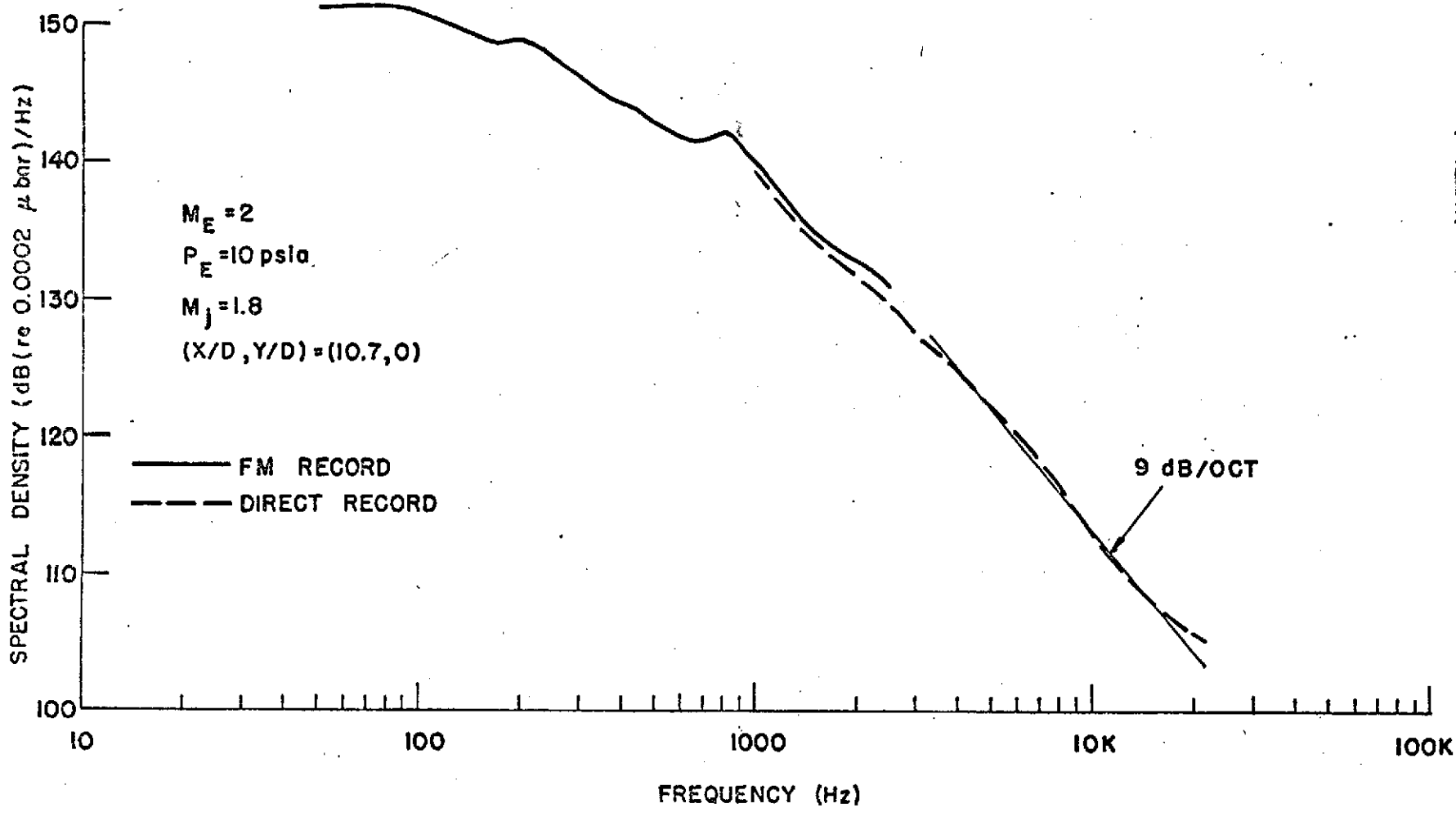

Fig. 19 Spectral Distribution of the Static Pressure Fluctuations at X/D=10.7 Along Centerline of Overexpanded Jet

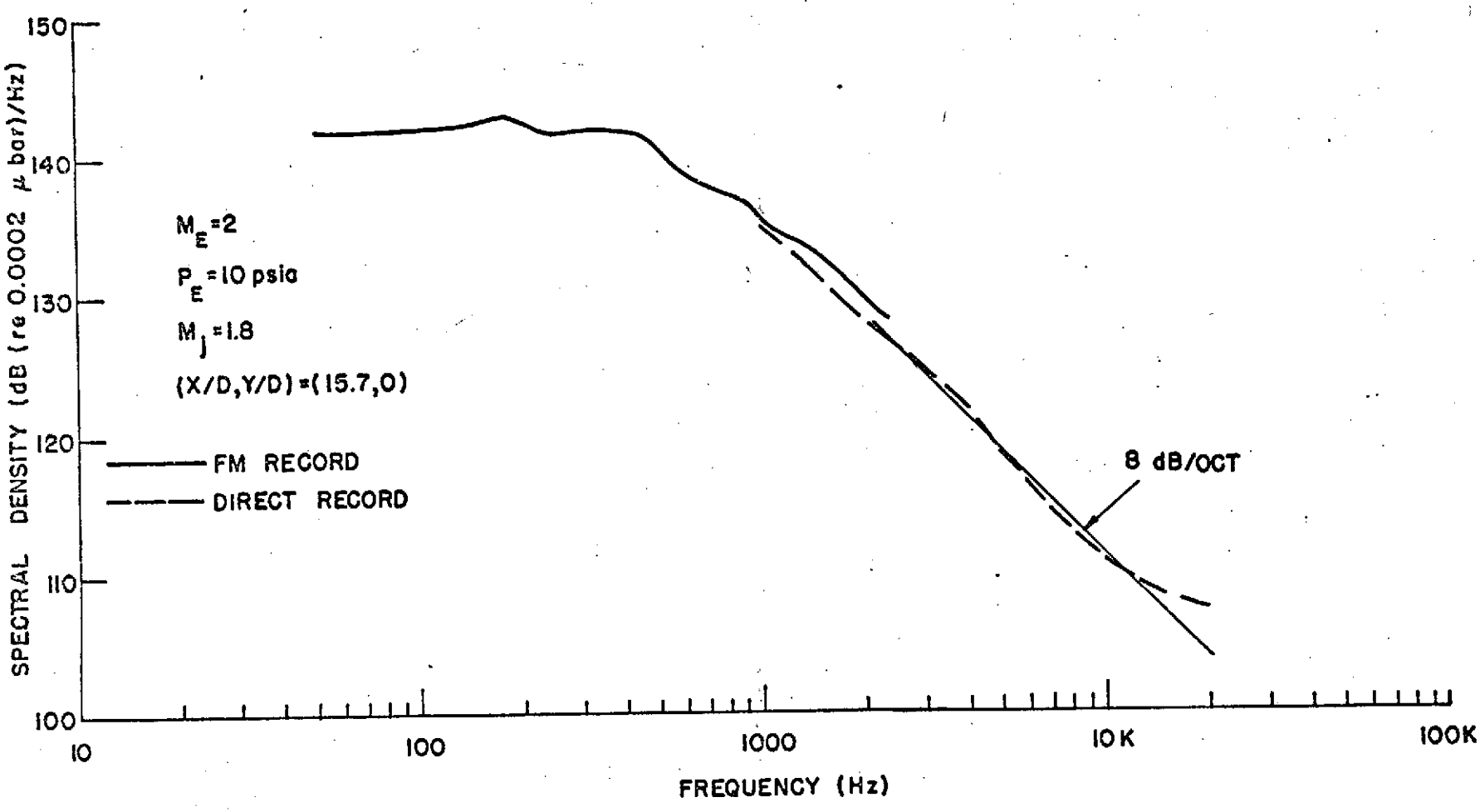

Fig. 20 Spectral Distribution of the Static Pressure Fluctuations at X/D=15.7 Along Centerline of Overexpanded Jet

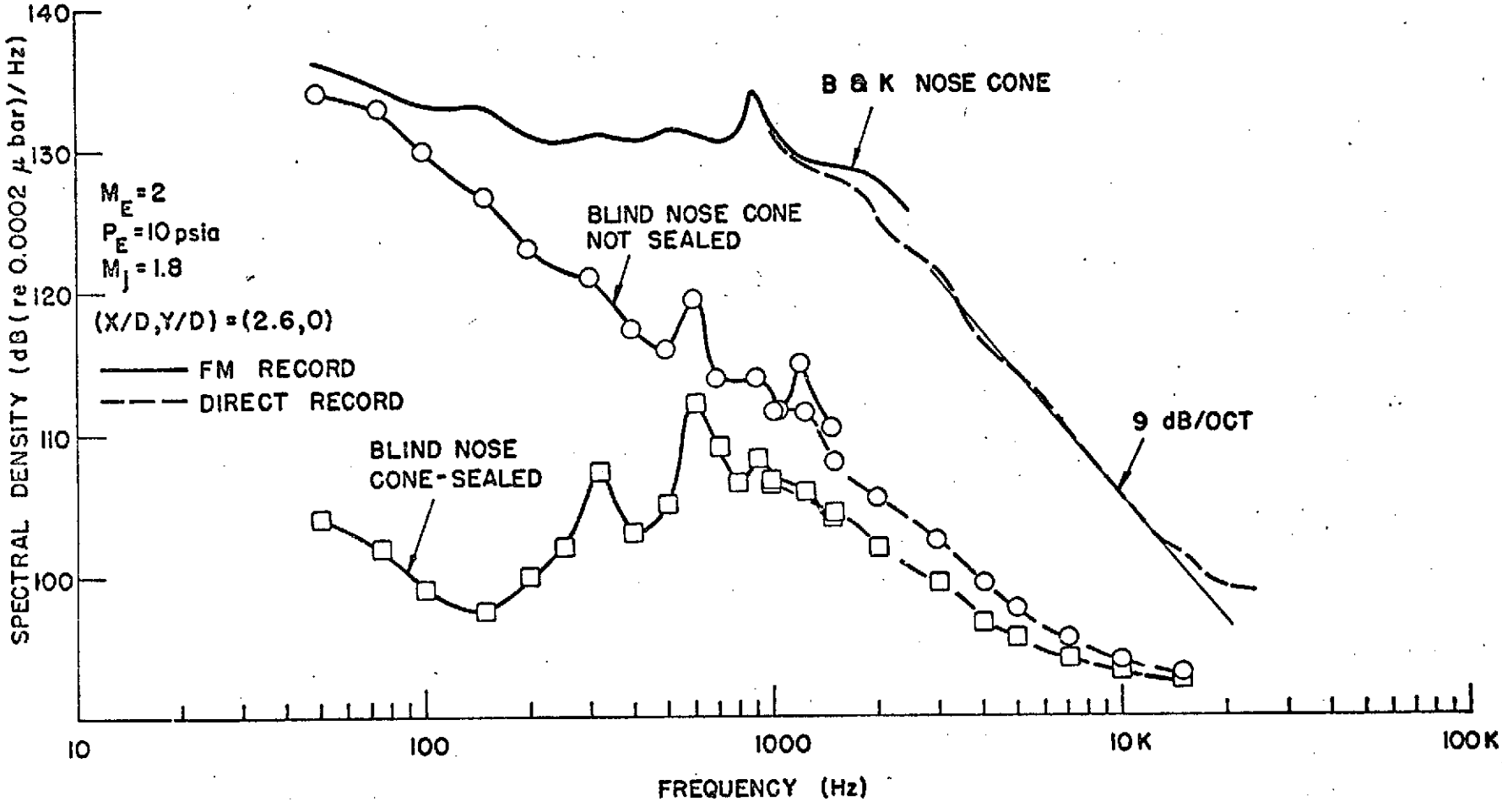

Fig. 21 Spectral Distribution of Vibration Induced Electrical Noise

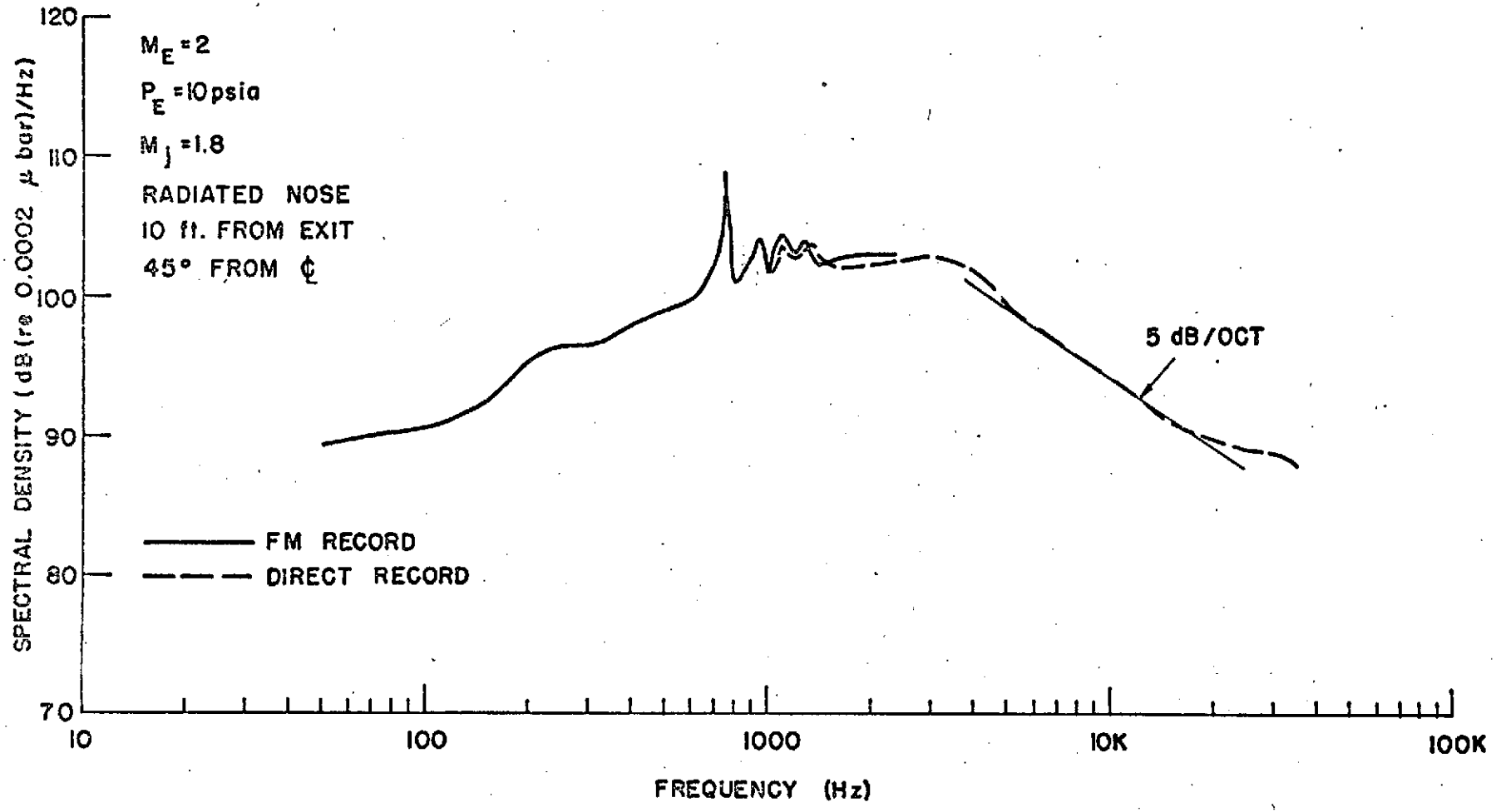

Fig. 22 Spectral Distribution of the Radiated Sound of the Overexpanded Jet

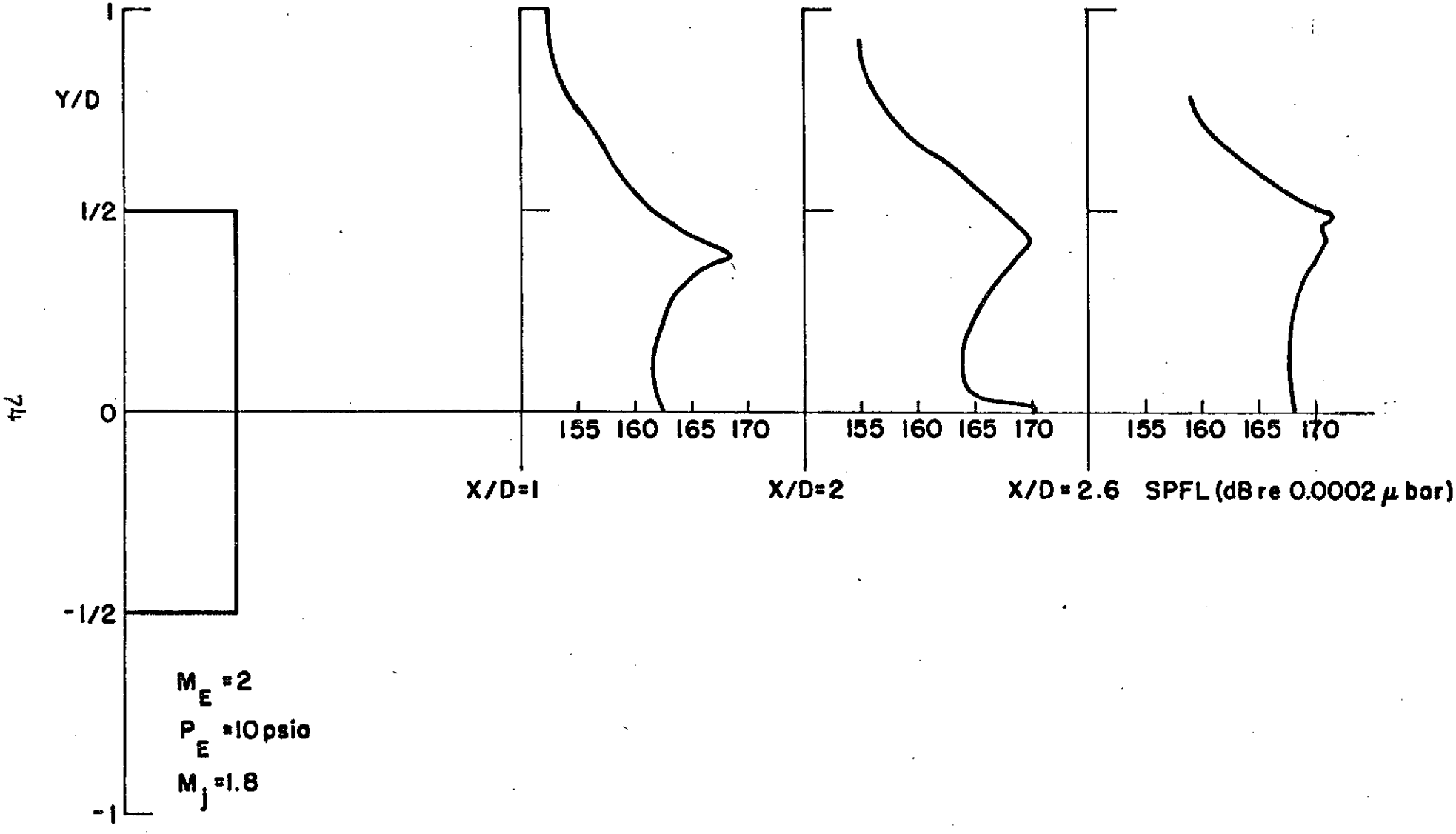

Fig. 23a Variation of Static Pressure Fluctuation Level with Radial Distance from Centerline of Overexpanded Jet

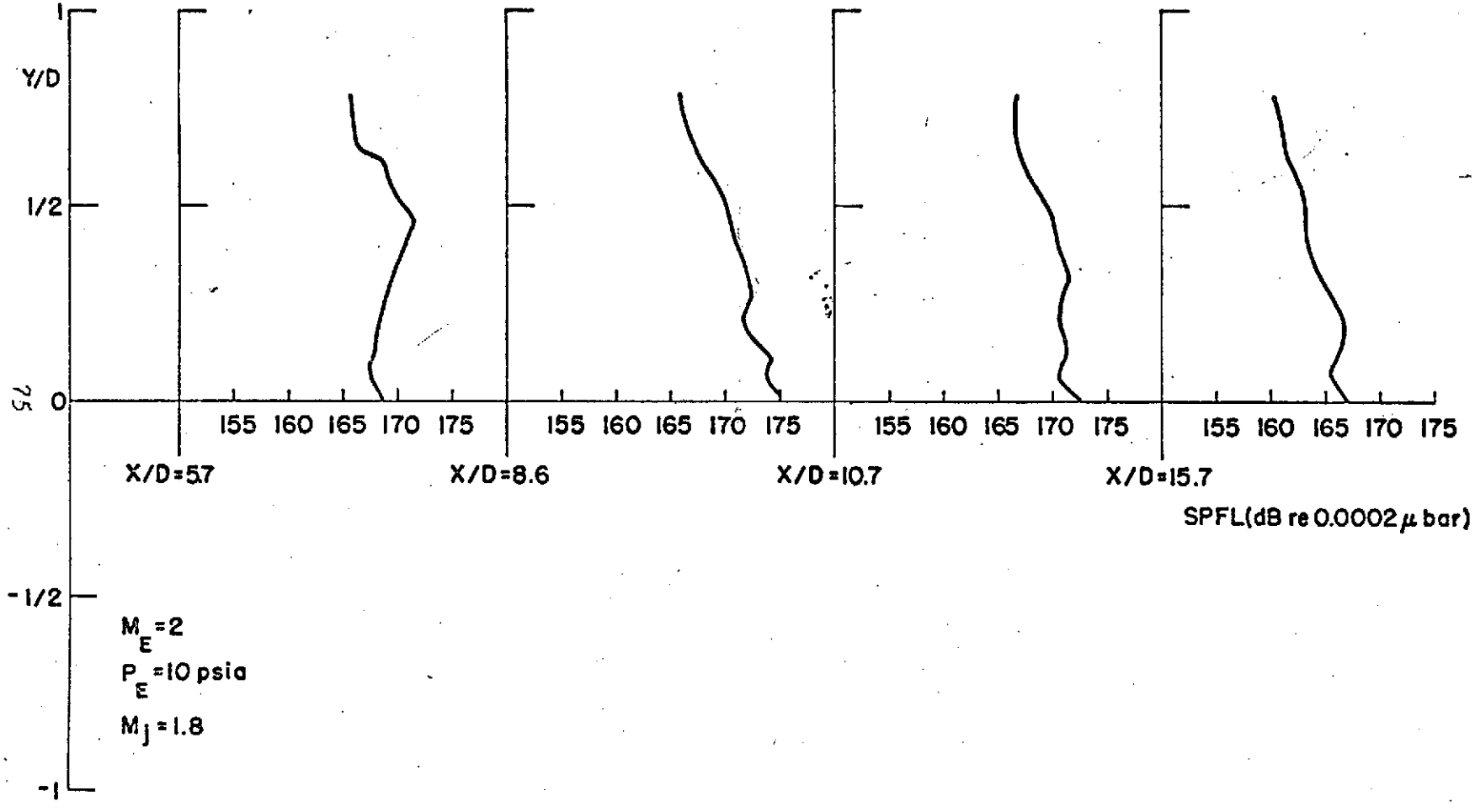

Fig. 23b Variation of Static Pressure Fluctuation Level with Radial Distance from Centerline of Overexpanded Jet

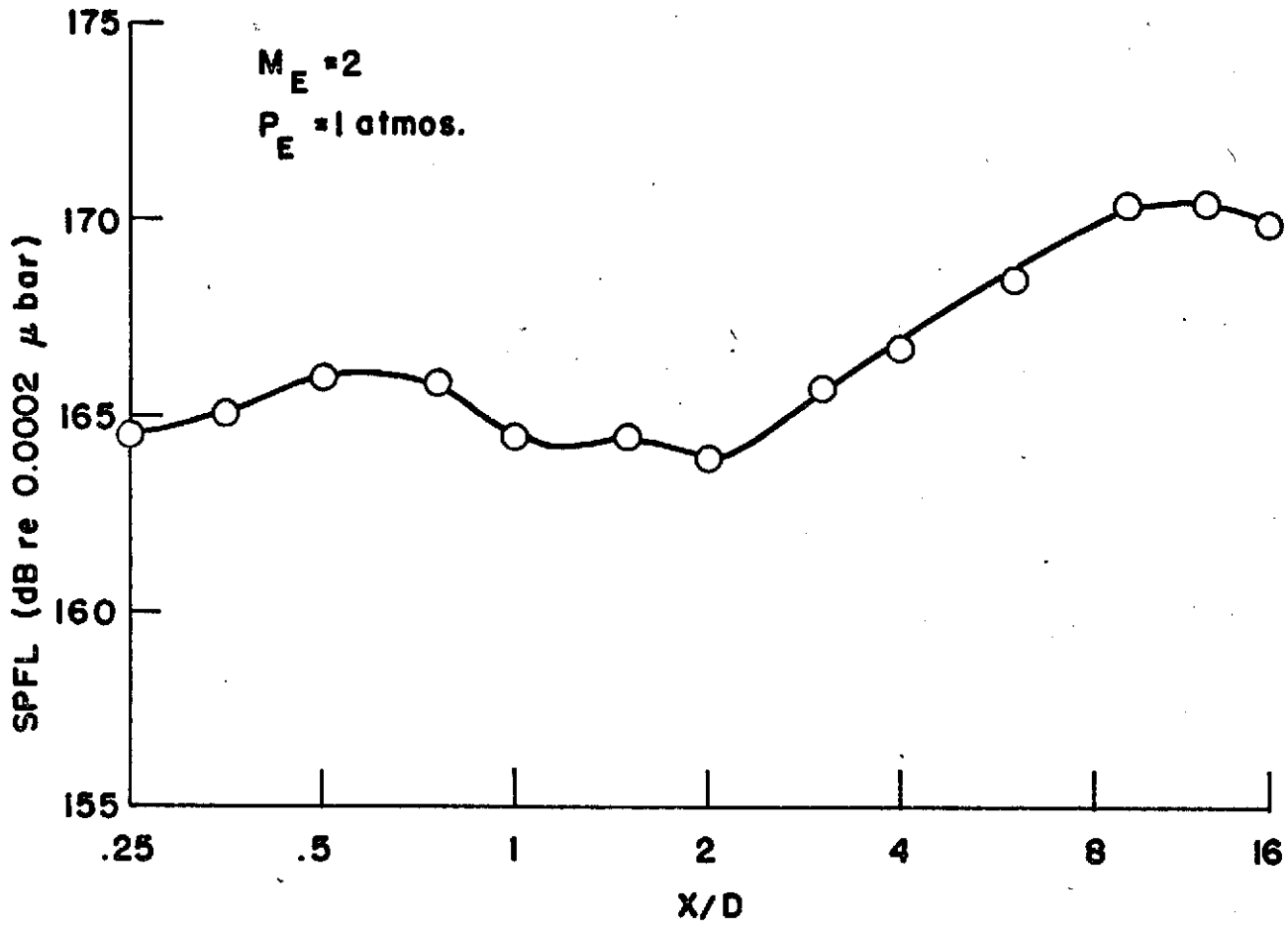

Fig. 24 Variation of Static Pressure Fluctuation Level Along Centerline of Balanced Jet

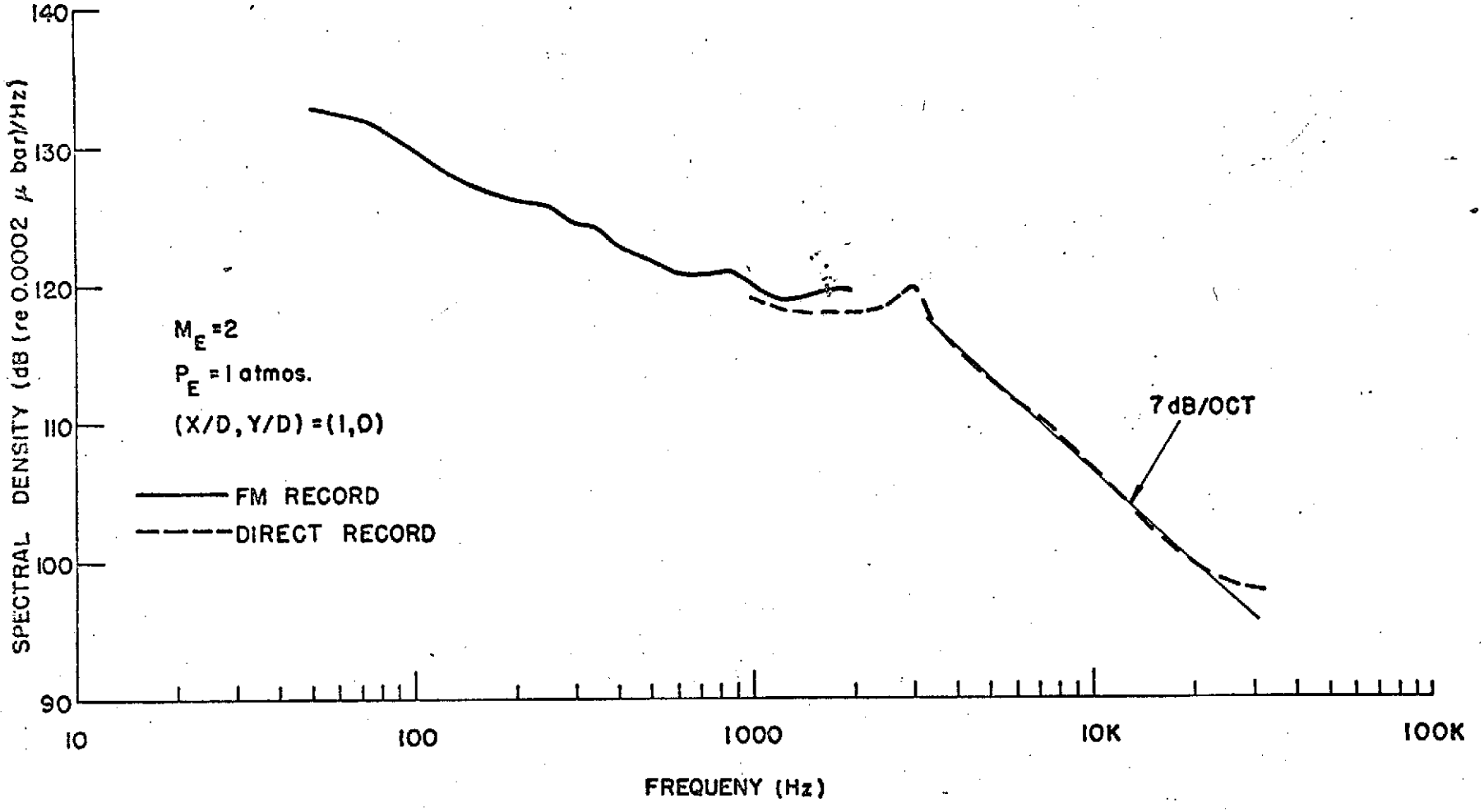

Fig. 25 Spectral Distribution of the Static Pressure Fluctuations at X/D=1 Along Centerline of Balanced Jet

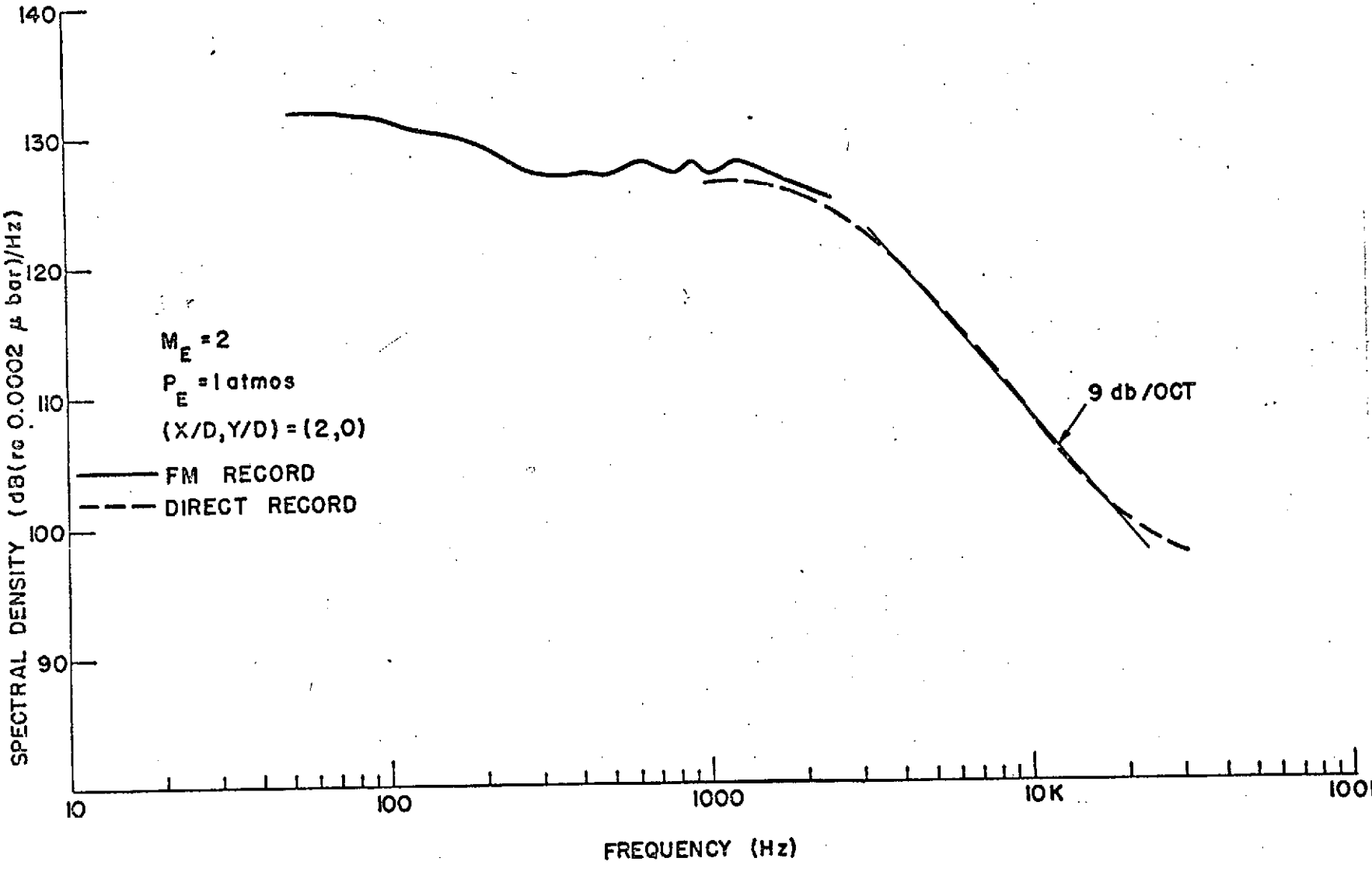

Fig. 26 Spectral Distribution of the Static Pressure Fluctuations at X/D=2 Along Centerline of Balanced Jet

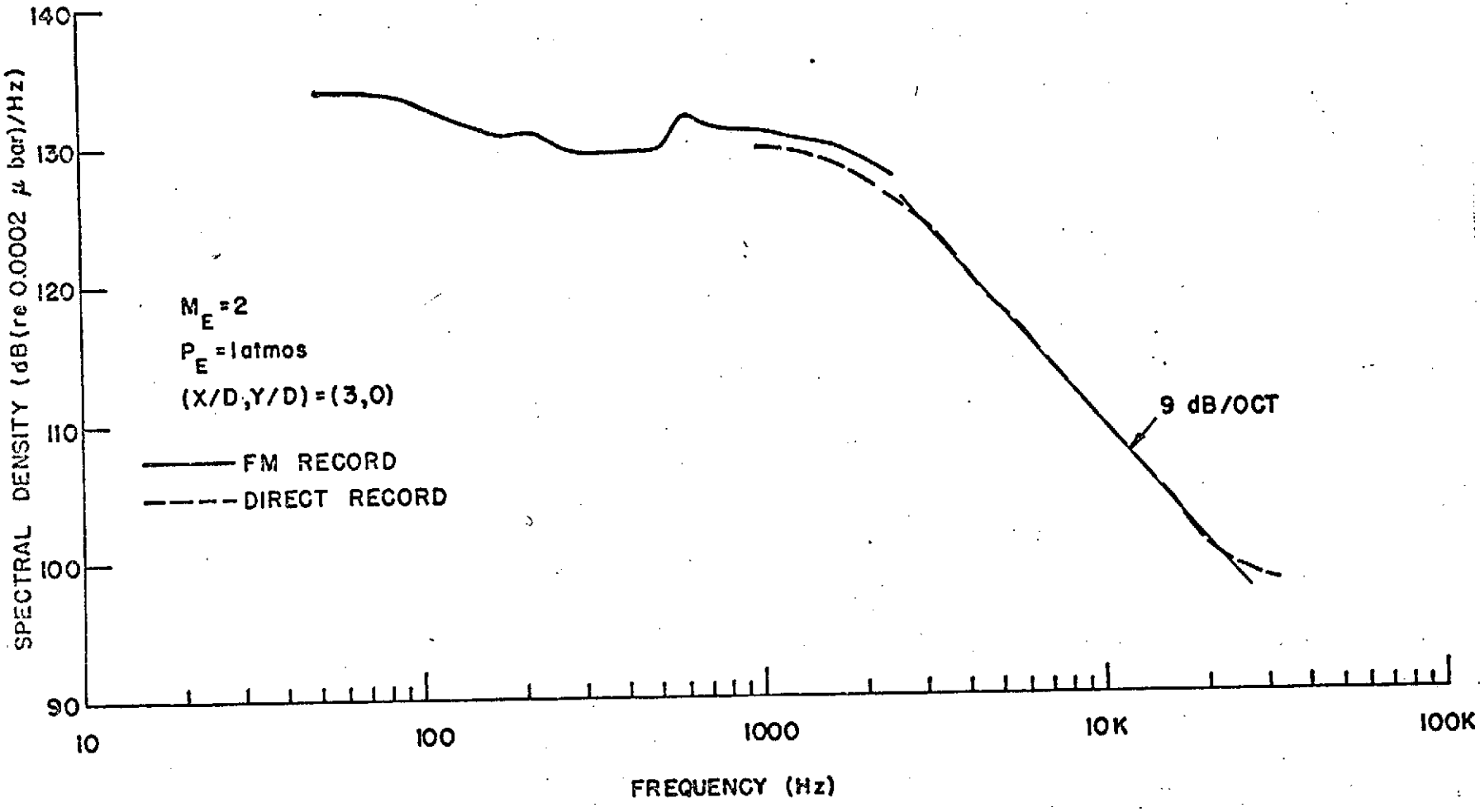

Fig. 27 Spectral Distribution of the Static Pressure Fluctuations at X/D=3 Along Centerline of Balanced Jet

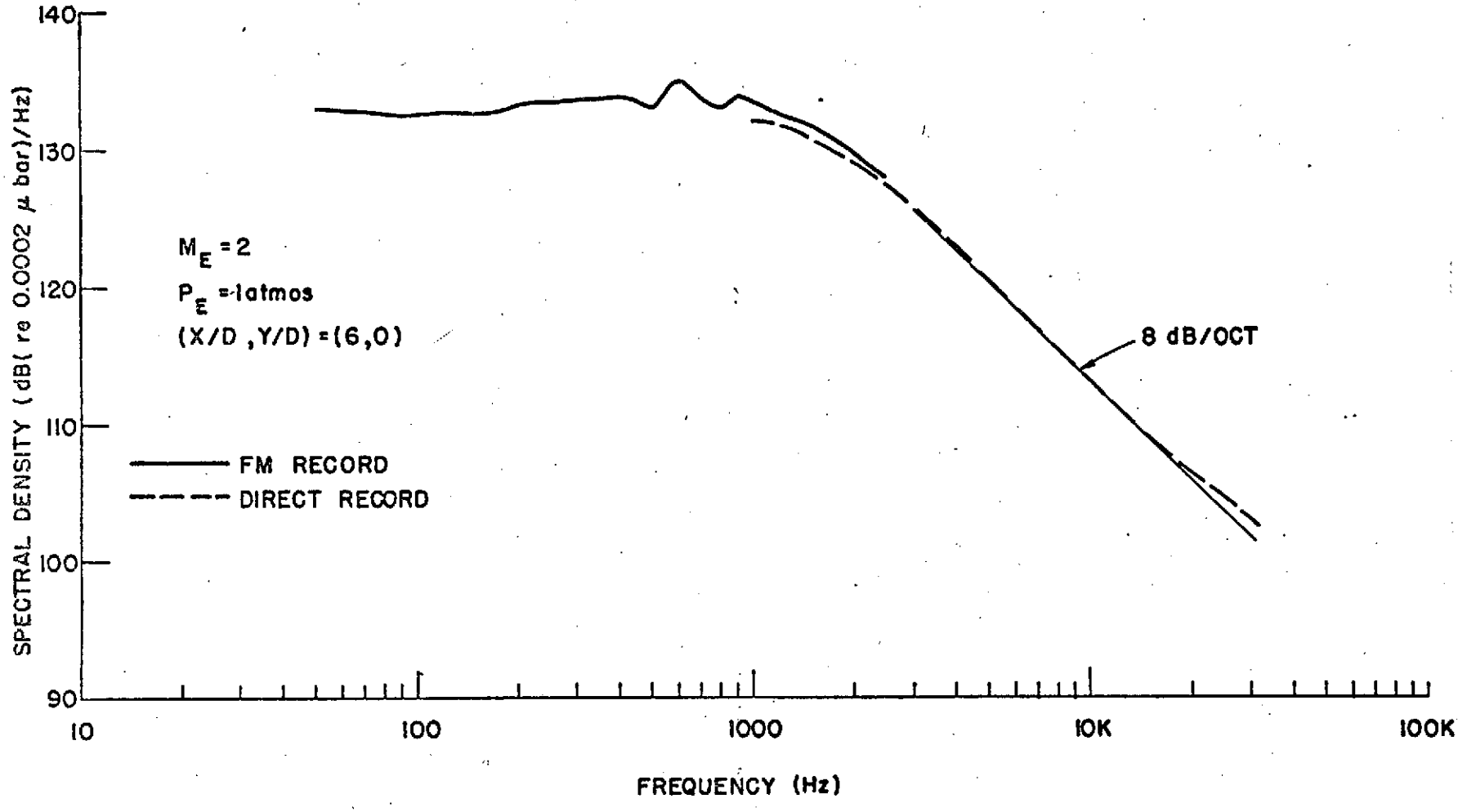

Fig. 28 Spectral Distribution of the Static Pressure Fluctuations at X/D=6 Along Centerline of Balanced Jet

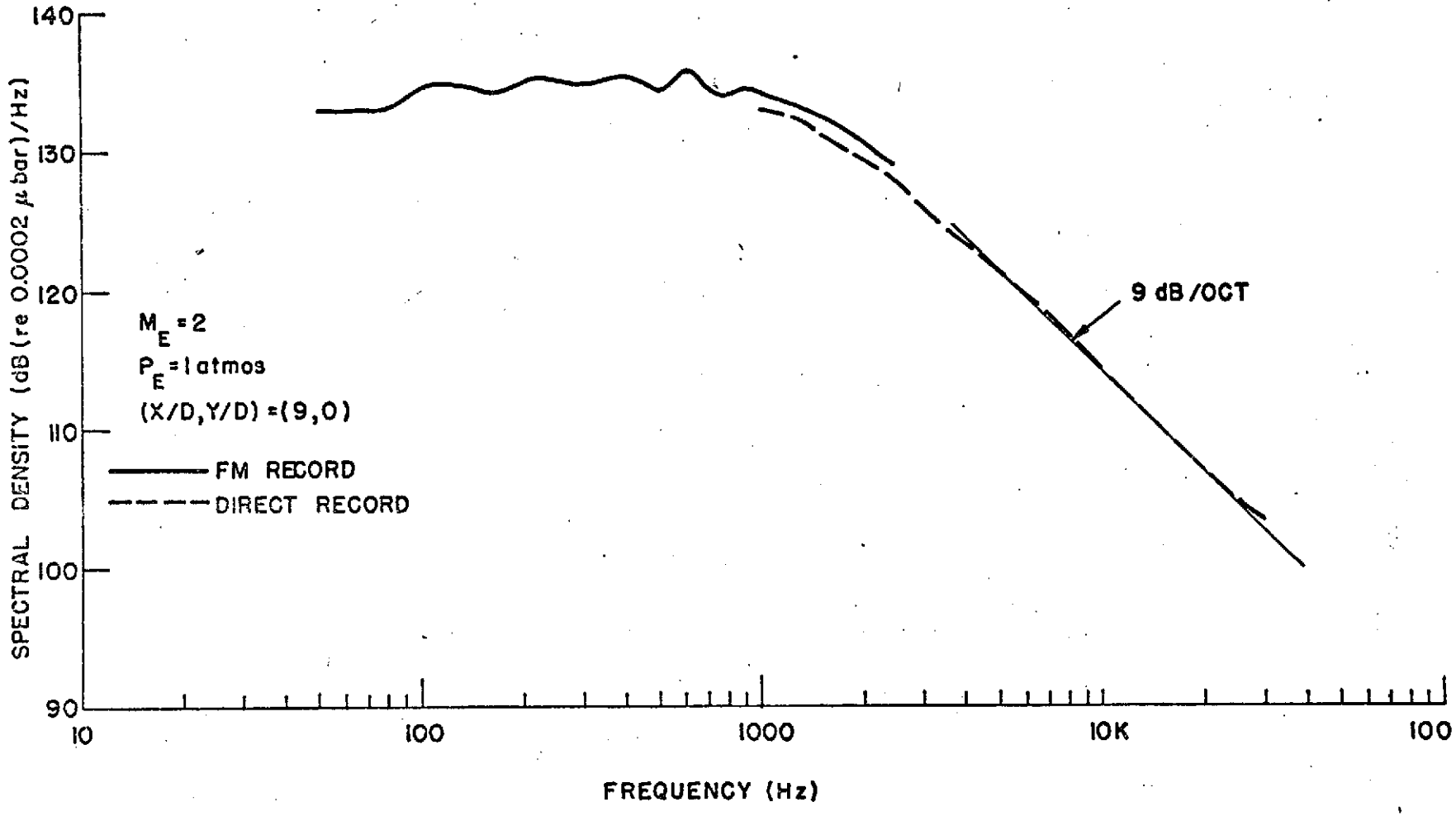

Fig. 29 Spectral Distribution of the Static Pressure Fluctuations at X/D=9 Along Centerline of Balanced Jet

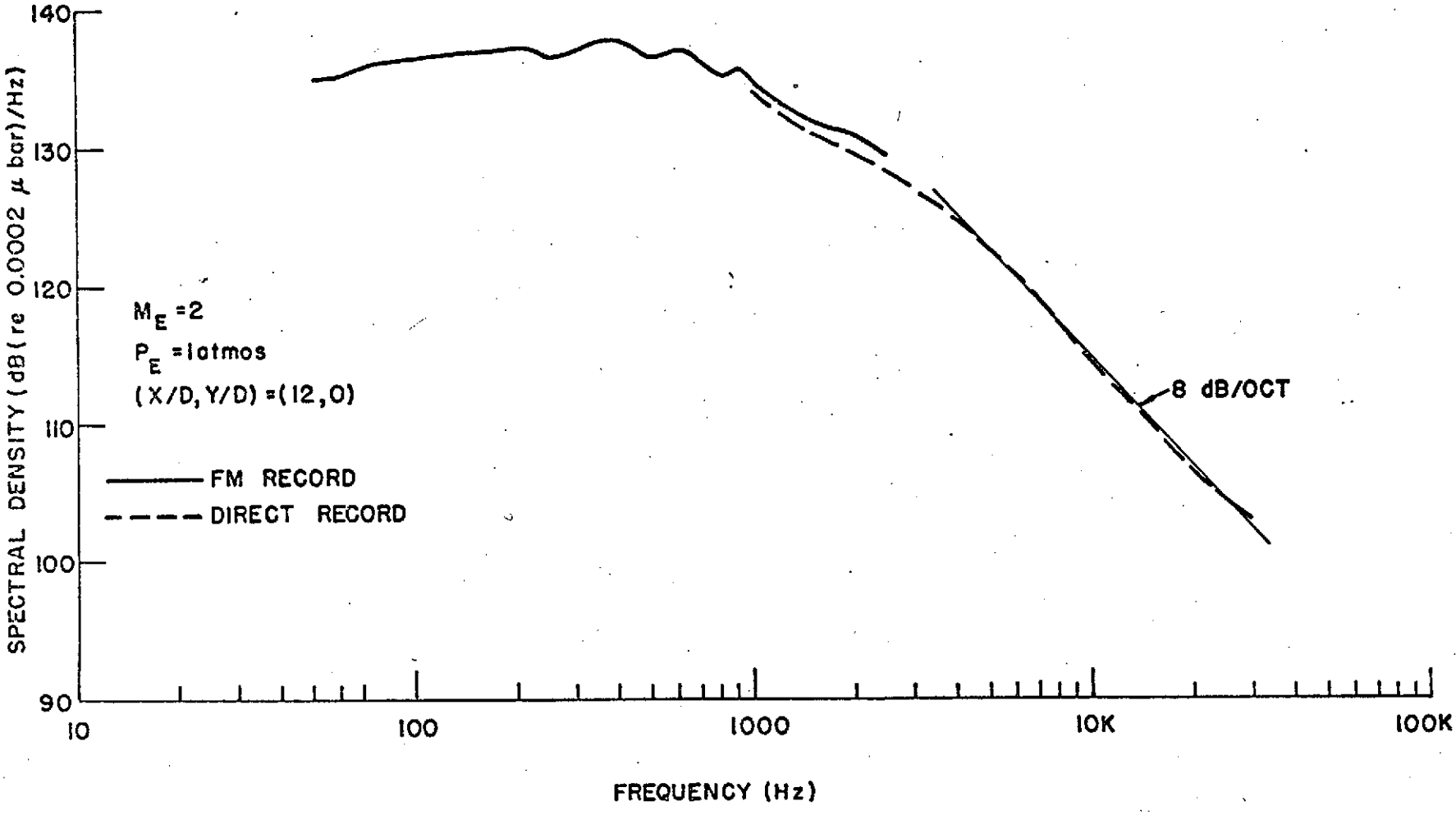

Fig. 30 Spectral Distribution of the Static Pressure Fluctuations at X/D=12 Along Centerline of Balanced Jet

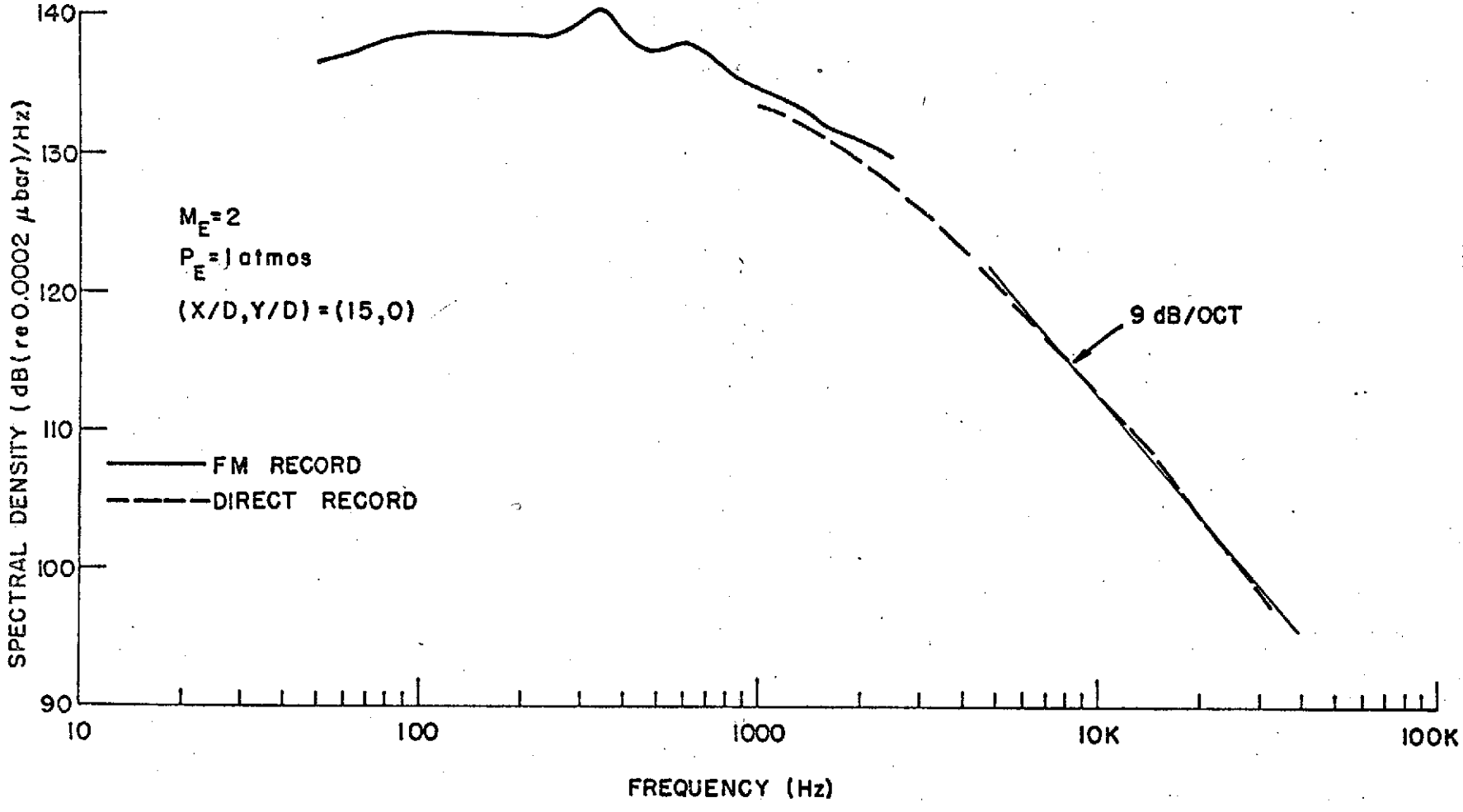

Fig. 31 Spectral Distribution of the Static Pressure Fluctuations at X/D=15 Along Centerline of Balanced Jet

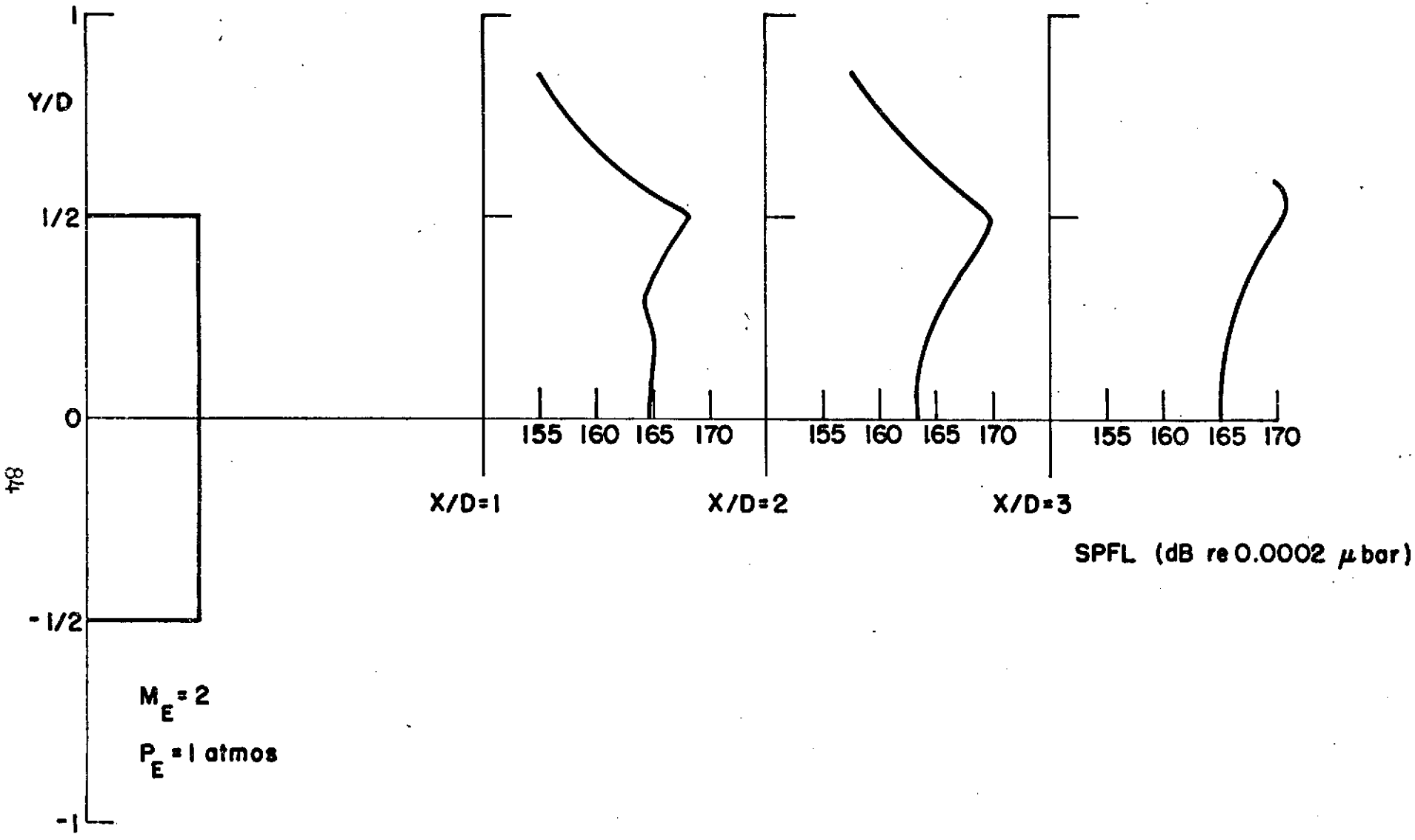

Fig. 32 Variation of Static Pressure Fluctuation Level with Radial Distance from Centerline of Balanced Jet

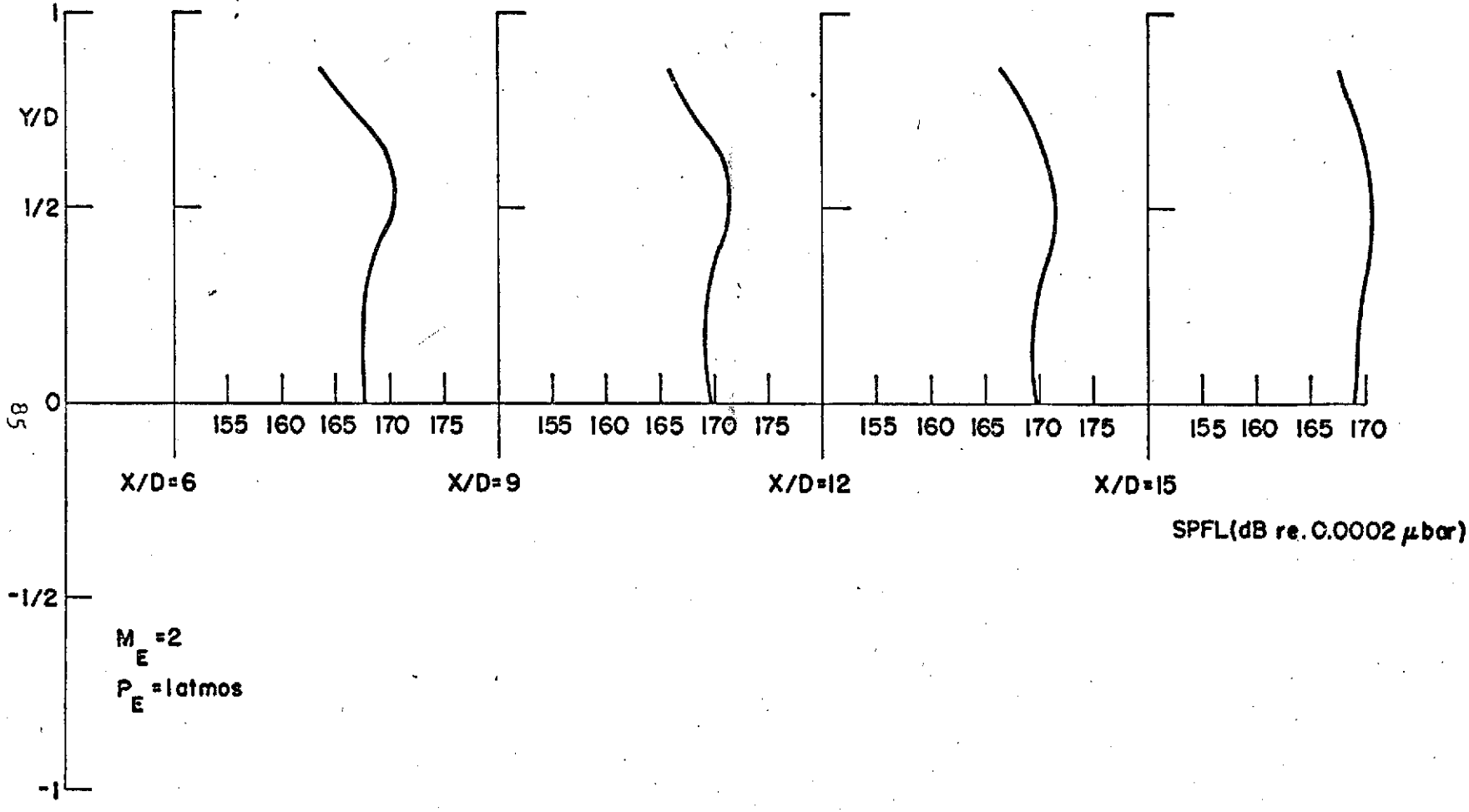

Fig. 33 Variation of Static Pressure Fluctuation Level with Radial Distance from Centerline of Balanced Jet

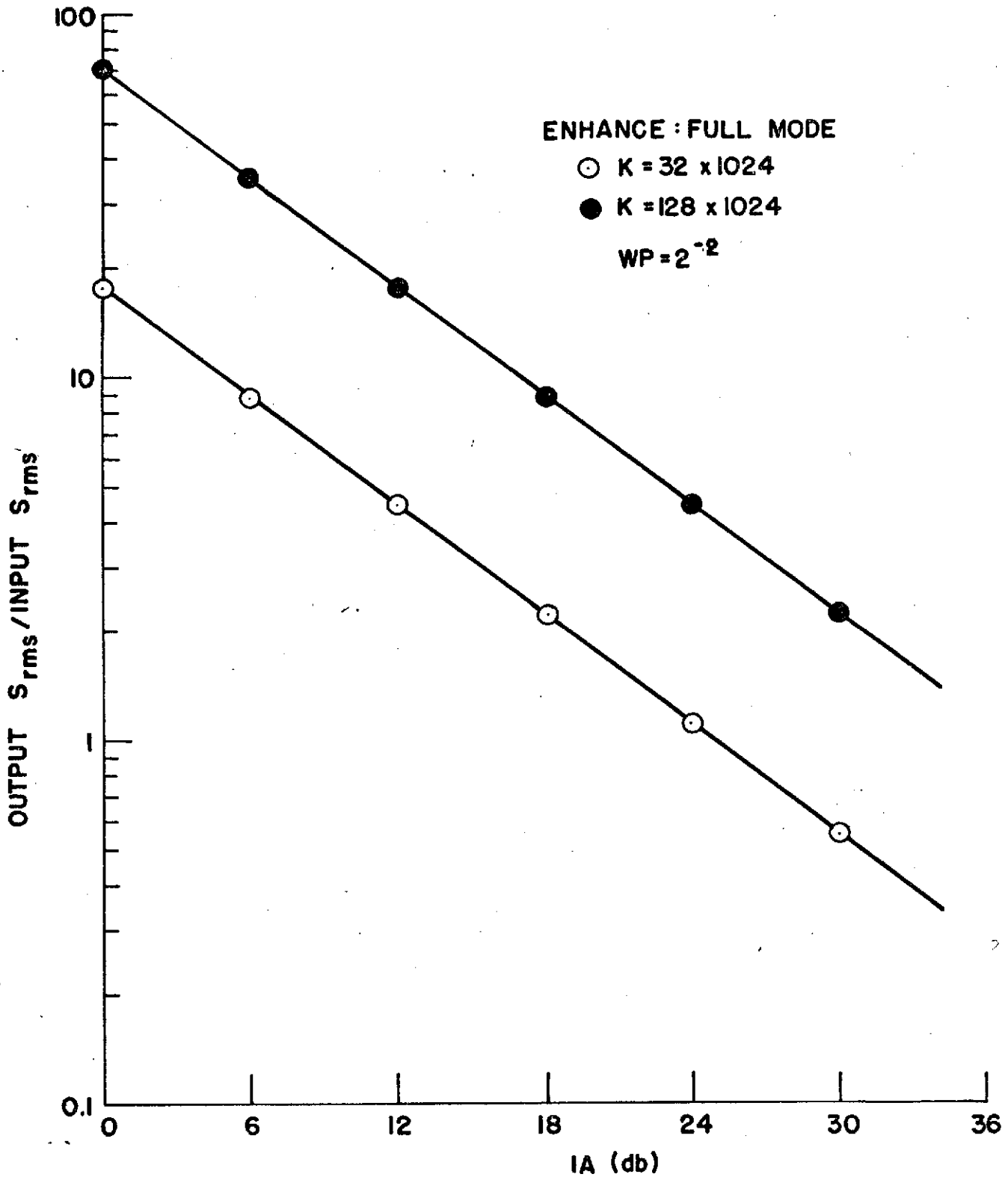

Fig. 34 Calibration of the Full Mode of Ensemble Averaging

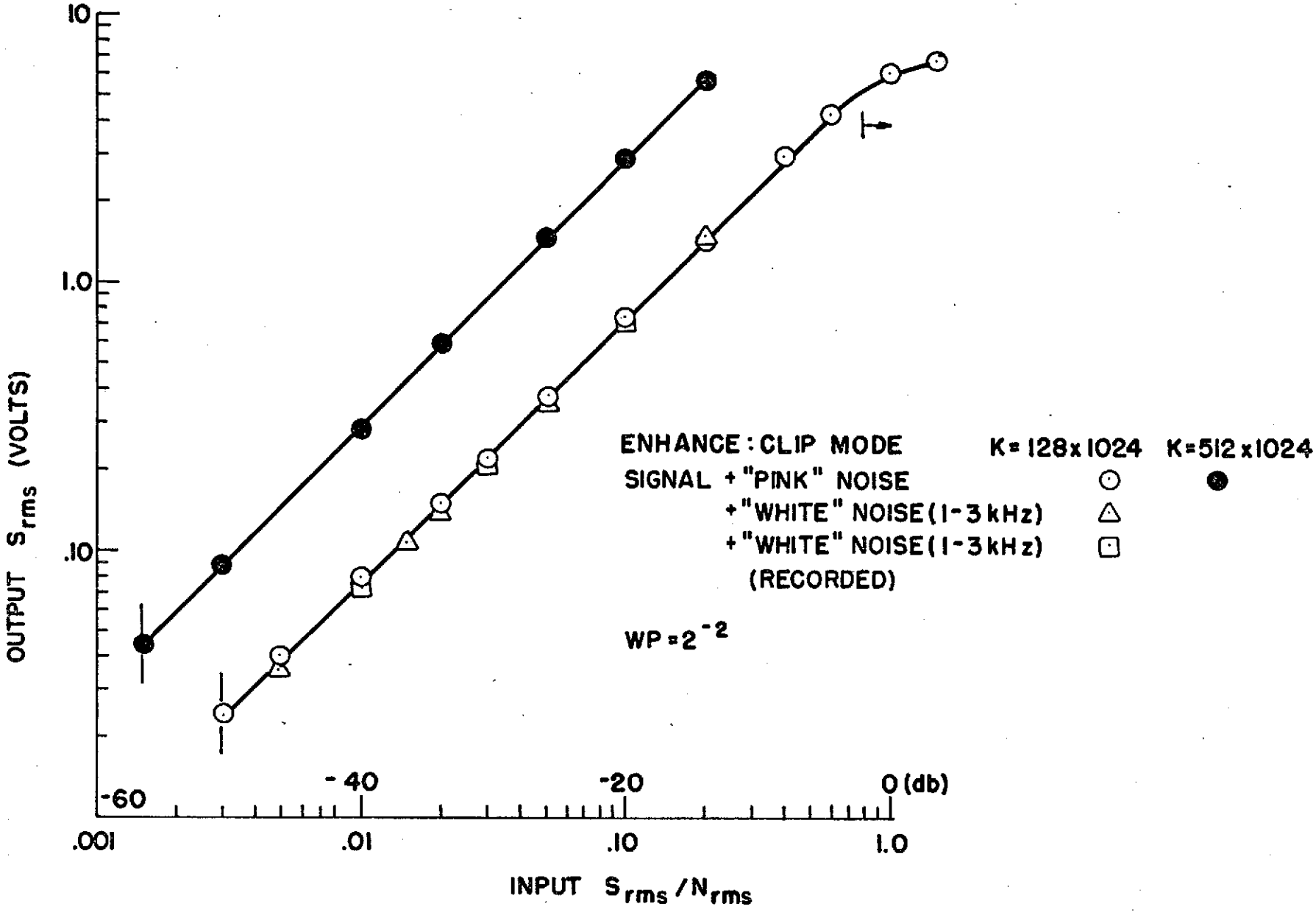

Fig. 35 Calibration of the Clip Mode of Ensemble Averaging

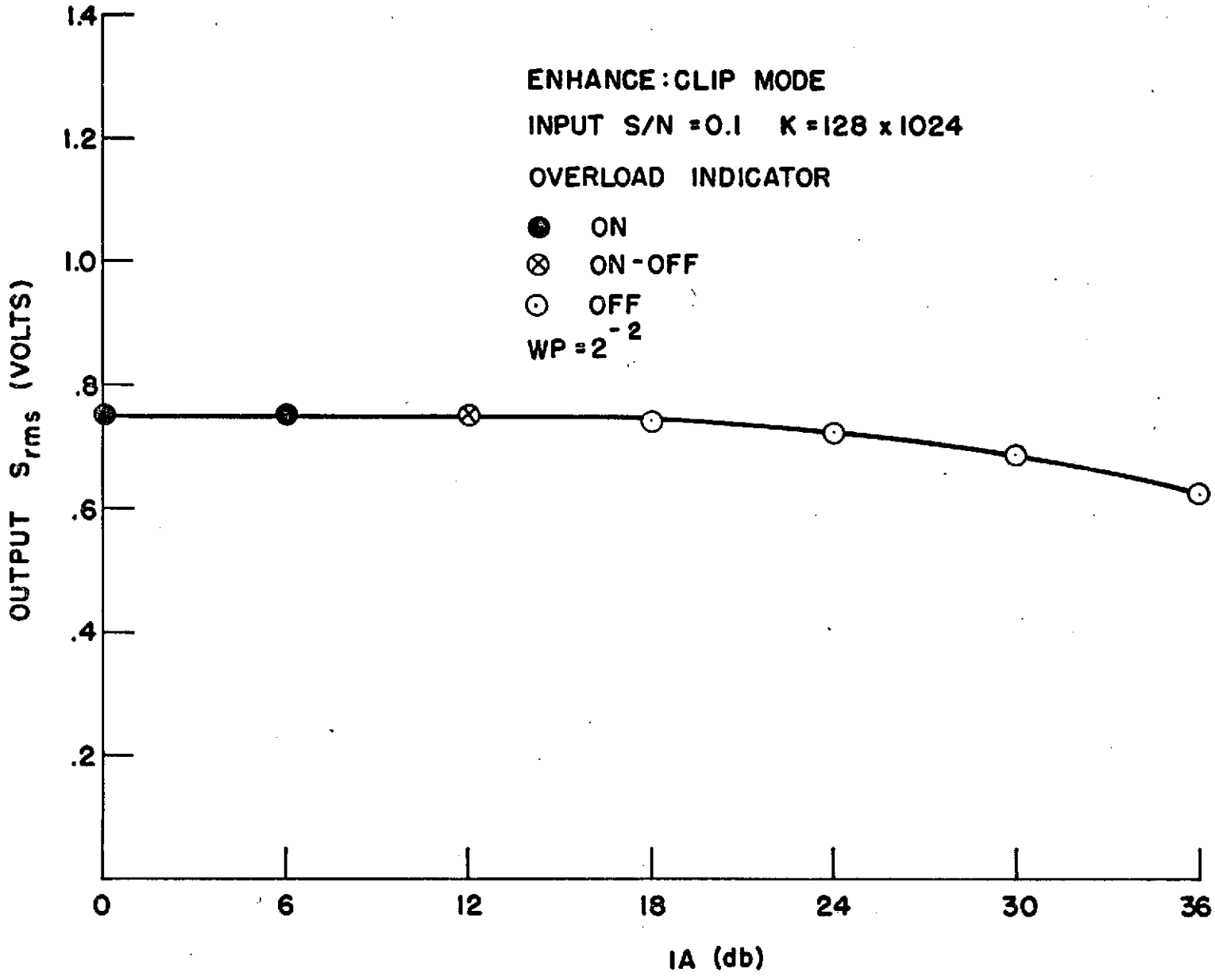

Fig. 36 Affect of the Input Attenuation on the Clip Mode of Ensemble Averaging

	OUTPUT S_{rms} (VOLTS)	INPUT S_{rms}/N_{rms}
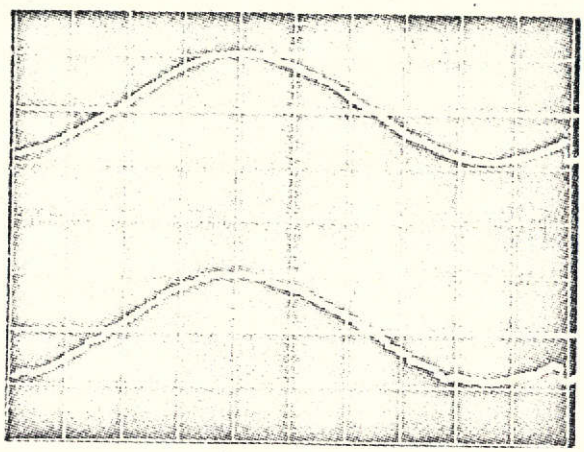	.74	-20 db
	.37	-26 db
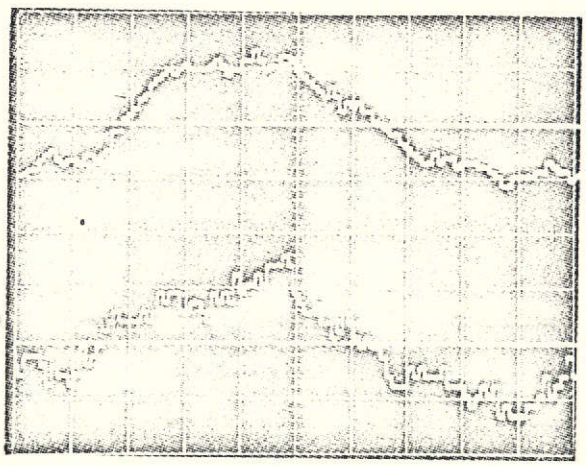	.079	-40 db
	.039	-46 db
PHOTOGRAPH NOT REPRODUCIBLE		
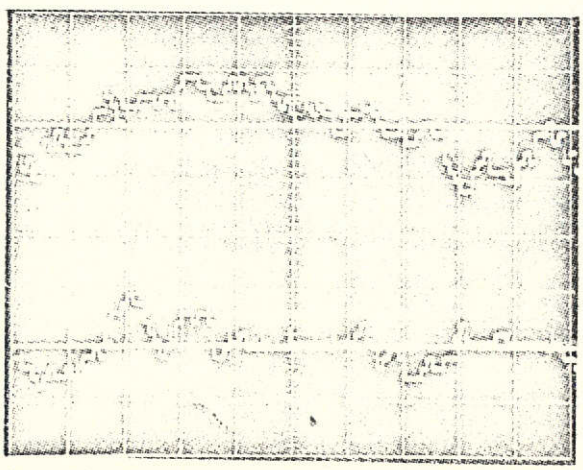	.024	-50 db
	< .024	-56 db

ENHANCE: CLIP MODE
SIGNAL +"PINK NOISE" K = 128 x 1024 WP = 2^{-2}

Fig. 37 Typical Signal Traces Obtained from the Clip Mode of Ensemble Averaging

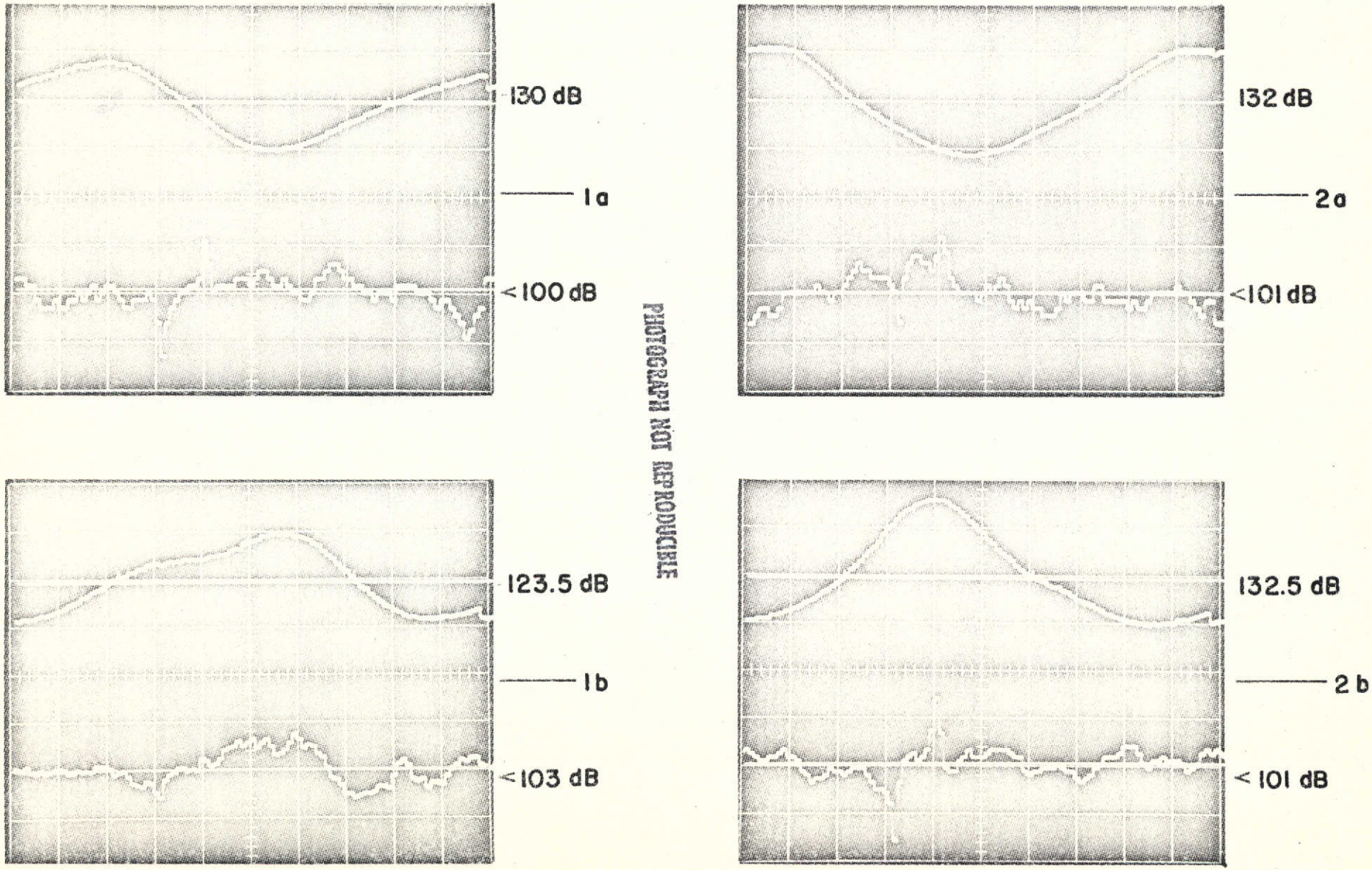

Fig. 38 Traces of the Acoustic Signal at Four Positions in Still Air and in the Balanced Jet

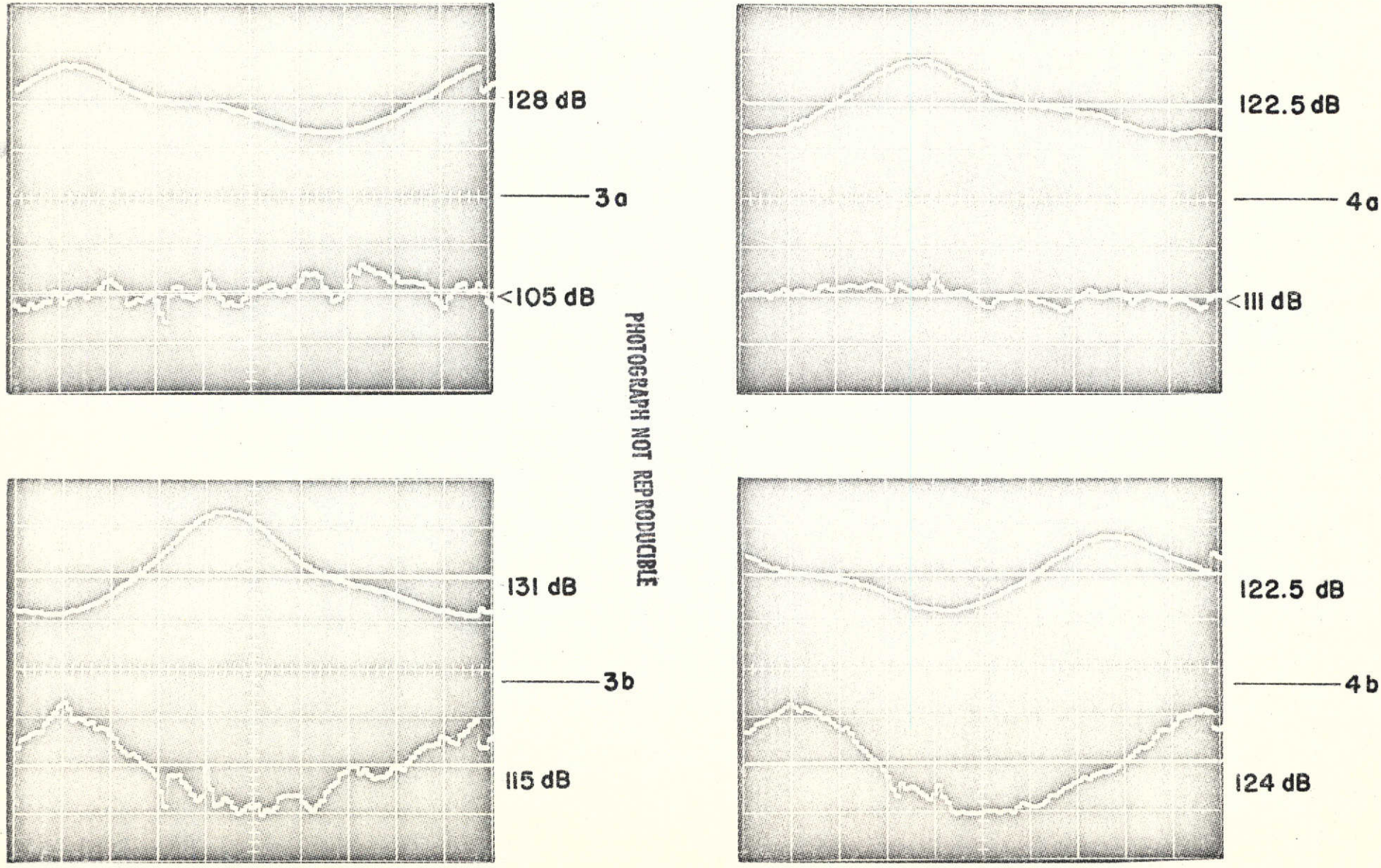

Fig. 39 Traces of the Acoustic Signal at Four Positions in Still Air and in the Balanced Jet

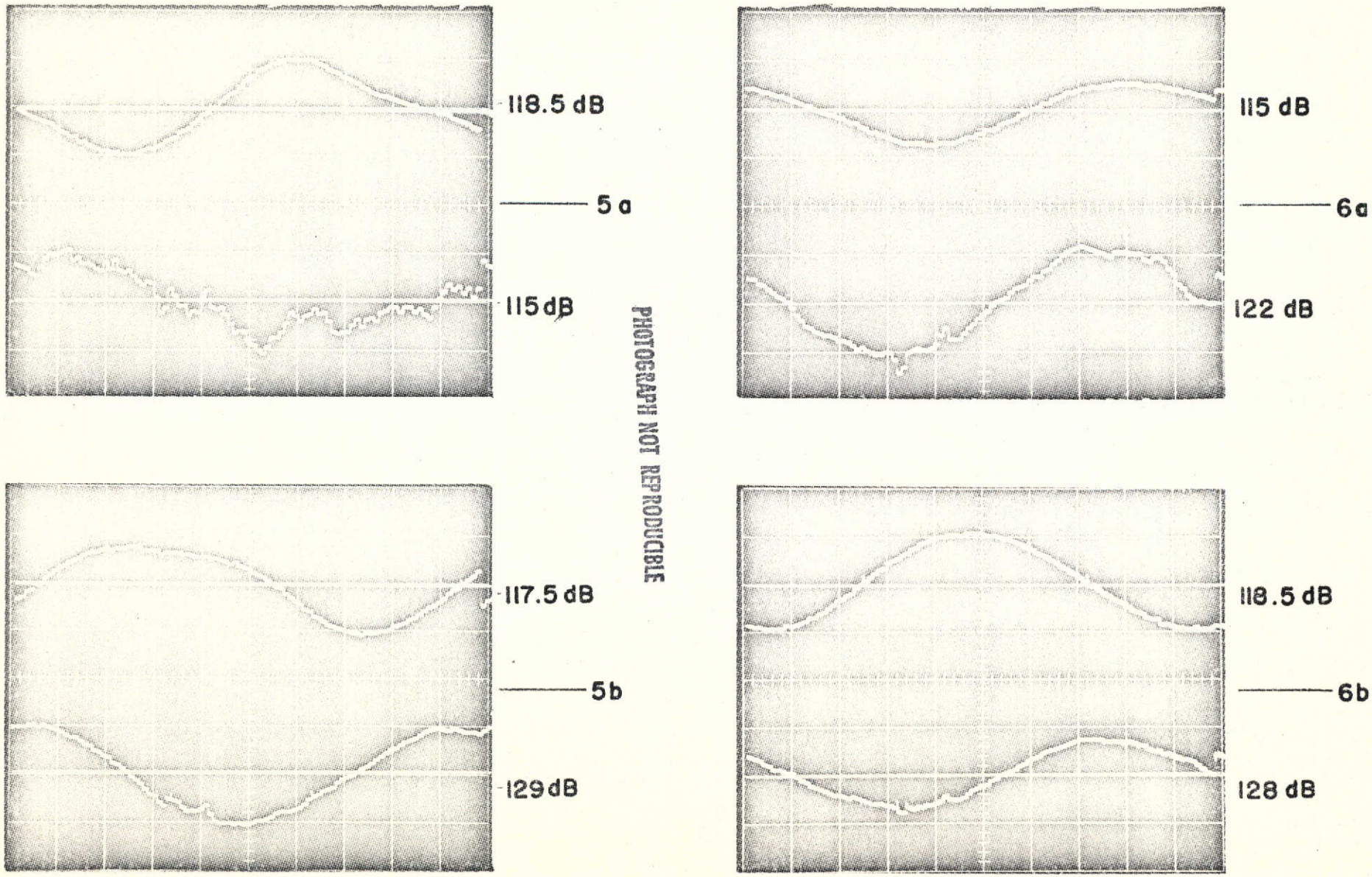

Fig. 40 Traces of the Acoustic Signal at Four Positions in Still Air and in the Balanced Jet

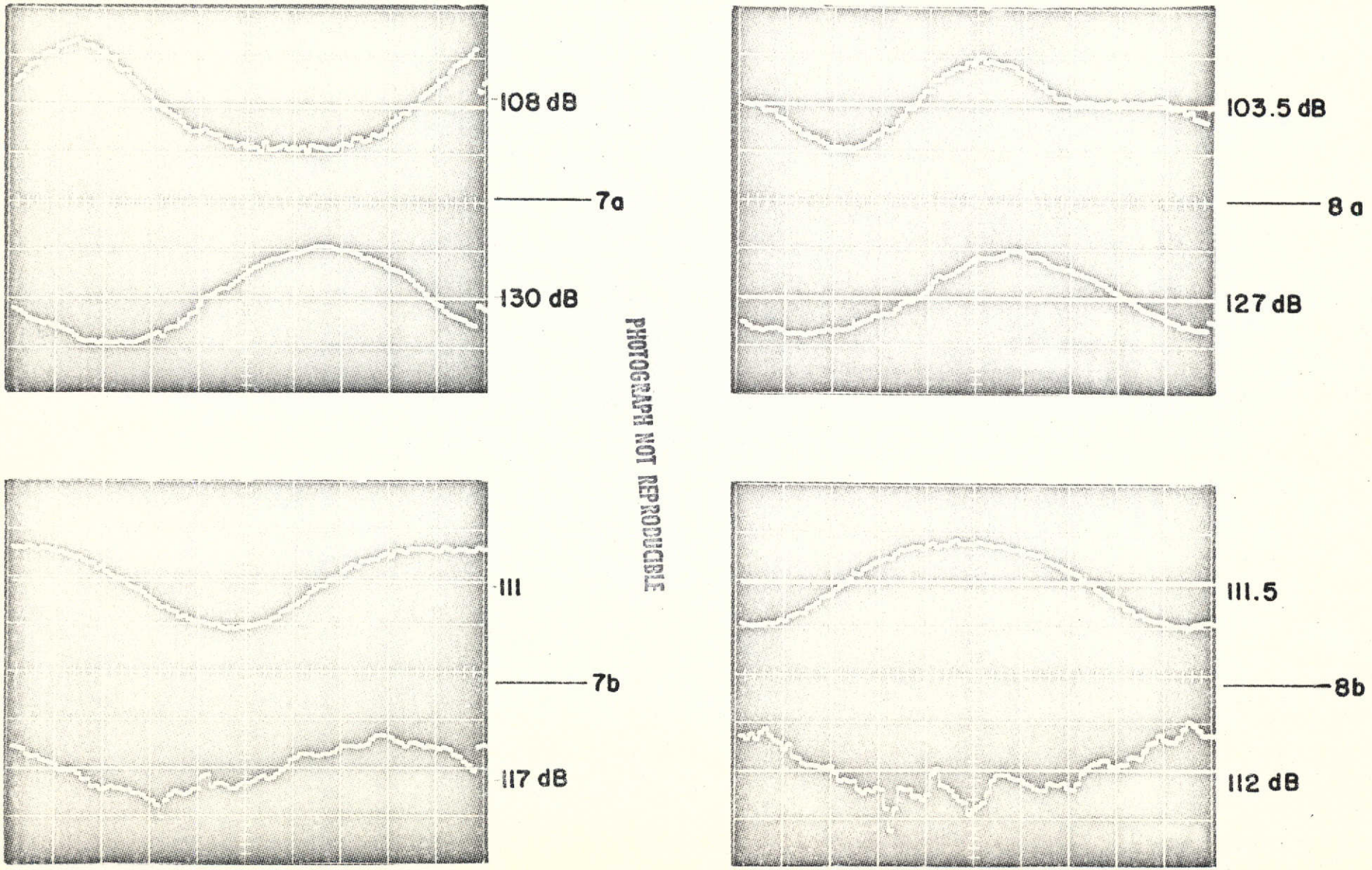

Fig. 41 Traces of the Acoustic Signal at Four Positions in Still Air and in the Balanced Jet

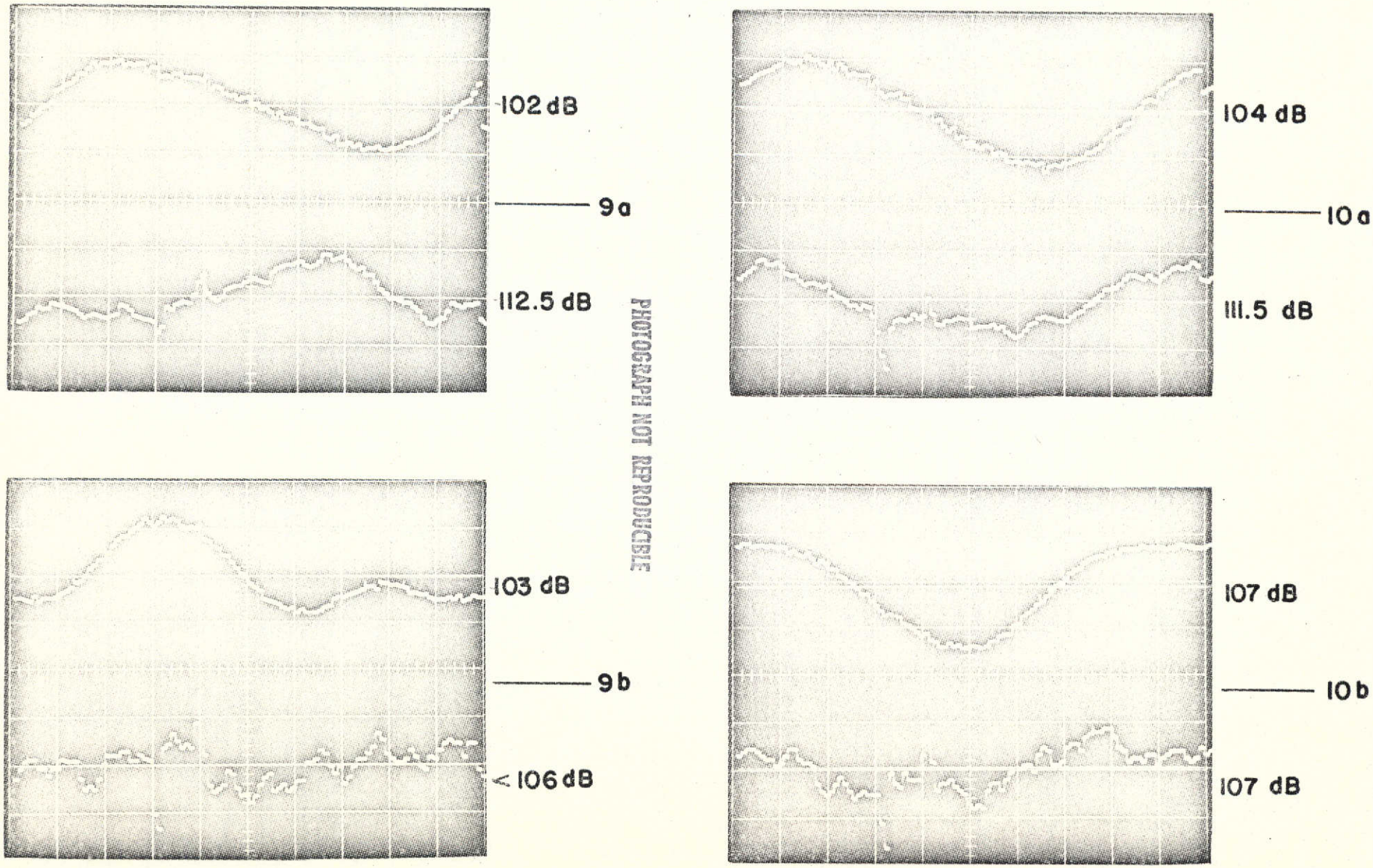

Fig. 42 Traces of the Acoustic Signal at Four Positions in Still Air and in the Balanced Jet

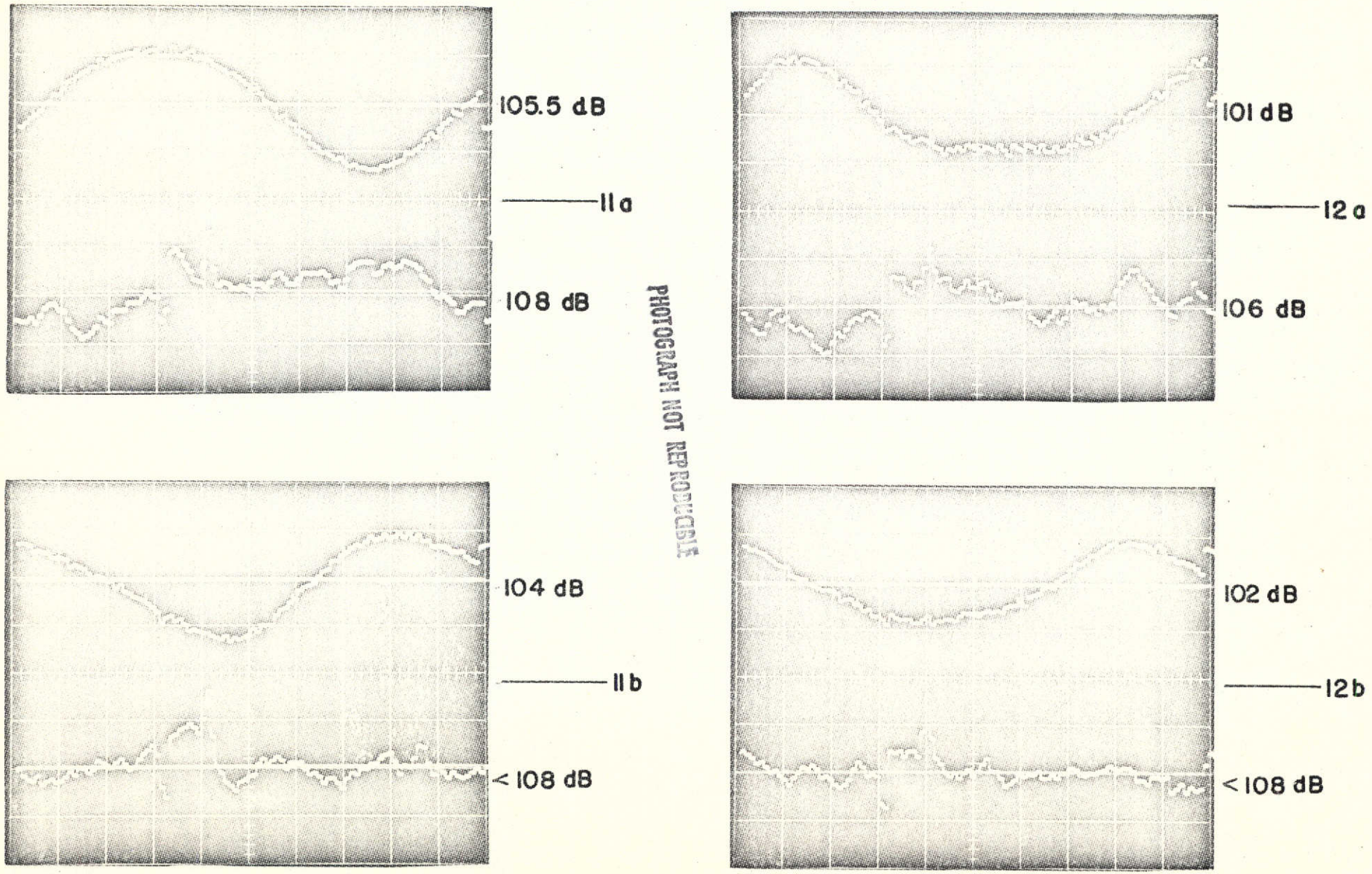

Fig. 43 Traces of the Acoustic Signal at Four Positions in Still Air and in the Balanced Jet

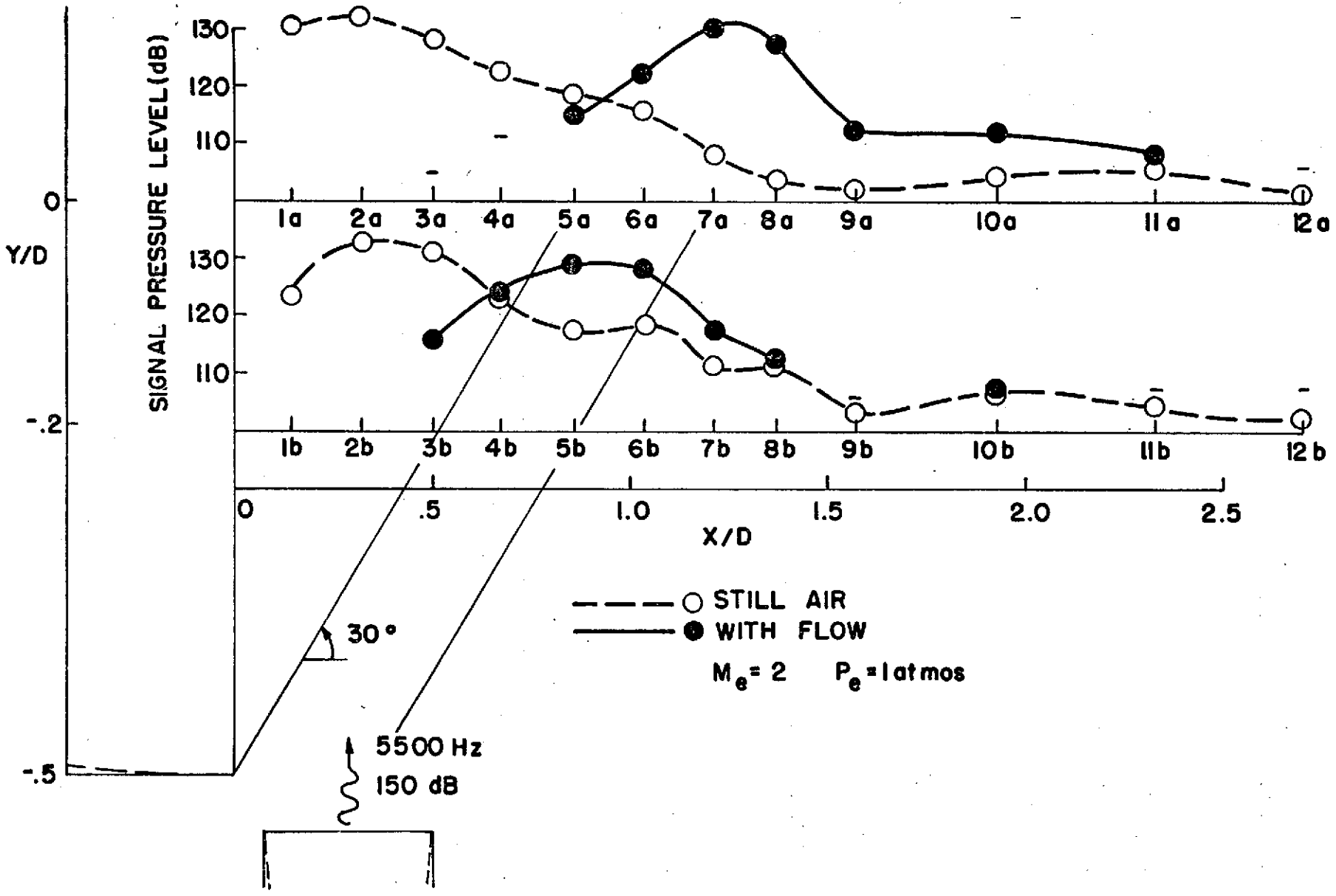

Fig. 44 Variation of the Acoustic Signal Level in Still Air and in the Balanced Jet

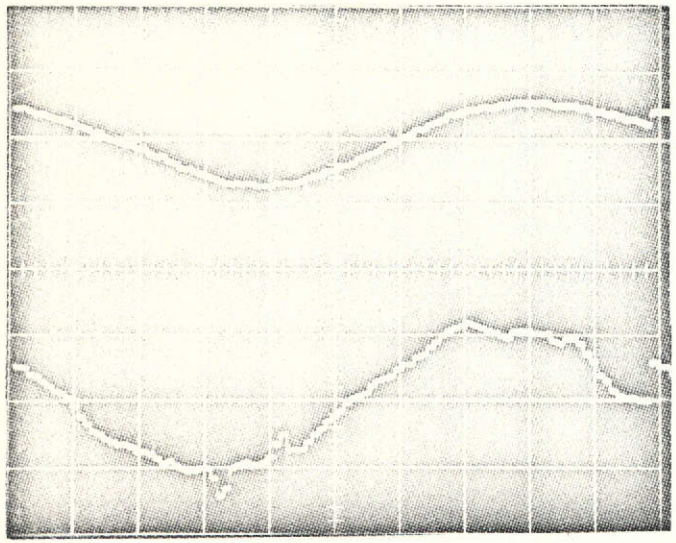

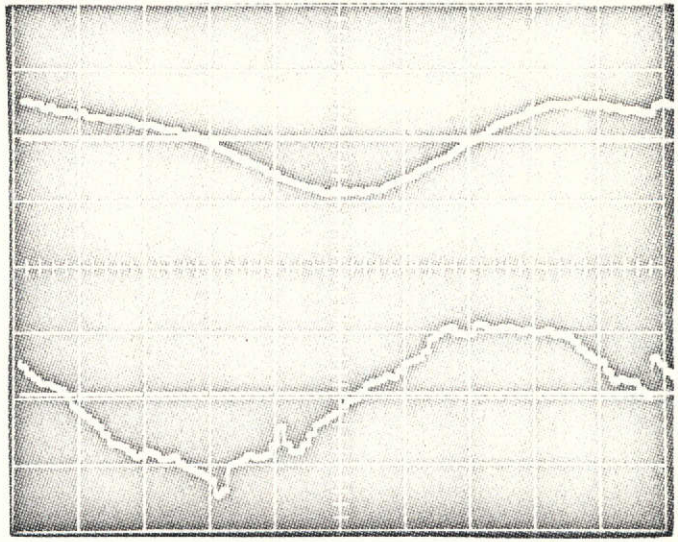

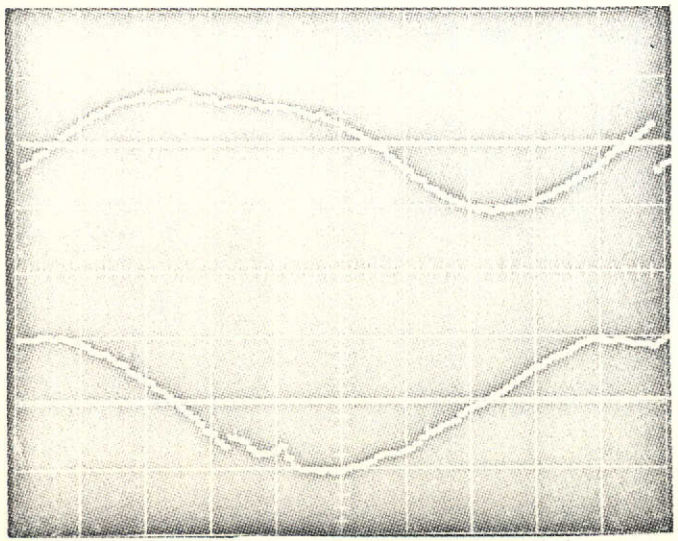

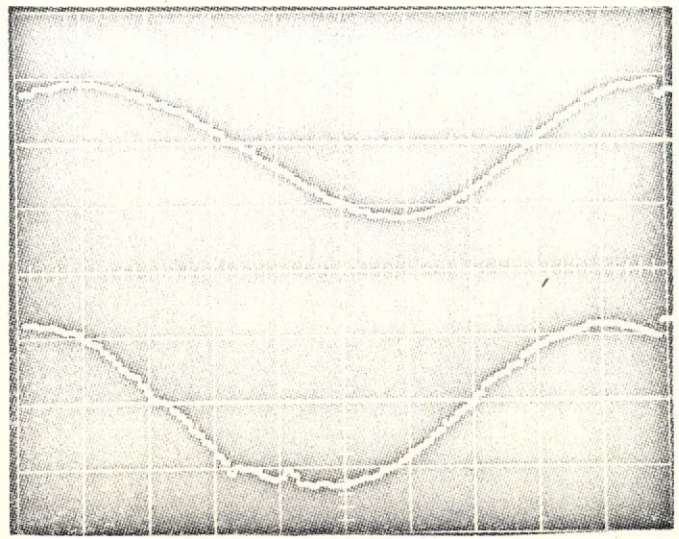

Fig. 45 Comparison of Two Repeated Measurements

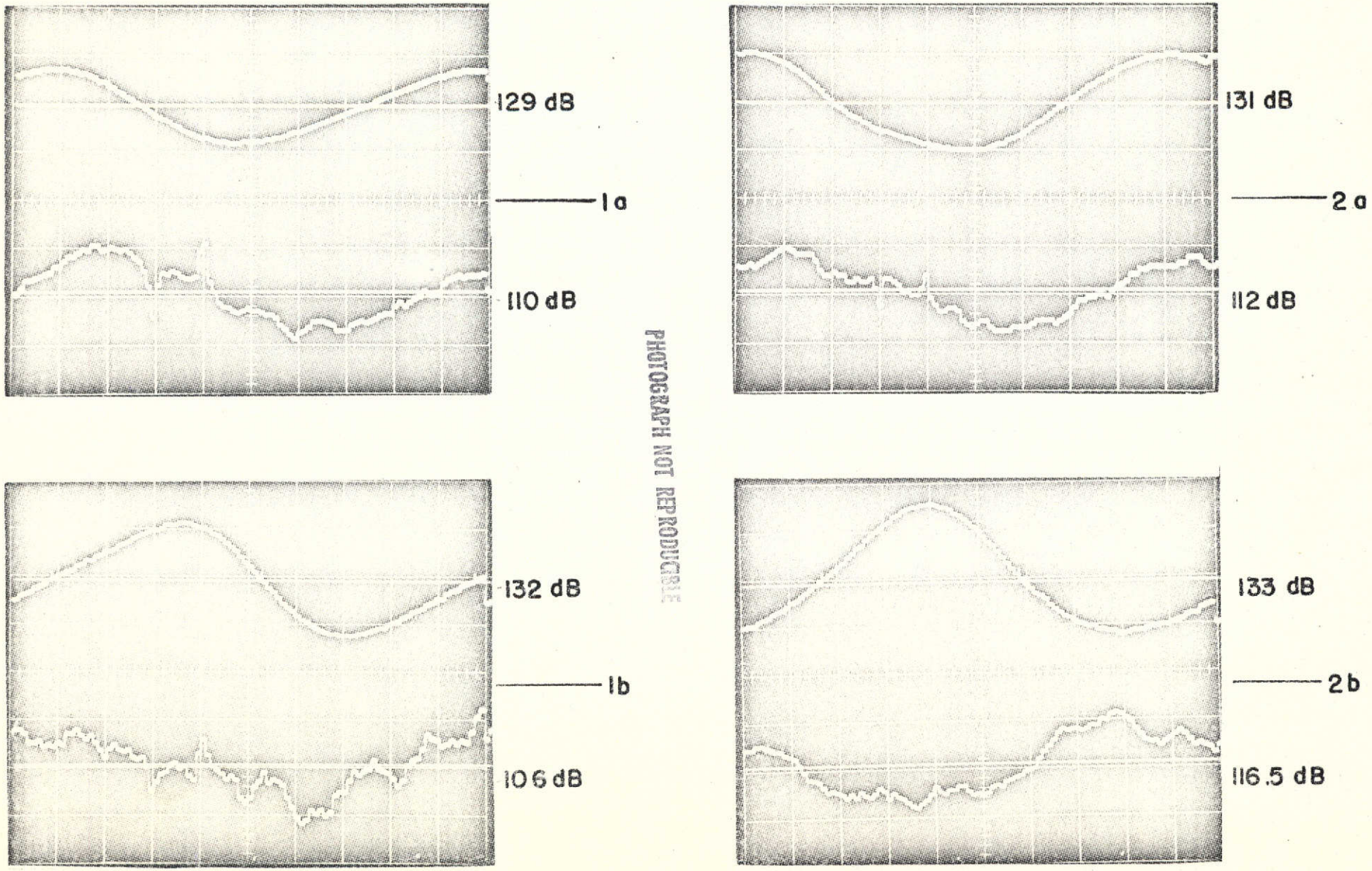

Fig. 46 Traces of the Acoustic Signal at Four Positions in Still Air and in the Overexpanded Jet

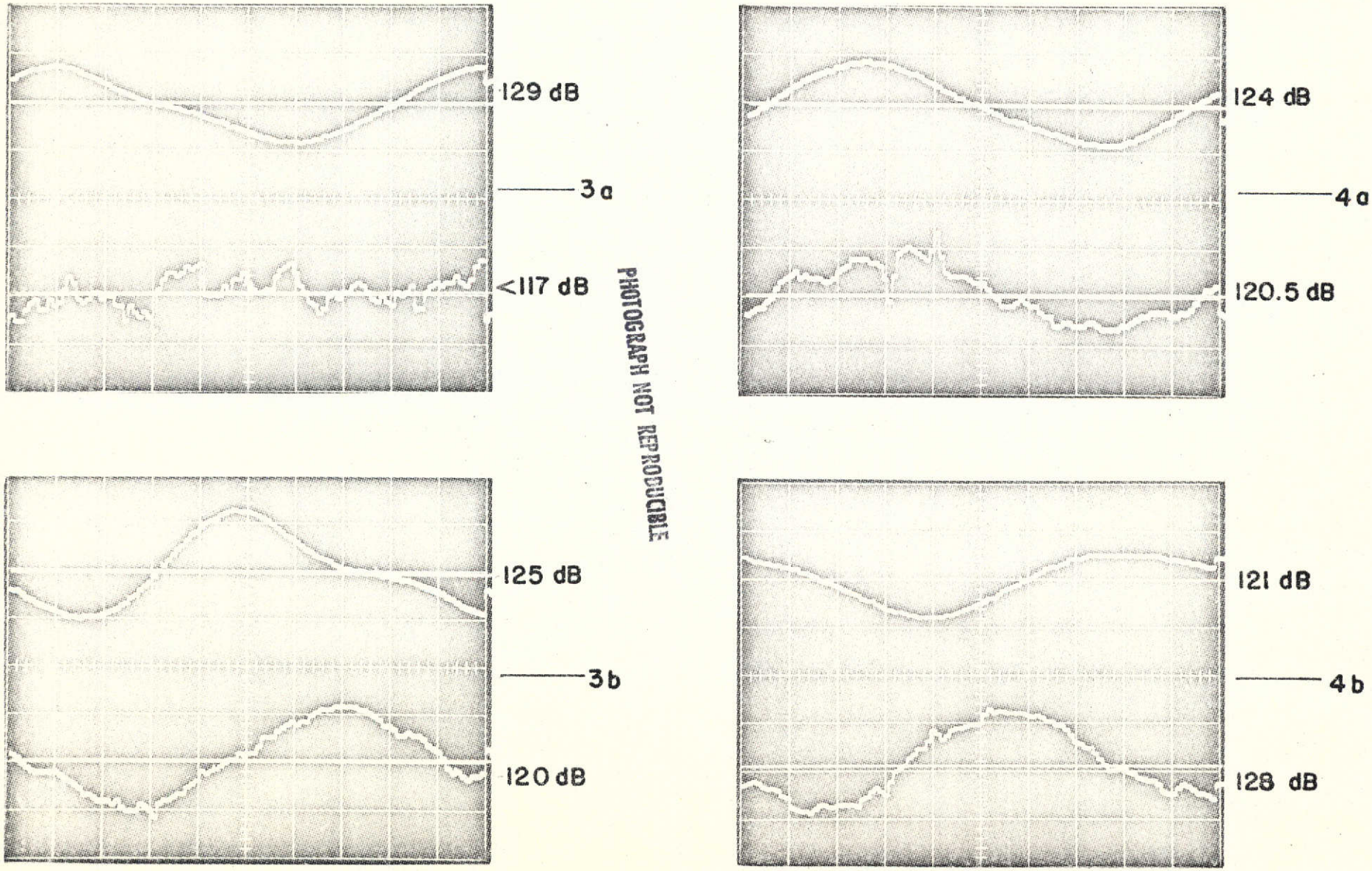

Fig. 47 Traces of the Acoustic Signal at Four Positions in Still Air and in the Overexpanded Jet

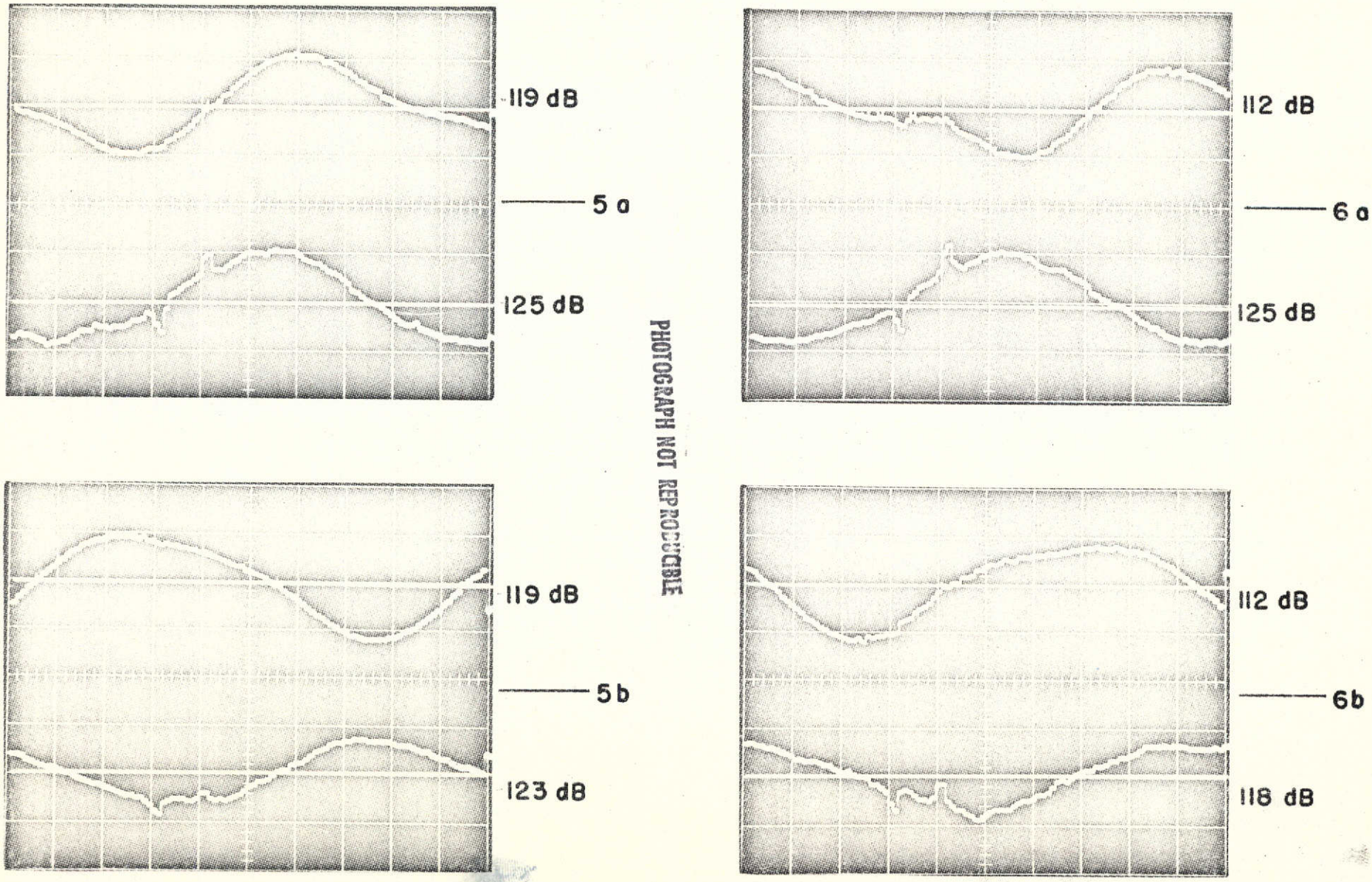

Fig. 48 Traces of the Acoustic Signal at Four Positions in Still Air and in the Overexpanded Jet

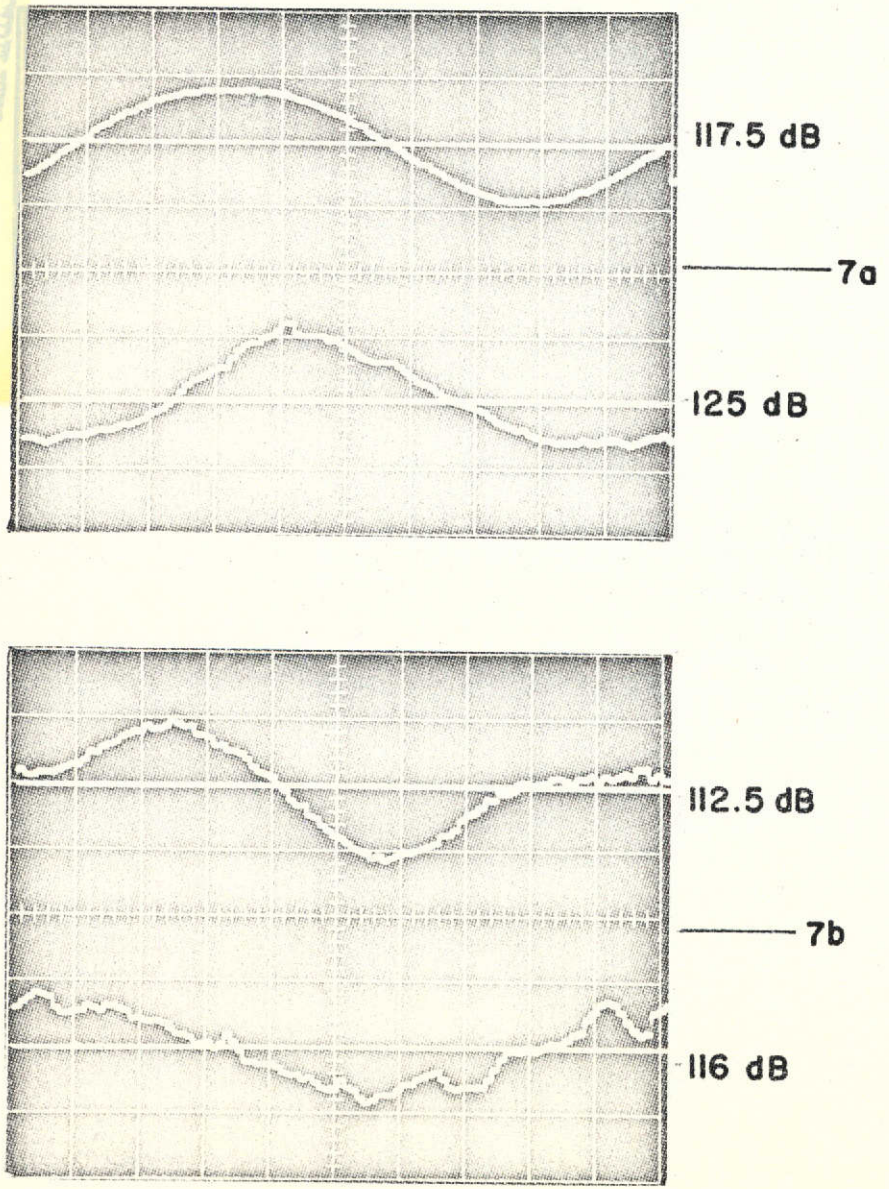

Fig. 49 Traces of the Acoustic Signal at Two Positions in Still Air and in the Overexpanded Jet

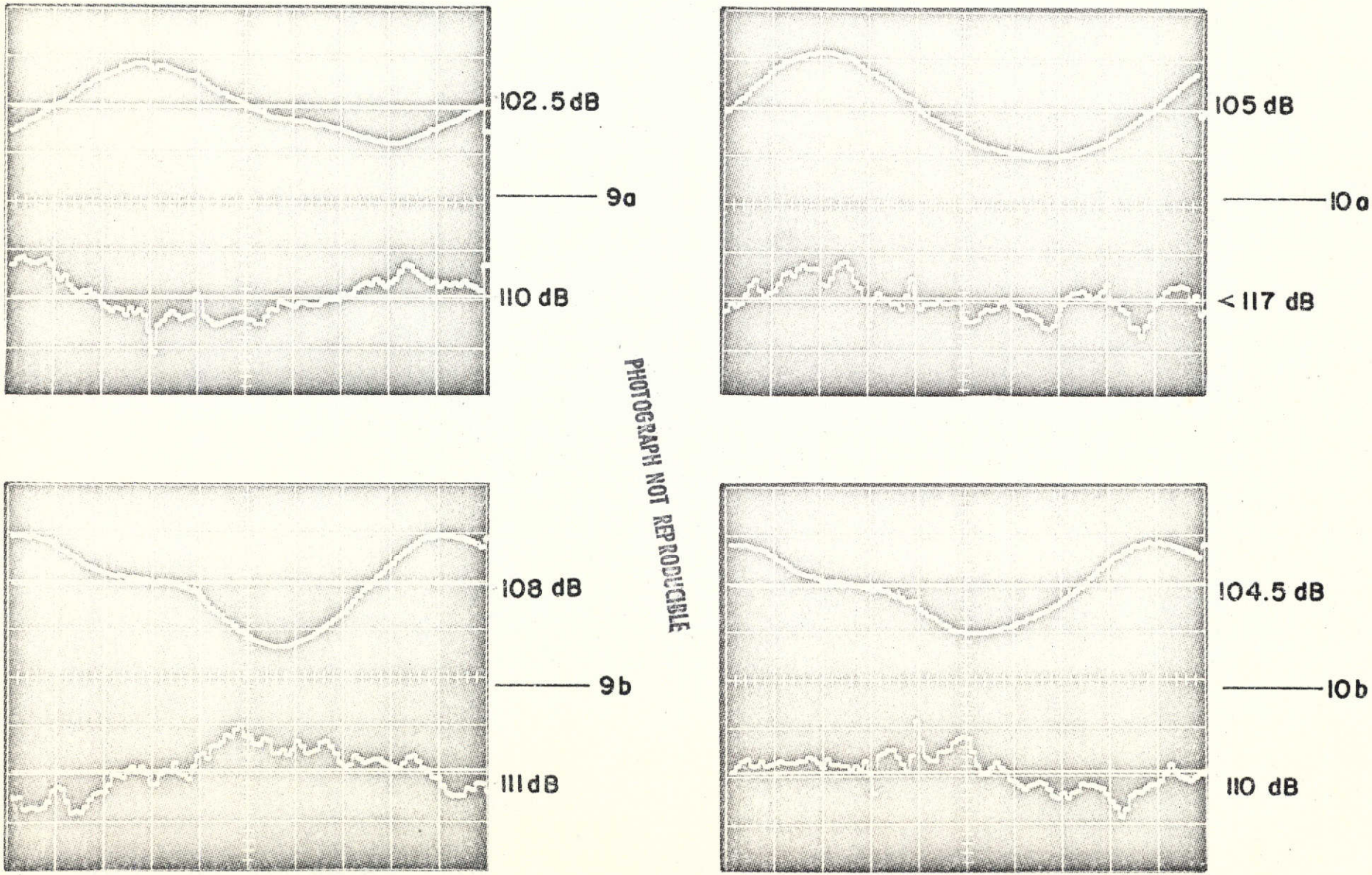

Fig. 50 Traces of the Acoustic Signal at Four Positions in Still Air and in the Overexpanded Jet

Page intentionally left blank

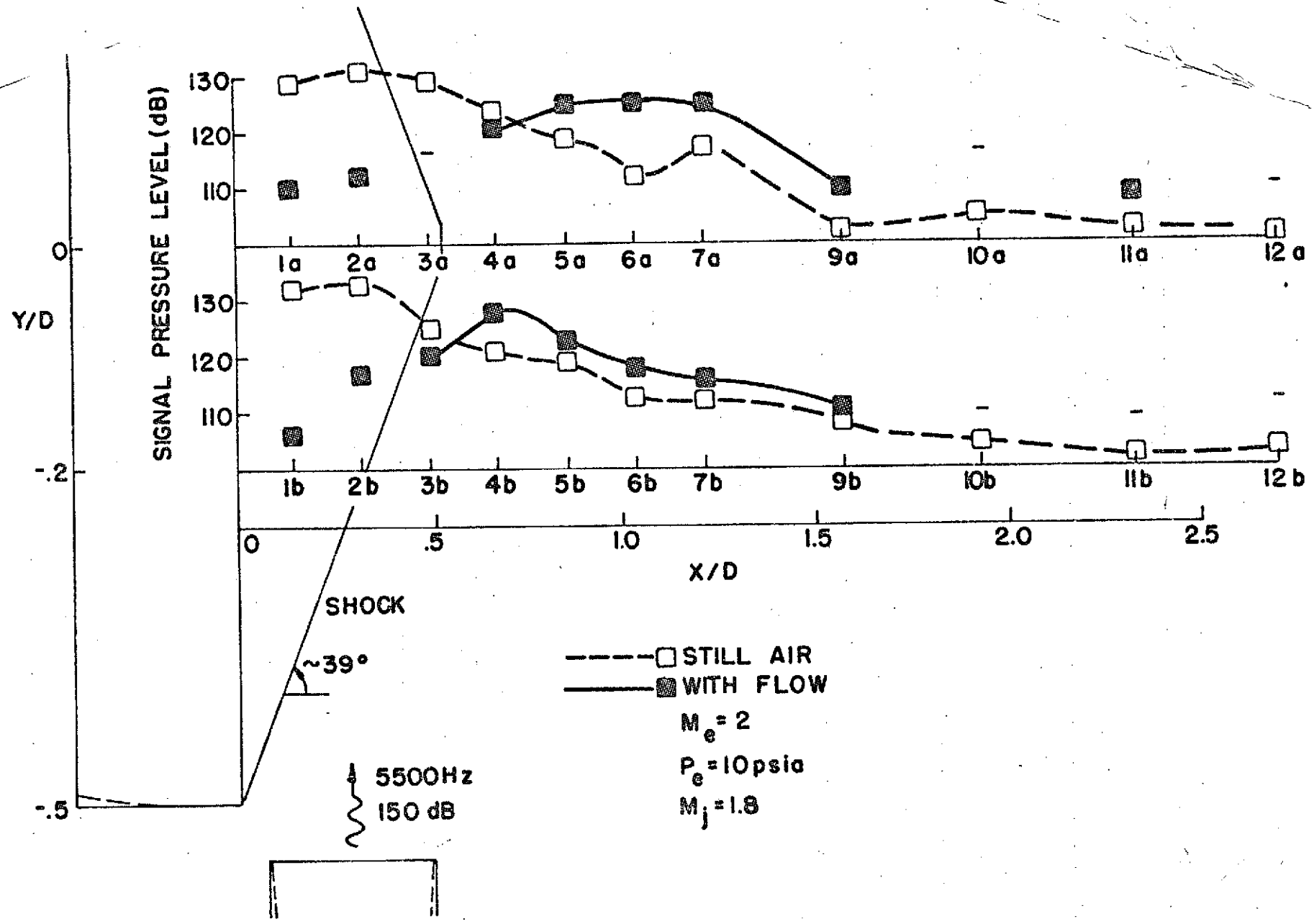

Fig. 52 Variation of the Acoustic Signal Level in Still Air and in the Overexpanded Jet